21

THREE-DIMENSIONAL ELASTODYNAMIC SHEAR FRACTURE PROPAGATION AND GROUND MOTION SIMULATION MODEL

by

E. SIEBRITS
B.Sc. (Civil) Engineering
Cape Town

Thesis submitted in partial fulfilment of the requirements for the degree of Master of Science in Engineering.

Department of Civil Engineering
UNIVERSITY OF CAPE TOWN

1986

DECLARATION

I, Eduard Siebrits, hereby declare that this thesis is essentially my own work, and that no part of it has been submitted for a degree at any other university.

Signed

.....

December 1986.

ACKNOWLEDGEMENTS

I would like to acknowledge the support of the following people and organisations:

1. Dr Howard T. Pearce for his excellent supervision and encouragement, and for his help in the "assemblage" process.

2. Dr John A. Ryder for introducing me to the topic, and for his help and critical reading of the thesis document.

3. Mrs Val Atkinson for deciphering my handwriting and typing the thesis document.

4. The Chamber of Mines Research Organisation of South Africa, and the Council for Scientific and Industrial Research for their financial support.

ABSTRACT

A boundary integral equation method (BIEM) is used to obtain the stress and slip on a shear crack plane of arbitrary shape propagating in an infinite, three-dimensional, homogeneous medium. The displacement at any point on the crack plane is written as an integral of a convolution between the tractions on the crack plane and the fundamental solution of the displacement due to a unit impulse.

The fundamental solution is discretised over a space and time grid (the tractions being assumed constant over each grid) to solve the integral equation numerically. The rupture process can be controlled by prescribing the rupture velocity or can automatically propagate using a prescribed fracture criterion. The method is checked against a simple analytical solution.

From the results of the dynamic slip on the fault plane, it is possible to obtain the ground motion response at near- and far-field locations away from the fault surface by means of a summation of the responses due to the slip on a small element of the crack surface. This ground motion simulation model is demonstrated for a linearly propagating ramp dislocation function and for a self-similar (radially propagating) shear crack.

NOMENCLATURE

α	compressional (P) wave speed
β	shear (S) wave speed
γ	Rayleigh (R) wave speed
$\delta_{ij}(.)$	Dirac delta function
Δt	grid time-step
Δx	grid spatial step length in x_1 and x_2 directions
θ_i	polar integration limit
λ	Lamé constant
μ	Lamé constant
μ_d	dynamic coefficient of friction
ν	Poisson's ratio
ν_ℓ	ℓ^{th} component of unit normal to fault element $d\Sigma(\underset{\sim}{\xi})$
ξ_i	source point in Cartesian coordinate system
π	pi
ρ	material density
σ_d	dynamic frictional stress
σ_{ij}°	initial uniform stress component on $x_3 = 0$ plane
σ_{ij}	total stress component on $x_3 = 0$ plane
τ_{ij}	incremental stress component on $x_3 = 0$ plane
τ_e	dynamic stress drop or effective stress
Γ	boundary of a domain Ω
$\phi_q(t)$	interpolation function
ϕ	radial polar coordinate
$\Psi_k(\underset{\sim}{\xi},t)$	double time integral of dislocation $D_k(\underset{\sim}{\xi},t)$
$\dot{\Psi}_k(\underset{\sim}{\xi},t)$	first time derivative of $\Psi_k(\underset{\sim}{\xi},t)$

$\ddot{\Psi}_k(\underset{\sim}{\xi},t)$	second time derivative of $\Psi_k(\underset{\sim}{\xi},t)$
$\dddot{\Psi}_k(\underset{\sim}{\xi},t)$	third time derivative of $\Psi_k(\underset{\sim}{\xi},t)$
Ω	domain
A	dimensionless constant α^2/β^2
a,b,c	constants
$c_{ijk\ell}$	elasticity tensor
c_1, c_2, c_3, c_4	constants
C(.)	dimensionless function
C_1, C_2	complex constants
CNUM	complex number
CROOT	complex square root
$d\Sigma(\underset{\sim}{\xi})$	fault element with central node point $\underset{\sim}{\xi}$
$D_k(\underset{\sim}{\xi},t)$	k^{th} component of the dislocation on fault element $d\Sigma(\underset{\sim}{\xi})$ at time t
D_p	$D_k(\underset{\sim}{\xi},t_p)$
E	Young's modulus
f_i, g_i	body force vectors
F_{ij}	$g^H_{ij}(.)$ integrated over an elemental volume
$G_{ni}(.)$	general three-dimensional Green's function
$g_{ni}(.)$	three-dimensional Green's function for a homogeneous half-space where source function is a unit impulse
$g^H_{ni}(.)$	three-dimensional Green's function for a homogeneous half-space where source function is a unit step
H(.)	Heaviside step function
$I_1(T), I_2(T)$	dimensionless functions within the Green's functions
i,j,k	receiver point indices
ℓ,m,n	source point indices
L, M	summation constants

n_j	direction vector
P	dimensionless slowness in Rayleigh cubic equations
$P_1, P_2, \ldots P_6$	spatial terms in Maruyama formula
$Q_1, Q_2, \ldots Q_6$	temporal terms in Maruyama formula
$\underset{\sim}{r}$	direction vector $(\underset{\sim}{x}-\underset{\sim}{\xi})$ from source $(\underset{\sim}{x})$ to receive $(\underset{\sim}{\xi})$ points
r	distance $\lvert\underset{\sim}{r}\rvert$ between source and receiver points
r	polar spatial coordinate
R_1, R_2, R_3	roots of the Rayleigh cubic equation in P^2
s	source time
S_1	cracked part of $x_3 = 0$ plane
S_2	uncracked part of $x_3 = 0$ plane
S	crack plane (S_1+S_2) in $x_3 = 0$ plane
t	receiver time
t_p	discretised time
T	dimensionless ratio $\alpha t/r$
T_i	traction
$u_m(\underset{\sim}{x},t)$	m^{th} component of displacement at receiver point $\underset{\sim}{x}$ and time t off the fault plane
$u_n(\underset{\sim}{x},t)$	n^{th} component of displacement at receiver point $\underset{\sim}{x}$ and time t on the fault plane $x_3 = 0$
x_i	receiver (field) point in Cartesian coordinates
u_i, v_i	displacement fields
$\dot{u}_i, \dot{v}_i$	velocity fields
$\ddot{u}_i, \ddot{v}_i$	acceleration fields

v_r	rupture velocity on crack plane
V_e	effective region of integration
V	volume of integration
X, Y	dimensionless values.

LIST OF ABBREVIATIONS

BEM('s)	boundary element method(s)
BIEM('s)	boundary integral equation method(s)
BP	backward P (-wave cone)
BR	backward R (-wave cone)
equ.	equation
FEM('s)	finite element method(s)
FP	forward P (-wave cone)
P-wave	compressional wave
R-wave	Rayleigh wave
S-wave	shear wave

LIST OF FIGURES

CONTENTS

CHAPTER 1

INTRODUCTION

1.1 Problem Statement

Rockbursts and rockfalls are two of the main problems affecting the safety of workers and the productivity of gold mining operations, especially on the Witwatersrand where the gold mines are over 3.5 kilometres in depth. The threat of rockbursts is intensified as gold mines become deeper because rock pressure increases with depth.

Mining alters the stress distribution in rock, thereby causing stress concentrations and releasing previously "locked-in" tectonic stresses. These conditions can precipitate a seismic event or shear failure in the vicinity of the excavations resulting in a violent failure of rock around, and often into, the mining excavations.

Significant progress has been made in understanding the patterns of rock fractures and deformations, and in controlling the fractured rock by the design of efficient mine layouts and support systems, but the effects of rock pressure still require the most urgent attention.

The aim of this thesis is to provide the framework in which further studies relating to the nature of slip on a fault, the criteria for rupture of a weakened zone, stopping mechanisms, and the interpretation of seismic records can be undertaken. This will comprise two main parts. The first consists of a model for fracture propagation in an infinite medium assuming

that rupture occurs on a given plane. The crack either propagates in a controlled (prescribed) way or is allowed to choose its own rupture path according to some fracture criterion. The second part consists of a method of computing, for an arbitrary slip function, the motion of the medium at any point away from the fault. With these two parts linked, it will be possible to use the slip histories obtained from the numerical simulation of the source process to synthesise the seismic wave field with the objective of gaining further knowledge of the rupture histories of real seismic sources.

1.2 Solution Approach

A large proportion of the literature dealing with models for fracture and wave propagation in the earth makes use of boundary element methods (BEM's). BEM's are particularly suited to solving this type of problem (as opposed to finite element methods (FEM's) for a number of reasons, some of which are outlined here.

Firstly, there is a reduction in the dimensionality of the problem if a BEM is used, since only the fracture surface or the plane containing the fracture need be discretised. Thus the boundary integral equations governing the problem have the boundary values as the only unknowns. The solution at interior points need not, in general, be considered, although it usually can be evaluated at these points directly from the integral representation once the boundary integral equations have been solved.

Besides having to discretise the fracture surfaces, a FEM would also require the surrounding domain to be discretised by means of a suitably graded mesh, which would be terminated at a sufficient distance from the

fracture surface, either directly or by the use of infinite elements. Apart from the difficulty involved in producing this extra mesh area, there are not at present suitable infinite elements available for use in transient elastodynamic problems (see Zienkiewicz et al 1981)[1] . Spurious wave reflections arise if the mesh is not properly graded, and at the boundaries of a curtailed mesh, and affect the accuracy of the results.

BEM's which use a time-stepping scheme, do require large amounts of data storage since results at <u>all</u> previous times are required to obtain results at the current time. However, various symmetry properties and the causal properties of the time-dependent Green's tensors can be included in the coding to reduce the storage requirements. These need only be computed once and are then written away to file.

The above factors plus the favouring of BEM approaches in the literature dealing with transient elastodynamic fracture propagation schemes provided the motivation for the choice of method seen to be most effective in modelling the fault dislocation problem.

1.3 Outline of Contents

We start with a review of past work in the field of elastodynamic fracture propagation and ground motion simulation which is presented in chapter 2.

In chapter 3, the theory describing the dynamic fracture process on a fault surface is presented, starting with the general elastodynamic and Green's function equations. We then show how the representation theorem of Betti

---

1. RAJAPAKSE and KARASUDHI (1986) have at time of final editing, reported work on an elastodynamic infinite element.

leads to the integral equations defining the displacements on the fracture surface in terms of a convolution of the Green's functions and the stresses. The Green's functions due to a unit impulse on the surface of a half-space (Richards 1979) are also presented.

The numerical discretisation of the integral equations and the solution procedure for determining the unknown stresses ahead of the rupture front as well as the unknown displacements on the crack surface, is contained in chapter 4.

Chapter 5 deals with the theory describing the near- and far-field ground motion due to a dislocation source as presented by Maruyama (1963). We also describe the numerical integration and discretisation of Maruyama's formulation for the case of a general dislocation source function.

The computational aspects of the theory in chapters 4 and 5 are discussed in chapter 6.

The analytical solution to the problem of a self-similar shear crack (which provides us with a check on our numerical results) is presented in chapter 7, after the work of Kostrov (1964) and Dahlen (1974).

In chapter 8 we discuss the results, which are presented in graphical form in appendices F and G. Conclusions and recommendations are found in chapter 9.

CHAPTER 2

REVIEW OF PAST WORK

A review of the literature pertaining to fracture and wave propagation problems as related to the faulting process in the earth is divided into three sections. The first section deals with the various approaches that are used to solve general elastodynamic BEM problems. The second section is specialised to fracture propagation models and the third deals with models that simulate ground motions due to seismic events.

We note here that the fundamental solutions appearing in the various elastodynamic boundary element methods appear in a variety of forms. All the forms employ a unit impulse as the source function. Some are written in terms of Dirac delta functions (e.g. Manolis 1983) while others are written in terms of Heaviside step functions (e.g. Rice and Sadd 1984). The step function forms are merely the integrated equivalents of the Dirac delta function forms. The various approaches are given in texts such as Eringen and Suhubi (1975) or Morse and Feshbach (1953).

2.1 General Elastodynamic Boundary Element Methods

The need to obtain solution formulations for boundary and initial value problems has resulted in researchers formulating various problems in static and dynamic linear elasticity in terms of integral equations. These integral formulations have been in existence since the 19th century, the basis for them being the reciprocal work theorem of Betti (1872-73). Early development in this field came from Italian elasticians such as Somigliana.

The theory of linear elastostatics in conjunction with the theory of linear integral equations was presented by Fredholm (1905), and the solution of the scalar wave equation as a potential function was introduced by Poisson (1820).

Many of the boundary value problems in geophysics and engineering preclude the use of analytical solutions due to such influences as non-linearities and complicated boundary conditions, and it therefore becomes necessary to resort to numerical techniques. The development and application of these numerical methods, as well as the extension from statics to dynamics, is much more recent, due largely to the dependency on the development of computer technology. Classical work in steady-state elastodynamics was done by Kupradze (1963). Integral formulae for the displacements in transient elastodynamics were introduced by Doyle (1966), by integrating the Laplace-transformed equations of classical elastokinetics, using Somigliana field equations.

Despite the rapid development in boundary integral methods, there is currently relatively little work reported on elastodynamics when compared with papers dealing with static problems. Two of the original papers on the use of the boundary integral equation method (BIEM) in solving an elastodynamic problem were by Cruse and Rizzo (1968a,b) and Cruse (1968). A wave propagation problem in an elastic half-space was solved in the Laplace transform domain. Their formulation used fundamental solutions of the Laplace transformed equations of motion corresponding to dynamic concentrated forces in an infinite medium, and was based on the work of Sternberg and Eubanks (1955 and 1957) and Doyle (1966). A numerical

inversion algorithm due to Papoulis (1957) was used to obtain the time-domain solutions, but this was found to give reasonable results only for short times.

Manolis (1980) and Manolis and Beskos (1981) extended Cruse's work to investigate stress concentrations around arbitrarily-shaped cavities due to the scattering of elastic waves of a general transient nature. They formulated the problem using a Fourier transform with an inversion algorithm due to Durbin (1974), which although more time consuming than Papoulis', was considerably more accurate, even to late times.

The steady-state solution and the reconstitution of the transient response by the Fourier transform method was done by Niwa et al (1975 and 1976) in investigating the transient stresses produced around cylindrical cavities during the passage of travelling waves, under conditions of plane strain. A three-dimensional BEM was used.

Cole et al (1978) developed a general time-domain formulation that was used to find the solution of elastic wave scattering for a simple elastodynamic antiplane problem in an infinite space. The equations were discretised using piecewise linear time interpolation functions for displacements and piecewise constant time interpolation functions for tractions. (Linear interpolation was found to be unstable for tractions). Constant spatial interpolation functions were used. The time-stepping scheme could be made explicit or implicit depending on whether the shear wave travelled less or more than half the smallest element length in one time-step. It was stressed that the interpolation scheme must not transmit information non-causally and must accurately represent the short-scale dynamics of the domain. This was accomplished using a very localised interpolation scheme.

Mansur and Brebbia (1982 a,b) presented the numerical formulation of the BEM to solve two-dimensional transient problems governed by the scalar wave equation with a time-stepping scheme similar to Cole et al (1978). Mansur and Brebbia (1983) later extended their work for two- and three-dimensional problems.

A comparison of the three BEM approaches, i.e. Fourier transform, Laplace transform and time-domain, was undertaken and reported by Manolis (1983). He used the three approaches to study the problem of the scattering of a pressure wave pulse by a circular cylindrical cavity in a linear, elastic, homogeneous and isotropic medium. He found that the Laplace transform formulation was more economical than either the Fourier transform formulation or the time-domain approach by a factor of 1.7 and 5.0 respectively. However, the time-domain scheme was more useful because it gave a better picture for the very early times. He also noted that the time-domain solution algorithm became more involved at later time-steps since information from all the earlier time-steps was required. The time-domain scheme could also be extended to three-dimensional problems.

Nardini and Brebbia (1983) introduced a general BEM for the transient dynamic analysis of elastic solids, using a different time integration procedure from previous methods. This approach employed a class of coordinate functions for approximation of the inertial forces in the domain. However, this method was only applicable to finite domain problems due to the formation of the mass matrix in the solution.

Rice and Sadd (1984) used the scheme developed by Cole et al (1978) to model the propagation and scattering of SH waves in a half-space containing

a cavity. The method of images was used to construct the half-space Green's functions from the infinite-space functions that Cole et al (1978) had used. The advantage of this superposition technique was that the boundary of the free surface did not have to be discretised, thus simplifying the problem.

Antes (1985) presented an integral formulation of the elastodynamic equations, with arbitrary initial conditions, using constant spatial and linear time-dependent interpolation functions in the discretisation process. The boundary element equations were solved using a time-stepping scheme. The Green's functions were transformed through partial integrations into equations with kernels that were only logarithmically singular and could be integrated as Cauchy principal values. An example of the response of an elastic half-plane under a discontinuous boundary stress distribution was shown to compare favourably with results of Cruse and Rizzo (1968 a,b) and Mansur (1983). Antes' method allowed a time-step four times larger than Mansur's procedure without loss in accuracy.

Advances have also been made in developing hybrid FEM and BEM schemes. Kobayashi (1985) discussed a FEM-BIEM combination with a time-domain formulation. Kobayashi and Kishima (1985) presented a FEM-BIEM scheme using the Fourier transform method. They applied their model to the dynamic analysis of an inclined fault in a half-space. Goto, Matsumoto and Urayama (1985) also developed a FEM-BIEM with a Fourier transform scheme which they applied to cavity problems.

2.2 Fault Propagation Models

A number of theoretical studies on fault propagation has been presented in the last twenty-five years. Some of the more relevant papers are discussed

in this review.

There are a large number of papers dealing with two-dimensional faults that rupture and move as an infinite line. The problem of finding the time history of crack-tip location from the cohesive-force distribution on the crack plane was first studied by Kostrov (1966). He solved the dynamic problem of a semi-infinite, instantaneous, anti-plane (mode III) shear crack in an infinite medium by reducing the problem to a mixed boundary value problem in a half-space. He found closed form expressions for the displacements inside the crack and the stresses outside the crack, both on the plane of the crack. It was found that mode III cracks which propagated according to the fracture criterion that the rate of energy flux into the crack tip was constant (Griffith criterion), gradually accelerated from zero to the shear wave speed.

Kostrov's work was the basis of work by Burridge (1969), who used a numerical technique to study the problem of in-plane as well as anti-plane finite shear cracks, when the crack-tip moved at a fixed velocity.

Hamano (1974) is reported to have extended Burridge's analysis to the case of finite two-dimensional cracks in an infinite medium where the time history of crack-tip location need not be known apriori. He determined the rupture velocity from the strength distribution on the crack-plane, with a critical stress-jump fracture criterion.

Andrews (1976) used the finite difference technique with Griffith's fracture criterion to solve for the rupture propagation of a finite, two-dimensional shear crack in an infinite medium. He showed the maximum in-plane rupture velocity to be sub-Rayleigh or supershear, depending on the material strength of the fault plane.

Das and Aki (1977) presented a numerical technique to determine the displacement and stress fields due to the propagation of two-dimensional shear cracks in an infinite, homogeneous medium, which was linearly elastic off the crack plane. They used a representation theorem to find an integral equation for the displacements inside the crack. This integral equation was solved by the method proposed by Hamano (1974) for various initial and boundary conditions on the crack surface. The fracture criterion used was a critical stress jump across the tip of the crack, which was found to be the finite difference approximation to the initial stress intensity factor used in Irwin's fracture criterion (1958). The accuracy of the numerical method was verified by comparison with the analytical solution of Kostrov (1966) and the numerical solution of Madariaga (1976).

Besides fault propagation models that use an infinite line source, other authors assume a point source. Kostrov (1964) found an analytical solution to the problem of the slip and stress fields for a self-similar circular shear crack (see chapter 7) in an infinite, homogeneous, elastic medium. The crack initiated at a point and grew at a speed less than the shear-wave speed.

Burridge and Willis (1969) found a solution for an expanding self-similar elliptical shear crack.

Richards (1976) solved analytically the problem of a three-dimensional elliptical self-similar shear crack in an infinite medium, where the crack dimension grew linearly with time. Madariaga (1976) used a finite difference technique to calculate the slip motion for a circular shear crack that grew at a fixed velocity and stopped suddenly.

Archuleta and Frazier (1978) solved the three-dimensional problem for a semi-circular fault by means of the finite-element method and Madariaga (1979) solved the three-dimensional problem for a rectangular fault by a finite difference method.

Brune (1970) derived an earthquake model in which the time function was directly related to the effective stress available to accelerate the sides of the fault, rather than a time function of the dislocation. The model described near- and far-field displacement time functions and spectra, and included the effect of fractional stress drop.

All these methods had the limitation that the overall growth of faulting had to be specified, rather than becoming a part of the solution for spontaneous crack growth. Thus, for example, there had been no investigation to see if an initially circular crack retained this shape during crack growth.

A method to determine the displacement and stress on a crack plane for a three-dimensional shear crack of arbitrary shape propagating in an infinite homogeneous, linearly elastic medium was presented by Das (1980). She extended the work done by Hamano (1974) for two-dimensional problems to three-dimensions. The method was based on the representation theorem in which the displacement at any point on the crack plane is given as an integral over the whole crack plane of the product of the traction and a Green's function. The Green's function used was obtained as the time-derivative of the response of the surface of a half-space to a unit step input force on the surface. The accuracy of the method was checked against known solutions for two simple cases.

Day (1982) used a finite-difference method to study crack propagation in a three-dimensional continuum with uniform and non-uniform prestress conditions. He found that, for uniform prestress and low cohesion, rupture velocity was predicted to exceed the shear wave velocity in directions for which shear (mode II) crack motion dominated. A sub-shear rupture velocity was predicted for the direction of anti-plane (mode III) crack motion. The introduction of stress heterogeneities was sufficient to reduce average rupture velocities to less than the shear wave velocity, but local super-shear rupture velocities could still occur in regions of high prestress.

Andrews (1985) showed how the boundary integral method could be adapted to a slip-dependent friction law on a crack plane, using a two-dimensional plane-strain geometry. Previous boundary integral approaches had only been applied to a brittle crack model, in which there was an abrupt transition from no slip to sliding at a constant prescribed traction. (See Hamano 1974, Das and Aki 1977 and Das 1980). Andrews tested his method on a crack growing at a constant sub-Rayleigh rupture speed and the solution for traction and slip velocity agreed well with the analytical solution.

Recently, work has been done on heterogeneous dynamic faulting models. The faulting process depends on the "dynamic stress drop", defined as the initial stress minus the dynamic frictional stress needed for sliding. In a physical situation, both these quantities vary over the fault surface. Das (1985) reviewed two models currently used to describe the heterogeneous faulting process, namely, the "barrier" and "asperity" models. She showed some results for a three-dimensional shear crack problem.

2.3 Simulation of Ground Motion

Methods of determining the form of the ground motion due to seismic events have been in existence since the early 1960's. The basis for these methods is the elastic dislocation theory.

The concepts of dislocation theory were first used in metallurgy and crystal physics, and were applied to earthquake problems in the late 1950's and early 1960's. Steketee (1958 a,b) constructed the mathematical foundations for the study of a three-dimensional crack or fault, using the classic work of Volterra (1907) as a basis. He entitled his theory the "elasticity theory of dislocations" to distinguish it from crystal dislocation theory, which only dealt with discrete or static dislocations as opposed to Steketee's continuous dislocation theory.

Knopoff and Gilbert (1959, 1960) combined the dynamic dislocation theory with a Green's function integral representation to obtain the radiation pattern of the first motions (high frequency terms only) of a moving fault in an infinite homogeneous medium.

A formulation for the total radiation pattern due to general dynamic dislocations (high and low frequency terms) was obtained by Maruyama (1963). His formulation was derived from Betti's reciprocal theorem and a displacement relation from Love (1927). Maruyama's formulation showed that the displacement field produced by a dynamic dislocation was equivalent to that due to a distribution of combinations of pairs of mutually perpendicular dynamic forces ("double couples") in the absence of the dislocation surface.

The work of Knopoff and Gilbert (1960) was employed by Haskell (1964, 1969) to obtain a representation of the ground motion due to a dislocation faulting source in an infinite medium. Haskell's formulation was equivalent to that obtained by Maruyama. A simple ramp dislocation function was used to provide displacement, velocity and acceleration records of ground motion.

The ground motion near a seismic source for several dislocation models and different sources was examined by Anderson and Richards (1975). They found that different dislocation models of the rupture could give very similar displacements at stations located one fault length from the fault in an infinite, elastic, homogeneous space. In particular, models with fault motions and rupture velocity quite different from the Haskell ramp, could often have near field motions very similar to those from a ramp model. Models in which the rupture velocity and rise time were varied over certain ranges (up to a factor of 3 for rise time) also showed similar near field motions. They inferred that there was considerable ambiguity in interpreting near field displacement data in favour of a particular model of fault rupture.

Besides the above-mentioned approaches, there are further ways of modelling the strong motions due to seismic events. A discrete wave number representation method of Bouchon and Aki (1977) was generalised to three dimensions by Bouchon (1979 a,b) to model the elastic wave fields in an infinite layered medium. The method was developed to cope with the problem of seismic scattering at boundaries in the vicinity of the seismic source.

Empirical methods have also been used to estimate strong ground motions occurring during large seismic events. Irikura (1983) formulated a

semi-empirical synthesis method for estimating the mainshock motions, using the records of small events as the "fundamental solutions". The method was based on the Haskell-type source model and the similarity law of earthquakes (which defines scaling relations between small and large events, involving fault length, width and dislocation rise time - see Aki 1967, Kanamori and Anderson 1975, and Geller 1976). Synthesised results showed good agreement with observed seismograms for frequencies up to 5 Hz.

All the schemes appearing in the literature have been applied to problems, using a specific dislocation function (e.g. step or ramp function), even though the theory allows a general dislocation function to be used. We will numerically discretise the Maruyama formulation allowing an arbitrary dislocation function as the input data.

CHAPTER 3

THE GOVERNING ELASTODYNAMIC EQUATIONS

3.1 Introduction

The problem of the dislocation of a fault plane may be posed mathematically at various levels of complexity but still within the framework of a continuum model.

In reality, the fault occurs in an anisotropic, non-homogeneous inelastic particulate medium which is under some arbitrary state of stress. Within this continuum there exist planes of weakness on which fracture is initiated and subsequently propagated. Propagation of the rupture occurs when the stresses have increased past some critical value due to an accumulation of strains in the surrounding medium. This critical value, and therefore the criterion for rupture, is in general a complicated function of the stress state, the material constitutive behaviour and the temperature. In any given body of material, the zones of weakness are unpredictable.

This most general state of a continuum poses an impossible problem and certain simplifying assumptions must be made.

In reality, knowledge of the fault planes within certain regions of the earth's crust is reasonably advanced. Investigative work can be done to increase that knowledge around a given site. We can therefore assume that the location and orientation of the faulting surfaces are known. In the

present work the surfaces are also assumed to be planar to reduce computational requirements involved in transformations from local curvilinear coordinates to a global system.

A second simplification is achieved by employing an empirical type fracture criterion to determine when rupture of a particular portion of the crack tip will occur. This critical stress level fracture criterion allows the crack to choose its own shape as rupture proceeds and stresses are relieved in the medium.

Perhaps the most elementary model of the complex problem as described is obtained by prescribing the way in which the crack will rupture and the distribution of the stresses across this ruptured region. This is the starting point for most studies together with the assumption of an elastic homogeneous isotropic material off the dislocation surface. The propagation of the waves into the surrounding medium then becomes a well understood analytical problem, but one which needs to be implemented numerically. The slip history is determined from the knowledge of the shape of the ruptured region, the values of stress on that region and previously computed stresses outside this region. This procedure is detailed analytically and numerically in what follows.

3.2 Reciprocal Relations

Consider a linear elastic solid in equilibrium under the action of two sets of forces. The reciprocity theorem derived by Betti equates the work done by the first set of forces as it displaces through the deformations due to the second set with the work of the reverse situation. We use this theorem for the case of dynamic equilibrium to arrive at an integral equation for

the displacement field in a body due to surface tractions and body forces.

A continuum has volume V and surface S. Applying Newton's second law to the particles within the volume, we equate the rate of change of momentum to the forces acting, to obtain

$$\frac{\partial}{\partial t}\iiint_V \rho \frac{\partial \underset{\sim}{u}}{\partial t}\, dV = \iiint_V \underset{\sim}{f}\, dV + \iint_S \underset{\sim}{T}(\underset{\sim}{u},\underset{\sim}{n})\, dS \tag{3.1}$$

The tractions $\underset{\sim}{T}$ are related to the stresses in component form by

$$T_i = \tau_{ij}\, n_j \tag{3.2}$$

Substituting this into the above and applying the divergence theorem, we arrive at the stress form of the equations of motion

$$\rho \ddot{u}_i = f_i + \tau_{ij,j} \tag{3.3}$$

We can, however use the form of equation (3.1) and obtain a statement of Betti's theorem for the dynamic case:

$$\iiint_V (\underset{\sim}{f} - \rho\ddot{\underset{\sim}{u}}).\underset{\sim}{v}\, dV + \iint_S \underset{\sim}{T}(\underset{\sim}{u},\underset{\sim}{n}).\underset{\sim}{v}\, dS =$$

$$\iiint_V (\underset{\sim}{g} - \rho\ddot{\underset{\sim}{v}}).\underset{\sim}{u}\, dV + \iint_S \underset{\sim}{T}(\underset{\sim}{v},\underset{\sim}{n}).\underset{\sim}{u}\, dS\ , \tag{3.4}$$

where $\underset{\sim}{u} = \underset{\sim}{u}(\underset{\sim}{x},t)$ is a displacement field due to body forces $\underset{\sim}{f}$ and boundary conditions on S and initial conditions at time t = 0 ,

$\underset{\sim}{v} = \underset{\sim}{v}(\underset{\sim}{x},t)$ is another displacement field due to body forces $\underset{\sim}{g}$ and boundary conditions and initial conditions at time $t = 0$, which in general are different to those for $\underset{\sim}{u}$,

and $\underset{\sim}{T}(\underset{\sim}{u},\underset{\sim}{n})$, $\underset{\sim}{T}(\underset{\sim}{v},\underset{\sim}{n})$ are tractions corresponding to $\underset{\sim}{u},\underset{\sim}{v}$ respectively.

Note that Betti's theorem does not involve initial conditions for $\underset{\sim}{u}$ or $\underset{\sim}{v}$. It also remains true even if $\underset{\sim}{u}$, $\ddot{\underset{\sim}{u}}$, $\underset{\sim}{T}(\underset{\sim}{u},\underset{\sim}{n})$ and $\underset{\sim}{f}$ are evaluated at time t_1, and $\underset{\sim}{v}$, $\ddot{\underset{\sim}{v}}$, $\underset{\sim}{T}(\underset{\sim}{v},\underset{\sim}{n})$ and $\underset{\sim}{g}$ are evaluated at a different time t_2.

If we choose $t_1 = t$, $t_2 = s - t$, and integrate over the range 0 to s, then the acceleration terms in Betti's theorem become,

$$\int_0^s \rho \{ \ddot{\underset{\sim}{u}}(t).\underset{\sim}{v}(s-t) - \underset{\sim}{u}(t).\ddot{\underset{\sim}{v}}(s-t) \} dt =$$

$$\rho \int_0^s \frac{\partial}{\partial t} \{ \dot{\underset{\sim}{u}}(t).\underset{\sim}{v}(s-t) + \underset{\sim}{u}(t).\dot{\underset{\sim}{v}}(s-t) \} dt =$$

$$\rho \{ \dot{\underset{\sim}{u}}(s).\underset{\sim}{v}(0) - \dot{\underset{\sim}{u}}(0).\underset{\sim}{v}(s) + \underset{\sim}{u}(s).\dot{\underset{\sim}{v}}(0) - \underset{\sim}{u}(0).\dot{\underset{\sim}{v}}(s) \}$$

Thus the acceleration terms depend only on initial and final values.

If there is some time s_0 before which $\underset{\sim}{u}$ and $\underset{\sim}{v}$ are zero everywhere in V (and hence $\dot{\underset{\sim}{u}} = \dot{\underset{\sim}{v}} = \underset{\sim}{0}$ for $s \leq s_0$), then the convolution

$$\int_{-\infty}^{\infty} \rho \{ \ddot{\underset{\sim}{u}}(t).\underset{\sim}{v}(s-t) - \underset{\sim}{u}(t).\ddot{\underset{\sim}{v}}(s-t) \} dt = 0$$

Hence, we deduce, for displacement fields with a quiescent past, the following equation :

$$\int_{-\infty}^{\infty} dt \iiint_V \{ \underset{\sim}{u}(\underset{\sim}{x},t).\underset{\sim}{g}(\underset{\sim}{x},s-t) - \underset{\sim}{v}(\underset{\sim}{x},s-t).\underset{\sim}{f}(\underset{\sim}{x},t) \} \, dV =$$

$$\int_{-\infty}^{\infty} dt \iint_S \{ \underset{\sim}{v}(\underset{\sim}{x},s-t).\underset{\sim}{T}(\underset{\sim}{u}(\underset{\sim}{x},t),\underset{\sim}{n}) - \underset{\sim}{u}(\underset{\sim}{x},t).\underset{\sim}{T}(\underset{\sim}{v}(\underset{\sim}{x},s-t),\underset{\sim}{n}) \} \, dS \qquad (3.5)$$

3.3 Elastodynamic Green's Function

Given a unidirectional unit impulse, localised precisely in space and time, the displacement field from such a simple source is the elastodynamic Green's function.

If the unit impulse is applied at $\underset{\sim}{x} = \underset{\sim}{\xi}$ at time $t = s$ in the n-direction, then one denotes the i^{th} component of displacement at a general position $(\underset{\sim}{x},t)$ by $G_{in}(\underset{\sim}{x},t;\underset{\sim}{\xi},s)$. This Green's function is a second-order tensor (i.e. a linear vector function) and depends on both receiver and source coordinates, and satisfies the equation of motion equ. (3.3) with the body force taken as a unit impulse expressed in terms of Dirac delta functions. Equilibrium is written in terms of displacements as

$$\rho \frac{\partial^2 G_{in}}{\partial t^2} = \delta_{in}\, \delta(\underset{\sim}{x}-\underset{\sim}{\xi})\delta(t-s) + \frac{\partial}{\partial x_j}\left(c_{ijk\ell} \frac{\partial G_{kn}}{\partial x_\ell} \right) \quad . \qquad (3.6)$$

In applying equ. (3.6) we choose to use the initial conditions that $\underset{\sim}{G}$ and $\partial\underset{\sim}{G}/\partial t$ are zero for $t \leq s$, $\underset{\sim}{x} \neq \underset{\sim}{\xi}$.

To specify $\underset{\sim}{G}$ uniquely we must still state the boundary conditions on S.

3.3.1 Properties of Green's Function

If the boundary conditions are time-dependent, i.e. boundary S is always rigid, then the time origin can be shifted at will, and one can see from equ. (3.6) that $\underset{\sim}{G}$ depends on t and s only via (t-s). Hence,

$$\underset{\sim}{G}(\underset{\sim}{x},t;\underset{\sim}{\xi},s) = \underset{\sim}{G}(\underset{\sim}{x},t-s;\underset{\sim}{\xi},0) = \underset{\sim}{G}(\underset{\sim}{x},-s;\underset{\sim}{\xi},-t) \quad ,$$

which is a reciprocal relation for source (s) and receiver (t) times.

If $\underset{\sim}{G}$ satisfies homogeneous boundary conditions, then equ. (3.5) can be used to obtain a reciprocal relation for source and receiver positions.

Take $\underset{\sim}{f}$ to be a unit impulse in the m-direction, at $\underset{\sim}{x} = \underset{\sim}{\xi}_1$ and at time $t = s_1$, and $\underset{\sim}{g}$ to be a unit impulse in the n-direction at $\underset{\sim}{x} = \underset{\sim}{\xi}_2$ and at time $t = -s_2$.

Then, $u_i = G_{im}(\underset{\sim}{x},t;\underset{\sim}{\xi}_1,s_1)$ and

$$v_i = G_{in}(\underset{\sim}{x},t;\underset{\sim}{\xi}_2,-s_2) \qquad (3.7)$$

Substituting equ. (3.7) into (3.5) directly yields :

$$G_{nm}(\underset{\sim}{\xi}_2,s + s_2;\underset{\sim}{\xi}_1,s_1) = G_{mn}(\underset{\sim}{\xi}_1,s - s_1;\underset{\sim}{\xi}_2,-s_2)$$

Choosing $s_1 = s_2 = 0$ yields :

$$G_{nm}(\underset{\sim}{\xi}_2,s;\underset{\sim}{\xi}_1,0) = G_{mn}(\underset{\sim}{\xi}_1,s;\underset{\sim}{\xi}_2,0) \qquad (3.8)$$

Equ. (3.8) is a purely spatial reciprocal relation.

Choosing s = 0 in equ. (3.7) yields :

$$G_{nm}(\underset{\sim}{\xi}_2,s_2;\underset{\sim}{\xi}_1,s_1) = G_{mn}(\underset{\sim}{\xi}_1,-s_1;\underset{\sim}{\xi}_2,-s_2) \quad . \tag{3.9}$$

Equ. (3.9) is a space-time reciprocal relation.

We will use these properties in the numerical discretisation of the integral equations to considerably reduce the storage requirements of the computer program.

3.4 Representation Theorem

The reciprocity theorem of Betti (3.4), which was specialised for quiescent apriori conditions to equ. (3.5), is used together with a Green's function for the one displacement term to obtain an integral equation which is a representation of the motion at a general point in the medium in terms of information on the boundaries and body forces (if they exist). This so named Representation Theorem is largely due to work by Knopoff and de Hoop in the late 1950's.

We set $g_i(\underset{\sim}{x},t) = \delta_{in}\,\delta(\underset{\sim}{x}-\underset{\sim}{\xi})\delta(t)$, and

$$v_i(\underset{\sim}{x},t) = G_{in}\,(\underset{\sim}{x},t;\underset{\sim}{\xi},0) \quad .$$

Then equ. (3.5) becomes

$$u_n(\underset{\sim}{\xi},s) = \int_{-\infty}^{\infty} dt \iiint_V f_i(\underset{\sim}{x},t)\, G_{in}(\underset{\sim}{x},s-t;\underset{\sim}{\xi},0)\, dV +$$

$$\int_{-\infty}^{\infty} dt \iint_S \{G_{in}(\underset{\sim}{x},s-t;\underset{\sim}{\xi},0)\, T_i(\underset{\sim}{u}(\underset{\sim}{x},t),\underset{\sim}{n}) -$$

$$u_i(\underset{\sim}{x},t)\, c_{ijk\ell}\, n_j\, G_{kn,\ell}(\underset{\sim}{x},s-t;\underset{\sim}{\xi},0)\}\, dS \quad .$$

Interchanging $\underset{\sim}{x}$ and $\underset{\sim}{\xi}$, and t and s one obtains

$$u_n(\underset{\sim}{x},t) = \int_{-\infty}^{\infty} ds \iiint_V f_i(\underset{\sim}{\xi},s)\, G_{in}(\underset{\sim}{\xi},t-s;\underset{\sim}{x},0)\, dV(\underset{\sim}{\xi}) +$$

$$\int_{-\infty}^{\infty} ds \iint_S \{G_{in}(\underset{\sim}{\xi},t-s;\underset{\sim}{x},0)\, T_i(\underset{\sim}{u}(\underset{\sim}{\xi},s),\underset{\sim}{n}) -$$

$$u_i(\underset{\sim}{\xi},s)\, c_{ijk\ell}(\underset{\sim}{\xi})\, n_j\, G_{kn,\ell}(\underset{\sim}{\xi},t-s;\underset{\sim}{x},0)\}\, dS(\underset{\sim}{\xi}) \qquad (3.10)$$

Equ. (3.10) is a representation theorem for the displacement $\underset{\sim}{u}$ at a particular point $\underset{\sim}{x}$ at time t, due to contributions from a force $\underset{\sim}{f}$ throughout V, and due to the traction $\underset{\sim}{T}(\underset{\sim}{u},\underset{\sim}{n})$ and the displacement $\underset{\sim}{u}$ itself on S.

If S is a free boundary (e.g. the surface of a half-space), then the traction given by $c_{ijk\ell}\, n_j\, \partial\, G^{free}_{kn}(\underset{\sim}{\xi},t-s;\underset{\sim}{x},0)/\partial\xi_\ell$ is zero for $\underset{\sim}{\xi}$ in S and

$$u_n(\underset{\sim}{x},t) = \int_{-\infty}^{\infty} ds \iiint_V f_i(\underset{\sim}{\xi},s)\, G_{ni}^{free}(\underset{\sim}{x},t-s;\underset{\sim}{\xi},0)\, dV(\underset{\sim}{\xi}) +$$

$$\int_{-\infty}^{\infty} ds \iint_S G_{ni}^{free}(\underset{\sim}{x},t-s;\underset{\sim}{\xi},0)\, T_i(\underset{\sim}{u}(\underset{\sim}{\xi},s),\underset{\sim}{n})\, dS(\underset{\sim}{\xi}) \qquad (3.11)$$

If the body forces are zero, then we get

$$u_n(\underset{\sim}{x},t) = \int_{-\infty}^{\infty} ds \iint_S G_{ni}^{free}(\underset{\sim}{x},t-s;\underset{\sim}{\xi},0)\, T_i(\underset{\sim}{u}(\underset{\sim}{\xi},s),\underset{\sim}{n})\, dS(\underset{\sim}{\xi}) \qquad (3.12)$$

Equ. (3.12) is an integral equation defining displacements in terms of a convolution of tractions and Green's functions over the free boundary S . We will use a slightly different version of this equation to solve our fracture propagation problem.

3.5 The Boundary Value Problem

The fault is modelled as a propagating shear crack in an infinite, isotropic, elastic solid medium. The crack surface will be confined to the $x_3 = 0$ plane (see figure 1) merely by reorienting the global coordinates.

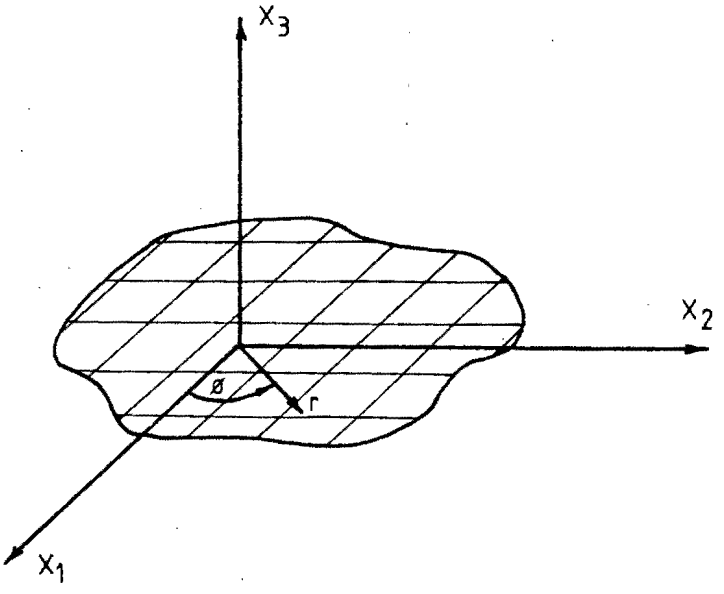

Figure 1 : Schematic representation of fault surface $x_3 = 0$

Initially, the domain is under a state of uniform stress given by normal stress σ^0_{33} and shear stress σ^0_{13} . The σ^0_{23} shear stress component will be taken as zero by assuming that the x_1-direction is the direction of maximum initial shear. The normal stress σ^0_{33} will remain constant during the fracture process (see Richards 1976) as long as the fracture surface is confined to the plane $x_3 = 0$. The other stress components σ^0_{11}, σ^0_{12} and σ^0_{22} are assumed to be zero (or constant) and have no effect on the shearing process.

The time origin $t = 0$ will be taken as the time when the fracture process starts. The fracture can be assumed to start at a particular point $(x_1 = x_2 = 0)$, or as an instantaneous circular fracture zone from which rupture proceeds. It is also possible to assume that rupture initiates from a line source or linear collection of point sources. However, this would require prohibitively large amounts of computer storage. The crack tip is generally assumed to propagate at a fixed rupture velocity or according to

a fracture criterion. We will present the former in this work, which together with preliminary results of a fracture criterion model are included in the appendices to demonstrate the adaptability of the formulation and coding for future studies.

Let the incremental stresses due to the displacements $\underset{\sim}{u}$ occurring on the fracture surface be τ_{ij} , so that $\sigma_{ij} = \sigma^{o}_{ij} + \tau_{ij}$. Thus τ_{ij} is the stress change due to the motion on the fault surface. The problem will be solved for τ_{ij} .

Once the rupture front passes a particular point, the residual stress on the fractured surface is simply the dynamic frictional stress $\sigma_d = \mu_d \sigma^{o}_{33}$, where μ_d is the dynamic coefficient of friction. Thus, the dynamic stress drop is the initial stress minus the dynamic frictional stress.

3.6 Determination of Boundary Conditions

For the case of a shearing displacement discontinuity it is not difficult to see that the problem is symmetric about the plane of the crack. Das (1980) notes that the following conditions hold across the shear fracture surface $x_3 = 0$:

τ_{23}, τ_{13}, u_3 are even, e.g., $u_3(x_1,x_2,x_3) = u_3(x_1,x_2,-x_3)$

τ_{33}, u_1 , u_2 are odd, e.g., $u_1(x_1,x_2,x_3) = -u_1(x_1,x_2,-x_3)$

Due to these symmetry properties, we need only consider a half-space to model the fracture propagation. The $x_3 = 0$ plane will be the boundary of this infinite half-space.

Assume that the cracked section of the $x_3 = 0$ plane is S_1 , and the uncracked part is S_2 . The incremental stress τ_{33} is zero everywhere along $x_3 = 0$ since τ_{33} is odd and continuous across $x_3 = 0$. The incremental stresses τ_{13}, τ_{23} are continuous across $x_3 = 0$, and are known in S_1 and unknown in S_2 . The displacements u_1, u_2, u_3 are unknown in S_1 . In S_2 , u_1 and u_2 are zero since they are odd and continuous on this part of the surface $x_3 = 0$. The displacement u_3 is unknown in S_2 .

Thus, we can summarise the mixed boundary value problem as follows :

In S_1 : $\tau_{23} = 0$, $\tau_{13} = \sigma_d - \sigma^0_{13} = -\tau_e$

$\tau_{33} = 0$

u_1, u_2, u_3 are unknown

where τ_e = dynamic stress drop or effective stress

In S_2 : τ_{13}, τ_{23}, u_3 are unknown

$u_1 = 0$, $u_2 = 0$, $\tau_{33} = 0$.

3.7 The Integral Equations

Equations (3.12) and (3.2) can be combined to give

$$u_n(\underset{\sim}{x},t) = \int_{-\infty}^{\infty} ds \iint_S G^{free}_{ni}(\underset{\sim}{x},t-s;\underset{\sim}{\xi},0)\ \tau_{ij}(\underset{\sim}{u}(\underset{\sim}{\xi},s))n_j\ dS(\underset{\sim}{\xi}) \qquad (3.13)$$

where S is the infinite plane $x_3 = 0$ containing the crack.

Integral equ. (3.13) defines the displacement in the n^{th} direction at point $(x_1,x_2,0)$ at time t, in terms of a convolution of the displacements $G^{free}_{ni}(\ .\ )$ due to a unit impulse acting in the i^{th} direction at $(\xi_1,\xi_2,0)$ at time s and the incremental stresses $\tau_{ij}(\ .\ )$ on the crack plane at $(\xi_1,\xi_2,0)$ at time s. The region of integration S is the crack plane.

Recalling the spatial and time translational properties of the Green's functions, we can see that the dependence of the Green's functions on $\underset{\sim}{x}$, t, $\underset{\sim}{\xi}$ and s is only via $(x_1-\xi_1),(x_2-\xi_2),(t-s)$ since $x_3 = \xi_3 = 0$, and thus we may write

$$G_{ni}^{free}(\underset{\sim}{x},t-s;\underset{\sim}{\xi},0) = g_{ni}(x_1-\xi_1,x_2-\xi_2,0,t-s;0,0,0,0) = g_{ni}(.) \qquad (3.14)$$

We can now write the three components of displacement on the surface S, in integral form as

$$u_1(x_1,x_2,0,t) = \int_{-\infty}^{\infty} ds \iint_{-\infty}^{\infty} \Big[g_{11}(.)\tau_{13}(\xi_1,\xi_2,0,s) + g_{12}(.)\tau_{23}(\xi_1,\xi_2,0,s) + g_{13}(.)\tau_{33}(\xi_1,\xi_2,0,s) \Big] d\underset{\sim}{\xi}$$

$$u_2(x_1,x_2,0,t) = \int_{-\infty}^{\infty} ds \iint_{-\infty}^{\infty} \Big[g_{21}(.)\tau_{13}(\xi_1,\xi_2,0,s) + g_{22}(.)\tau_{23}(\xi_1,\xi_1,0,s) + g_{23}(.)\tau_{33}(\xi_1,\xi_2,0,s) \Big] d\underset{\sim}{\xi}$$

$$u_3(x_1,x_2,0,t) = \int_{-\infty}^{\infty} ds \iint_{-\infty}^{\infty} \Big[g_{31}(.)\tau_{13}(\xi_1,\xi_2,0,s) + g_{32}(.)\tau_{23}(\xi_1,\xi_2,0,s) + g_{33}(.)\tau_{33}(\xi_1,\xi_2,0,s) \Big] d\underset{\sim}{\xi} \qquad (3.15)$$

Note that $n_1 = n_2 = 0$, $n_3 = 1$ since the crack plane is confined to $x_3 = 0$. The terms $g_{13}(.)$, $g_{23}(.)$, $g_{33}(.)$ apply only to tension cracks, and will thus be dropped in this formulation. Also $\tau_{33} = 0$ for shear cracks, since planar shearing cannot change the normal stresses on the fracture plane $x_3 = 0$.

The region of integration in equ. (3.15) is given by the causality condition defining the region over which the Green's functions are non-zero as

$$x_1^2 + x_2^2 \leq \alpha^2 t^2 \tag{3.16}$$

Equ. (3.16) defines a conical region (see figure 2) over which integration is carried out. Note that the apex of this "forward" cone is at the origin if rupture starts at the point (0,0,0,0). The cone defines all the (receiver) points $(x_1,x_2,0,t)$ which may experience wave effects at any particular time due to a rupture originating at the cone apex. The region outside the cone does not experience any disturbance, since we are assuming a rupture velocity less than the compressional wave speed of the medium.

A further two "backward" cones define all the (source) points $(\xi_1,\xi_2,0,s)$ which contribute to the wave motion at a particular receiver point $(x_1,x_2,0,t)$. These equations are given by

$$\sqrt{(x_1-\xi_1)^2 + (x_2-\xi_2)^2} \leq \alpha(t-s) \quad , \quad t \geq s \geq 0 \quad . \tag{3.17}$$

$$\sqrt{(x_1-\xi_1)^2 + (x_2-\xi_2)^2} \geq \gamma(t-s) \quad , \quad t \geq s \geq 0 \quad . \tag{3.18}$$

It can be seen from figure 2 that any point outside the compressional (BP) wave "backward" cone or inside the Rayleigh (BR) wave "backward" cone does <u>not</u> contribute to the motion felt at the relevant receiver or field point.

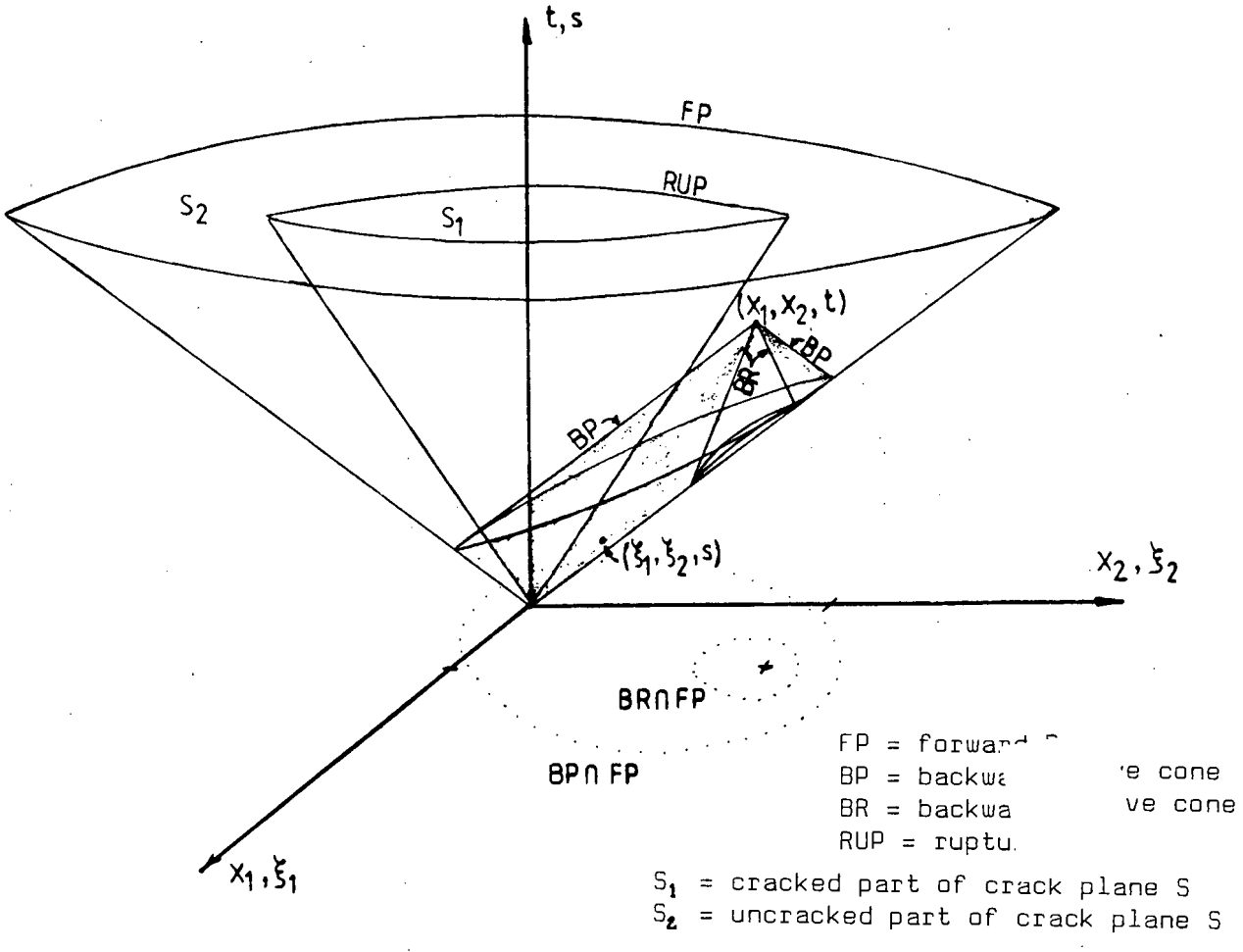

Figure 2 : Region of integration in (x_1,x_2,t) space, shown shaded

If rupture does not originate at the origin as a point source, but rather as an instantaneous circular shear crack of some desired radius r_{min}, then the forward cone in figure 2 has an initial radius at time t = 0, corresponding to the desired radius (see figure 3). This option is desirable in view of the fact that there is a minimum crack radius necessary for rupture propagation to occur, given a particular yield strength. (See Griffith 1921; Andrews 1976). Note that a point source, as in figure 2, does not prevent one from carrying out the integration process. A minimum crack radius is merely a physical condition and thus more realistic.

It is also possible to physically confine the fracture zone to some pre-defined maximum radius r_{max} . This ensures that the slip time-history reaches a saturation level, and does not escalate indefinitely (see figure 3).

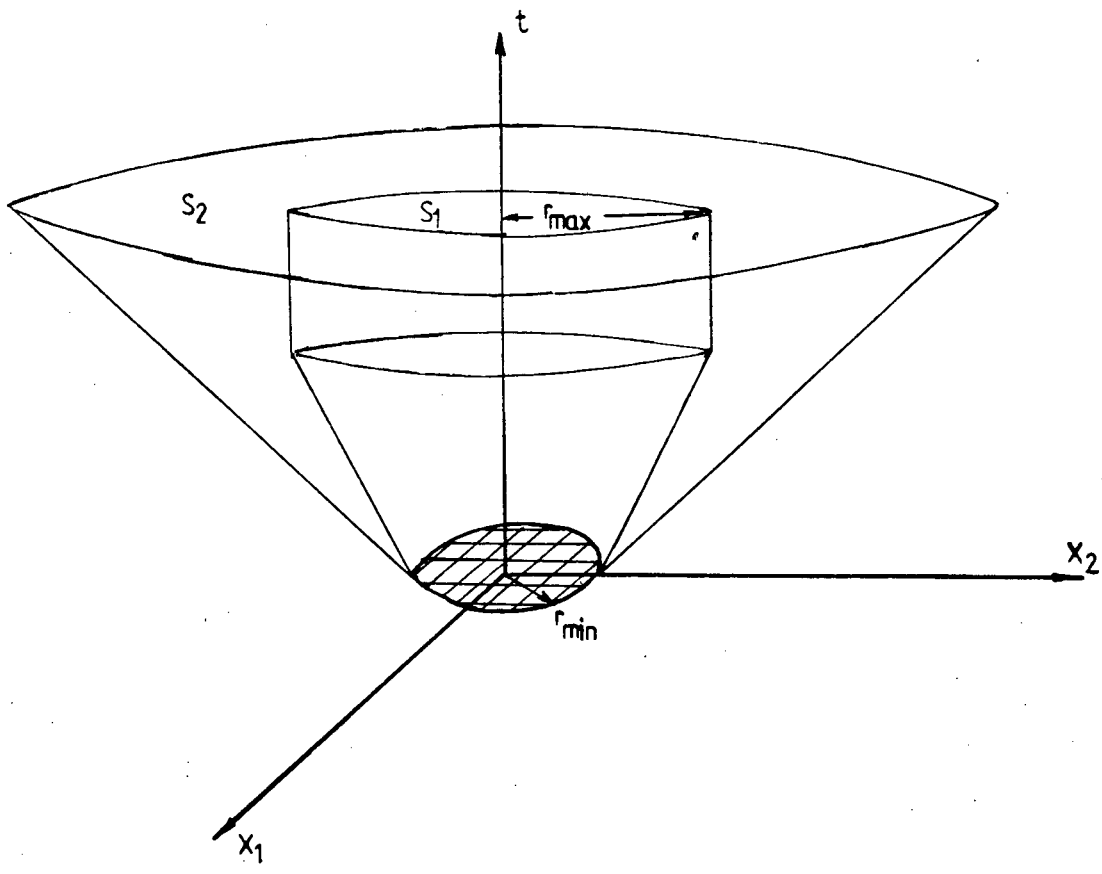

S_1 = cracked part of crack plane S
S_2 = uncracked part of crack plane S

Figure 3 : Forward and rupture cones when minimum and maximum crack radii r_{min} and r_{max} respectively, occur.

The fact that the three-dimensional Green's tensors are quiescent after the passage of the Rayleigh wave, in the infinite half-space, greatly reduces the amount of storage required when computing the Green's functions. (In the two-dimensional case there is no quiescence after the passage of the slowest wave).

To calculate the unknown displacements inside the crack, it will be necessary to solve the three integral equations (3.15) under the boundary conditions mentioned earlier. The region of integration includes the uncracked part S_2 of the fracture plane, but within the causality cone as defined in equ. (3.16), where the stresses τ_{13} and τ_{23} are unknown.

Thus, one must first determine these stresses before calculating the displacements. This will be possible provided the rupture velocity is known apriori, or provided a suitable fracture criterion is implemented.

3.8 The Fundamental Solution

The choice of Green's function for use in equ.(3.15) is made such that the boundary conditions of the problem are satisfied and the receiver and source points are both on the surface of the half-space. Richards (1979) analytically solved Lamb's problem[1] to obtain closed form solutions for the motions of the free surface due to a force applied as a step in time at a point on the free surface. Let these fundamental solutions be called g^H_{11}, g^H_{12}, and g^H_{22}. Then, in order to obtain the Green's function (i.e. the

1. LAMB (1904) studied the displacement set up by forces applied at a point along a line on the free surface of a half-space.

solution due to an impulse rather than a unit step) required in equ. (3.15), one simply needs to find the time-derivatives of g^H_{11} , g^H_{12} , and g^H_{22}. Thus, for example

$$g_{12} = \frac{dg^H_{12}}{dt} \text{ , etc. (see Das 1980).}$$

The Green's functions, as given by Richards (1979), are written in terms of dimensionless functions $I_1(T)$ and $I_2(T)$ as :

$$g^H_{11} = \left[I_1(T)\cos^2\phi - I_2(T)\sin^2\phi\right]/(\mu\pi r) \quad ,$$

$$g^H_{12} = g^H_{21} = \left[I_1(T) + I_2(T)\right]\cos\phi\ \sin\phi/(\mu\pi r) \quad ,$$

$$g^H_{22} = \left[I_1(T)\sin^2\phi - I_2(T)\cos^2\phi\right]/(\mu\pi r) \quad , \qquad (3.19)$$

where $x_1 = r\cos\phi$,

$x_2 = r\sin\phi$, (3.20)

and $T = \frac{\alpha t}{r}$. (3.21)

The dimensionless functions $I_1(T)$ and $I_2(T)$ depend on the compressional (P), shear (S) and Rayleigh (R) wave speeds, and are given below:

For times prior to, and including, the P-wave arrival, $T \leq 1$:

$$I_1(T) = I_2(T) = 0 \quad . \qquad (3.22)$$

For times between the P- and S-wave arrivals, $1 < T < \frac{\alpha}{\beta}$, there are two cases to consider, depending on whether Poisson's ratio is less or more than a critical value:

For a value of Poisson's ratio $\nu < 0.263$,

$$I_1(T) = T^2[c_1(T^2-R_1)^{-1/2} - c_2(T^2-R_2)^{-1/2} - c_3(R_3-T^2)^{-1/2}]$$

$$I_2(T) = -c_4 + c_1(T^2-R_1)^{1/2} - c_2(T^2-R_2)^{1/2} + c_3(R_3-T^2)^{1/2} \quad , \qquad (3.23)$$

where constants c_1 , c_2 , c_3 , c_4 are given in Appendix A , and constants R_1 , R_2 , R_3 are given in Appendix B.

If $\nu \geq 0.263$, then one needs to define a complex square root, since R_2 is complex, given by

$$CROOT = [(1-R_2)(T^2-R_2)]^{1/2} \quad , \qquad (3.24)$$

where the sign choice is made such that the complex number CNUM has magnitude less than unity :

$$|CNUM| = |1 + 2(1-R_2-CROOT)/(T^2-1)| < 1 \qquad (3.25)$$

Then $I_1(T) = -T^2[\text{Real}\{C_1/CROOT\} + c_3(R_3-T^2)^{-1/2}]$

$$I_2(T) = -c_4 - \text{Real}\{C_2 \times CROOT\} + c_3(R_3-T^2)^{1/2} \quad , \qquad (3.26)$$

where C_1 , C_2 are given in Appendix A.

For times between the S- and R-wave arrivals, $\frac{\alpha}{\beta} \leq T < \frac{\alpha}{\gamma}$:

$$I_1(T) = 0.5 - 2c_3T^2(R_3-T^2)^{-1/2}$$

$$I_2(T) = -2c_4 + 2c_3(R_3-T^2)^{1/2} \quad . \qquad (3.27)$$

For times after the Rayleigh wave has passed, $\frac{\alpha}{\gamma} \leq T$:

$$I_1(T) = 0.5$$

$$I_2(T) = -2c_4 \quad . \tag{3.28}$$

Note, from equ.(3.19), that the Green's functions g_{11} and g_{22} are simply 90° rotations of each other so that we only have to determine g_{11} and g_{12}. Also, g_{11} is symmetric about the x_1 and x_2 axes, and thus only needs to be calculated in one quadrant. Also, g_{12} has an 8-fold symmetry in terms of magnitude, and thus must only be calculated in one half of one quadrant. A sign difference occurs between the "even" and "odd" quadrants, i.e. "even" if x_1 and x_2 are both positive or negative, and "odd" if not.

The Green's functions with impulsive source are zero once the Rayleigh wave has passed, resulting in a very significant reduction in computer storage.

Figure 4 shows the dimensionless functions $I_1(T)$ and $I_2(T)$ as found by Richards (1979) as well as their time derivatives, for the case $\alpha^2 = 3\beta^2$.

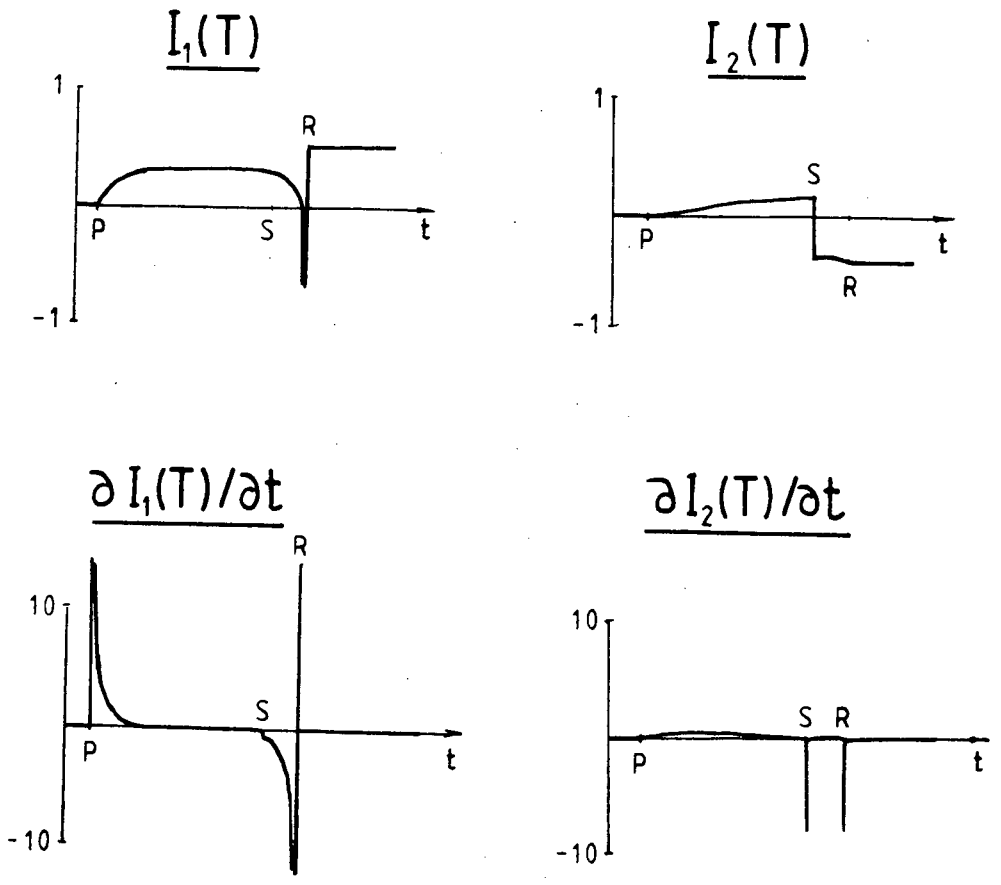

Figure 4 : Dimensionless functions $I_1(T)$, $I_2(T)$, $\partial I_1(T)/\partial t$ and $\partial I_2(T)/\partial t$ for the case $\alpha^2 = 3\beta^2$

Notice that $\partial I_1(T)/\partial t$ is singular at the P- and R-wave arrival points. $\partial I_2(T)/\partial t$ is singular at the S- and R-wave arrival points. Function $I_1(T)$ is singular at the R-wave arrival point. In the numerical discretisation scheme, the time-derivatives of $I_1(T)$ and $I_2(T)$ will be found numerically using the less singular functions $I_1(T)$ and $I_2(T)$.

CHAPTER 4

NUMERICAL DISCRETISATION

4.1 Integral Discretisation

Simplifying equ.(3.15) for shear cracks only ($\tau_{33} = 0$), one obtains

$$u_p(x_1,x_2,o,t) = \iiint_V \{g_{p1}(.)\tau_{13}(\xi_1,\xi_2,0,s) + g_{p2}(.)\tau_{23}(\xi_1,\xi_2,0,s)\}d\xi_1\, d\xi_2\, ds \qquad (4.1)$$

where V = space-time integration "volume" (ξ_1,ξ_2,s)

p = 1 or 2 .

To solve equ.(4.1) numerically, one must divide volume (x_1,x_2,t) into volume elements, each of size $\Delta x_1\Delta x_2\Delta t$. We will assume $\Delta x_1=\Delta x_2=\Delta x$ so as to take full advantage of the various symmetry properties in the Green's functions. The node point for each elemental volume is taken as the centre of the element.

Thus define the node points by $x_{1\ell} = \ell\Delta x$, $x_{2m} = m\Delta x$, $t_n = n\Delta t$, where ℓ,m = 0, $\pm$ 1, $\pm$ 2, $\pm$ 3, ... and n = 0, 1, 2, 3, ... Subscripts ℓ, m, n refer to source points and i, j, k refer to receiver or field points.

Discretising the integral equ. (4.1) gives

$$u_p(x_{1i},x_{2j},0,t_k) =$$

$$\sum_{\ell}\sum_{m}\sum_{n} \int_{t_n-\frac{\Delta t}{2}}^{t_n+\frac{\Delta t}{2}} \int_{\xi_m-\frac{\Delta x}{2}}^{\xi_m+\frac{\Delta x}{2}} \int_{\xi_\ell-\frac{\Delta x}{2}}^{\xi_\ell+\frac{\Delta x}{2}} \left[\begin{matrix} g_{p1}(.)\tau_{13}(\xi_{1\ell},\xi_{2m},0,s_n) \\ +g_{p2}(.)\tau_{23}(\xi_{1\ell},\xi_{2m},0,s_n) \end{matrix} \right] d\underset{\sim}{\xi} ds \quad , \quad (4.2)$$

where $g_{p1}(.) = g_{p1}(x_{1i}-\xi_{1\ell},x_{2j}-\xi_{2m},0,t_k-s_n)$

$$g_{p2}(.) = g_{p2}(x_{1i}-\xi_{1\ell},x_{2j}-\xi_{2m},0,t_k-s_n)$$

The stresses will be assumed constant over each spatial and temporal element and can thus be removed from within the integrals in equ. (4.2) to yield

$$u_p(x_{1i},x_{2j},0,t_k) =$$

$$\sum_{\ell}\sum_{m}\sum_{n} \left[\begin{matrix} \tau_{13}\left(\xi_{1\ell},\xi_{2m},0,s_n\right) \iiint_{V_e} g_{p1}\left(x_{1i}-\xi_{1\ell},x_{2j}-\xi_{2m},0,t_k-s_n\right) d\underset{\sim}{\xi}\, ds \\ + \tau_{23}\left(\xi_{1\ell}\xi_{2m},0,s_n\right) \iiint_{V_e} g_{p2}\left(x_{1i}-\xi_{1\ell},x_{2j}-\xi_{2m},0,t_k-s_n\right) d\underset{\sim}{\xi}\, ds \end{matrix} \right] \quad (4.3)$$

where V_e = elemental volume.

Interchanging the order of integration (allowed since integration limits over $\underset{\sim}{\xi}$ are not functions of time), and introducing the step function form of the Green's functions, gives

$$u_p(x_{1i},x_{2j},0,t_k) =$$

$$\sum_{\ell}\sum_{m}\sum_{n}\left[\begin{array}{l} \tau_{13}\left(\xi_{1\ell},\xi_{2m},0,s_n\right)\iint\limits_{\underset{\sim}{\xi}}\left[\begin{array}{l} g^H_{p1}\left(x_{1i}-\xi_{1\ell},x_{2j}-\xi_{2m},0,t_k-t_n-\frac{\Delta t}{2}\right)- \\ g^H_{p1}\left(x_{1i}-\xi_{1\ell},x_{2j}-\xi_{2m},0,t_k-t_n+\frac{\Delta t}{2}\right)\end{array}\right]d\underset{\sim}{\xi} \\ + \tau_{23}\left(\xi_{1\ell},\xi_{2m},0,s_n\right)\iint\limits_{\underset{\sim}{\xi}}\left[\begin{array}{l} g^H_{p2}\left(x_{1i}-\xi_{1\ell},x_{2j}-\xi_{2m},0,t_k-t_n-\frac{\Delta t}{2}\right)- \\ g^H_{p2}\left(x_{1i}-\xi_{1\ell},x_{2j}-\xi_{2m},0,t_k-t_n+\frac{\Delta t}{2}\right)\end{array}\right]d\underset{\sim}{\xi}\end{array}\right] \qquad (4.4)$$

The discretised integral equs. (4.4) are identical to those obtained by Das (1980) in her discretisation scheme, involving averaging the Green's functions over each volume element.

If the integrals in equ. (4.4) are transformed to polar coordinates (r,ϕ), then it is possible to do the integration over r analytically. Details of this are given in appendices C and D. The integration over ϕ must be done numerically, using a suitable integration scheme.

4.2 Numerical Solution Procedure

The first step in solving for the displacements on the fracture surface S_1, is to calculate the unknown stresses on the unfractured part S_2 of the fracture plane, using the boundary condition that $u_1 = u_2 = 0$ in S_2 .

From the discretised integral equs. (4.3), one may write for region S_2 ,

$$0 = \sum_{\ell}\sum_{m}\sum_{n}\left\{\tau_{13}(.)\iiint_{V_e} g_{11}(.)d\underset{\sim}{\xi}\ ds + \tau_{23}(.)\iiint_{V_e} g_{12}(.)d\underset{\sim}{\xi}\ ds\right\}$$

$$0 = \sum_{\ell}\sum_{m}\sum_{n}\left\{\tau_{13}(.)\iiint_{V_e} g_{21}(.)d\underset{\sim}{\xi}\ ds + \tau_{23}(.)\iiint_{V_e} g_{22}(.)d\underset{\sim}{\xi}\ ds\right\} \quad (4.5)$$

Taking the term, for which $x_{1i} = \xi_{1\ell}$, $x_{2j} = \xi_{2m}$, $t_k = t_n$, across to the left hand side, gives

$$F_{11}\tau_{13}(.)+F_{12}\tau_{23}(.) = -\sum_{\ell}\sum_{m}\sum_{n}\left\{\tau_{13}(.)\iiint_{V_e} g_{11}(.)d\underset{\sim}{\xi}\ ds + \tau_{23}(.)\iiint_{V_e} g_{12}(.)d\underset{\sim}{\xi}\ ds\right\}$$

$$= L$$

$$F_{21}\tau_{13}(.)+F_{22}\tau_{23}(.) = -\sum_{\ell}\sum_{m}\sum_{n}\left\{\tau_{13}(.)\iiint_{V_e} g_{21}(.)d\underset{\sim}{\xi}\ ds + \tau_{23}(.)\iiint_{V_e} g_{22}(.)d\underset{\sim}{\xi}\ ds\right\}$$

$$= M \quad ,$$

(4.6)

where F_{ij} denotes the singular Green's function g_{ij} integrated over its volume element. The summation terms L and M extend over every point of the integration cone except the apex of the backward cones.

Due to the symmetries in the Green's functions mentioned earlier, it follows that at the apex, $F_{11} = F_{22}$, and $F_{12} = F_{21} = 0$.

Thus the unknown stresses are determined as

$$\tau_{13}(x_{1i},x_{2j},0,t_k) = L/F_{11}$$

$$\tau_{23}(x_{1i},x_{2j},0,t_k) = M/F_{11} \tag{4.7}$$

Having determined these stresses, the displacements on part S_1 of the cone S can be found simply by substituting values obtained from equs. (4.7) into equs. (4.4). Velocities are found directly from the displacements using a central difference relation given by

$$\dot{u}(t) = (u(t+\Delta t) - u(t-\Delta t))/2\Delta t \tag{4.8}$$

4.3 Singular Integrals

Das (1980) analytically integrated over r and ϕ for points along the time axis t in evaluating the Green's function values. For this project, we used Gaussian quadrature to numerically approximate the value of the singular Green's function integrals when $t_k = t_n$, $x_{1i} = x_{1\ell}$, $x_{2j} = x_{2m}$.

The singular integral is given by

$$F_{11}(0,0,0,0) = \int_{-\frac{\Delta x}{2}}^{\frac{\Delta x}{2}} \int_{-\frac{\Delta x}{2}}^{\frac{\Delta x}{2}} \left[g^H_{11}\left(\xi_1,\xi_2,0+\frac{\Delta t}{2}\right) - g^H_{11}\left(\xi_1,\xi_2,0-\frac{\Delta t}{2}\right)\right] d\underset{\sim}{\xi}$$

Noting that $g^H_{11}(.)$ is symmetric about the x_1 and x_2 axes, and that $I_1(T) = I_2(T) = 0$ for $T \leq 1$, the above equation reduces to

$$F_{11}(0,0,0,0) = 4 \int_{0}^{\frac{\Delta x}{2}} \int_{0}^{\frac{\Delta x}{2}} g^H_{11}\left(\xi_1,\xi_2,0+\frac{\Delta t}{2}\right) d\underset{\sim}{\xi}$$

Two-dimensional Gaussian quadrature can thus be applied over one quarter of an element at the origin to obtain an approximation to the averaged value of the Green's function around r = 0.

The results obtained with a 40-point quadrature were cross-checked against results obtained by a simple right-hand Riemann sum approximation over a quarter element given by

$$4 \int_0^{\frac{\Delta x}{2}} \int_0^{\frac{\Delta x}{2}} g_{11}^{H}\left(\underset{\sim}{\xi}, \frac{\Delta t}{2}\right) d\underset{\sim}{\xi} \simeq 4h^2 \sum_{i=1}^{N} \sum_{j=1}^{N} g_{11}^{H}\left(ih, jh, \frac{\Delta t}{2}\right),$$

where $h = \frac{\Delta x}{2N}$

This was done to check the accuracy of the quadrature results because Ligget (1982) found that the approximations to singular integrals by this method were not always successful. In our case, the results from the two methods differ by less than ten percent.

CHAPTER 5

GROUND MOTION SIMULATION AWAY FROM THE FAULT SURFACE

5.1 Introduction

The Chamber of Mines has small and large seismic recording networks set up at some of the deep-level gold mines on the Witwatersrand which continuously monitor the mining-induced seismicity. Part of their aim is to try to interpret the seismic data in order to understand the type of source mechanism of the shear failures that occur in the rock mass surrounding the mining excavations. A ground motion simulation model allows us to use the results of the slip on the fault surface to predict the ground response at points away from the fault plane.

The formulation that we presented in chapters 3 and 4 was limited to the fault surface only. We require a formulation that allows us to determine the displacements at any point in the infinite domain so as to obtain a "complete" picture of the motion on and off the fault surface.

We cannot use the integral formulation in sections 3 and 4 to determine the response away from the fault plane since the Green's functions are only valid on the fault plane, i.e. both source and receiver points must be on the fault plane (Richards 1979). We must therefore resort to another formulation to obtain the response away from the fault surface.

5.2 Maruyama's Formulation

In order to obtain a displacement and velocity record at a field point remote from the fault surface, we can make use of a relation that links the response at a receiver or field point to the process occurring at each element on the fault surface.

The wave effects radiating from each source point are synchronised via the delay times between source and receiver points to give the combined effects experienced at each receiver point.

Maruyama (1963) developed a general formula to determine the displacement $u_m(\underset{\sim}{x},t)$ at a general position $\underset{\sim}{x}$ in an infinite domain, due to a dislocation process $D_k(\underset{\sim}{\xi},t)$ on fault surface elements $d\Sigma(\underset{\sim}{\xi})$ for a general fault surface Σ. (see figure 5).

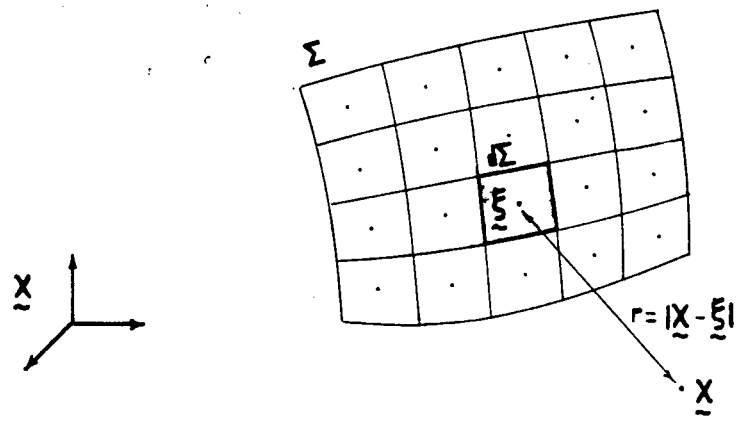

Figure 5 : Discretised fault surface showing source and receiver points.

Consider an infinite homogeneous, isotropic, elastic body, unstrained and at rest at time t = 0. Imagine a crack surface Σ with sides denoted by Σ^+ and Σ^- . The Maruyama formula considers the force distributions applied to this crack surface equivalent to a dynamic dislocation.

Define the surface tractions $\tau_{k\nu}$ on Σ as components of the force per unit area on a surface area by $\tau_{k\nu} = \tau_{k\ell}\nu_\ell$, where ν_ℓ is the direction cosine of the outward normal to the surface element, and $\tau_{k\ell}$ is a component of the stress tensor. (See figure 6).

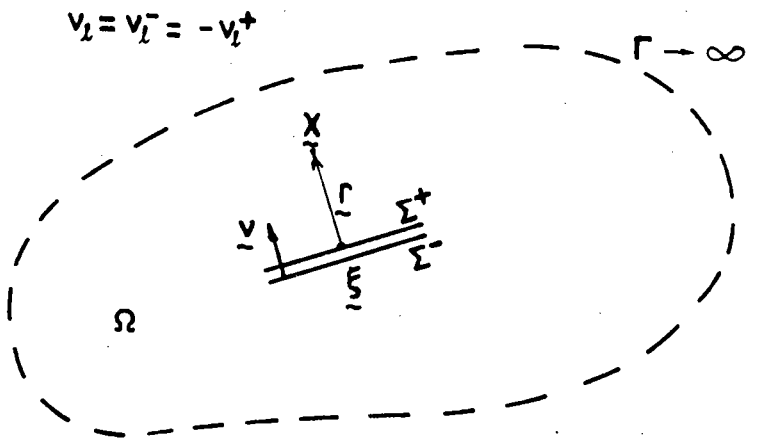

Figure 6 : Dislocation surface Σ showing direction cosines.

Define vector $\underset{\sim}{r}$ from source point $\underset{\sim}{\xi}$ to receiver point $\underset{\sim}{x}$ by $\underset{\sim}{r} = \underset{\sim}{x} - \underset{\sim}{\xi}$, or

$$r_k = x_k - \xi_k \ , \ k = 1,2,3 \ . \qquad (5.1)$$

Thus distance $|\underset{\sim}{r}| = r = \sqrt{r_1^2 + r_2^2 + r_3^2}$ (5.2)

For the most general form of the Maruyama formula, the displacements $u_k^m(\underset{\sim}{\xi},t)$ and stresses $\tau_{k\ell}^m(\underset{\sim}{\xi},t)$ are discontinuous across Σ . Define the stress and displacement discontinuities across Σ by

$$D_k = u_k^+ - u_k^- \quad , \tag{5.3}$$

and

$$\Delta\tau_{k\ell} = \tau_{k\ell}^+ - \tau_{k\ell}^- \tag{5.4}$$

By combining the reciprocal theorem of Betti (which relates two different displacement fields, stress fields and body forces to each other in a bounded elastic body $\Omega + \Gamma$) with a displacement expression from Love (1927) for an infinite elastic medium, and letting the boundary Γ in Betti's theorem recede to infinity, Maruyama obtained his fundamental formula for an infinite medium. The principle used in the development of this formula is fundamental in the boundary element method. If we apply tractions on surfaces Γ , Σ^+ and Σ^- of a finite body, the body will be deformed as if it were part of an infinite body. When a force is applied in Ω , and when such surface tractions as would be produced by the force in an infinite elastic medium, are applied on Γ , Σ^+ and Σ^- , then the displacement and stress fields in Ω will be identical to those in an infinite elastic medium.

Thus, in Betti's theorem, one takes as the first set, a unit body force in Ω , displacement field $u_k^m(\underset{\sim}{\xi},t)$ and stress field $\tau_{k\ell}^m(\underset{\sim}{\xi},t)$ which are generated in $\underset{\sim}{\xi}$ by the force, in an infinite elastic medium. As the second set, take an arbitrary (unknown) displacement field $u_k(\underset{\sim}{\xi},t)$ and the corresponding stress field $\tau_{k\ell}(\underset{\sim}{\xi},t)$.

The Love (1927) displacement formula provides an expression for $u_k^m(\underset{\sim}{\xi},t)$ due to a unit impulse. Stress components $\tau_{k\ell}^m(\underset{\sim}{\xi},t)$ are obtained from the usual stress-strain relations.

The combined equations are then integrated with respect to time t (see Maruyama 1963 for details) to give an expression for the displacement field at a point $\underset{\sim}{x}$ in the infinite medium, written in terms of the shear and displacement dislocations across a crack element $d\Sigma(\underset{\sim}{\xi})$.

For our fracture propagation problem the tractions τ_{13}, τ_{23}, τ_{33} are continuous across the crack plane (see section 3.6) and thus the shear stress discontinuity terms are zero.

Thus, the displacement field is written only in terms of the displacement discontinuities and is given by:

$$u_m(\underset{\sim}{x},t) = \frac{d\Sigma(\underset{\sim}{\xi})}{4\pi\rho} \sum_{\ell=1}^{3} \nu_\ell \sum_{k=1}^{3} \{6\mu\ Q_1P_1 + 6\mu\ Q_2P_2 + Q_3P_3 + \ldots + Q_6P_6\} \qquad (5.5)$$

where u_m = m^{th} component of u

ν_ℓ = ℓ^{th} component of the normal to $d\Sigma$

k,ℓ,m = (1,2,3) each = direction indices

and $$Q_1 = -\delta_{k\ell}\frac{r_m}{r^5} - \delta_{mk}\frac{r_\ell}{r^5} - \delta_{\ell m}\frac{r_k}{r^5} + 5\frac{r_k r_\ell r_m}{r^7}$$

$$P_1 = \Phi_k\left(\underset{\sim}{\xi},t - \frac{r}{\alpha}\right) - \Phi_k\left(\underset{\sim}{\xi},t - \frac{r}{\beta}\right)$$

$$Q_2 = -\delta_{k\ell}\frac{r_m}{r^4} - \delta_{mk}\frac{r_\ell}{r^4} - \delta_{\ell m}\frac{r_k}{r^4} + 5\frac{r_k r_\ell r_m}{r^6}$$

$$P_2 = \frac{1}{\alpha}\dot{\Psi}_k\left(\underset{\sim}{\xi}, t - \frac{r}{\alpha}\right) - \frac{1}{\beta}\dot{\Psi}_k\left(\underset{\sim}{\xi}, t - \frac{r}{\beta}\right)$$

$$Q_3 = (\lambda - 2\mu)\,\delta_{k\ell}\frac{r_m}{r^3} - 2\mu\,\delta_{mk}\frac{r_\ell}{r^3} - 2\mu\,\delta_{\ell m}\frac{r_k}{r^3} + 12\mu\frac{r_k r_\ell r_m}{r^5}$$

$$P_3 = \frac{1}{\alpha^2}\ddot{\Psi}_k\left(\underset{\sim}{\xi}, t - \frac{r}{\alpha}\right)$$

$$Q_4 = 2\mu\,\delta_{k\ell}\frac{r_m}{r^3} + 3\mu\,\delta_{mk}\frac{r_\ell}{r^3} + 3\mu\,\delta_{\ell m}\frac{r_k}{r^3} - 12\,\mu\,\frac{r_k r_\ell r_m}{r^5}$$

$$P_4 = \frac{1}{\beta^2}\ddot{\Psi}_k\left(\underset{\sim}{\xi}, t - \frac{r}{\beta}\right)$$

$$Q_5 = \lambda\,\delta_{k\ell}\frac{r_m}{r^2} + 2\mu\frac{r_k r_\ell r_m}{r^4}$$

$$P_5 = \frac{1}{\alpha^3}\dddot{\Psi}_k\left(\underset{\sim}{\xi}, t - \frac{r}{\alpha}\right)$$

$$Q_6 = \mu\,\delta_{mk}\frac{r_\ell}{r^2} + \mu\,\delta_{\ell m}\frac{r_k}{r^2} - 2\mu\frac{r_k r_\ell r_m}{r^4}$$

$$P_6 = \frac{1}{\beta^3}\dddot{\Psi}_k\left(\underset{\sim}{\xi}, t - \frac{r}{\beta}\right)$$

where $\Psi_k(\underset{\sim}{\xi}, t) = \int_0^t dt' \int_0^{t'} D_k(\underset{\sim}{\xi}, t'')\, dt''$ (5.6)

$\dot{\varphi}_k(\underset{\sim}{\xi},t)$ = the first time derivative of $\varphi_k(\underset{\sim}{\xi},t)$

$\ddot{\varphi}_k(\underset{\sim}{\xi},t)$ = the second time derivative of $\varphi_k(\underset{\sim}{\xi},t)$

$\dddot{\varphi}_k(\underset{\sim}{\xi},t)$ = the third time derivative of $\varphi_k(\underset{\sim}{\xi},t)$

r = $(r_1^2 + r_2^2 + r_3^2)^{1/2}$

α,β = compressional and shear wave speeds

λ,μ = Lamé constants

$D_k(.)$ = discontinuity in displacement in direction k.

In equ. (5.5), in the case of a fault plane confined to two orthogonal directions only (i.e. $x_3 = 0$), the normal $\underset{\sim}{\nu}$ to $d\Sigma$ is perpendicular to the direction of the displacement discontinuity $D_k(.)$ so that $\delta_{k\ell}$ vanishes. Since we exclude tensile fracture in this work, the k = 3 component of the discontinuity term is zero.

Equation (5.5) can be shortened if one notes that terms Q_1 and Q_2 differ merely by a factor of r . We can thus write

$$6\mu\, Q_1\, P_1 + 6\mu\, Q_2\, P_2 =$$

$$6\mu\, Q_1 \left\{ \left[\varphi_k\left(\underset{\sim}{\xi},t - \frac{r}{\alpha}\right) + \frac{r}{\alpha}\dot{\varphi}_k\left(\underset{\sim}{\xi},t - \frac{r}{\alpha}\right)\right] - \left[\varphi_k\left(\underset{\sim}{\xi},t - \frac{r}{\beta}\right) + \frac{r}{\beta}\dot{\varphi}_k\left(\underset{\sim}{\xi},t - \frac{r}{\beta}\right)\right]\right\}$$

5.3 Integration of Maruyama's Formula

In order to obtain the response for a known dislocation function, and to incorporate this in a numerical solution, we integrate Maruyama's formulation using a time-stepping technique obtained from an interpolation of the dislocation over small time increments.

The following assumptions will be made in the numerical discretisation:

- assume that the displacement discontinuity is constant over a fault element $d\Sigma$
- assume a linear variation in slip over a short time interval,
- assume a single node point j at the centre of each fault element $d\Sigma$.

From the second assumption, using linear interpolation functions (see figure 7) over time interval $t_{p-1} \leq t \leq t_p$, for p = 0,1,2,3, ... P ,

$$D_k(\underset{\sim}{\xi},t) = \sum_{q=1}^{2} D_k(\underset{\sim}{\xi},t_q)\, \phi_q(t) \qquad (5.7)$$

where $\phi_1(t) = \dfrac{t_p - t}{\Delta t_p}$

$$\phi_2(t) = \frac{t - t_{p-1}}{\Delta t_p}$$

and $\Delta t_p = t_p - t_{p-1}$ (5.8)

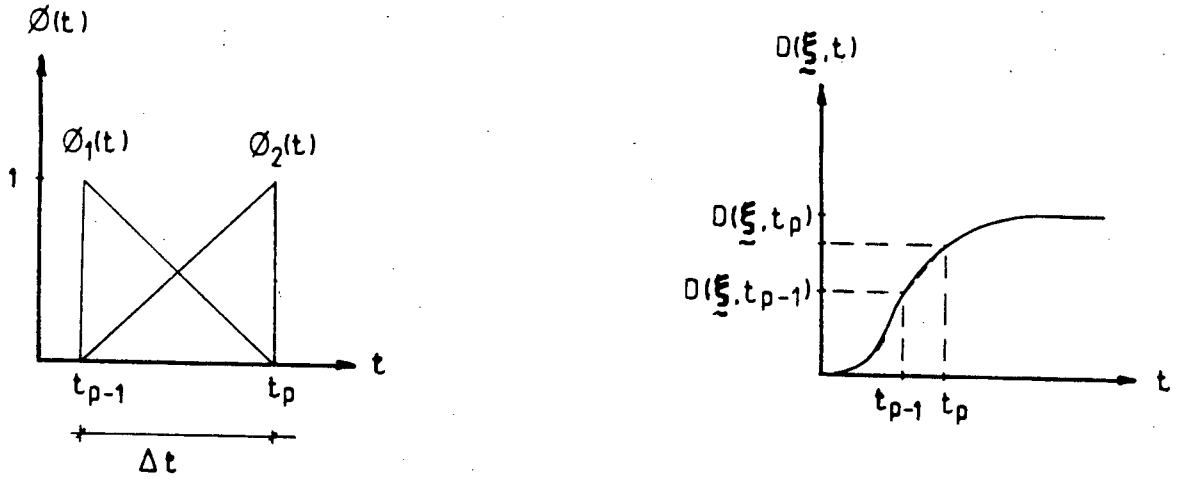

Figure 7 : Interpolation functions and numerical discretisation of dislocation function.

The linear approximation to equ. (5.6) thus becomes

$$\Psi_k(\underset{\sim}{\xi},t_n) = \sum_{p=1}^{n} \int_{t_{p-1}}^{t_p} \left[\sum_{q=1}^{p-1} \int_{t_{q-1}}^{t_q} D_k(\underset{\sim}{\xi},t'')dt'' + \int_{t_{p-1}}^{t'} D_k(\underset{\sim}{\xi},t'')dt'' \right] dt' \qquad (5.9)$$

where $t_0 = 0$,

and $$D_k(\underset{\sim}{\xi},t'') = D_k(\underset{\sim}{\xi},t_p) \frac{t'' - t_{p-1}}{\Delta t_p} + D_k(\underset{\sim}{\xi},t_{p-1}) \frac{t_p - t''}{\Delta t_p}$$

Define $D_p = D_k(\underset{\sim}{\xi},t_p)$.

After performing the integrations in equ. (5.9), the first double integral becomes

$$\int_{t_{p-1}}^{t_p} \int_{t_{q-1}}^{t_q} D_k(\underset{\sim}{\xi},t'')dt'' \, dt' = \frac{\Delta t_p . \Delta t_q}{2} (D_q + D_{q-1}) \qquad (5.10)$$

and the second double integral becomes

$$\int_{t_{p-1}}^{t_p} \int_{t_{p-1}}^{t'} D_k(\underset{\sim}{\xi},t'')dt'' \, dt' = \Delta t_p^2 \left(\frac{D_p}{6} + \frac{D_{p-1}}{3} \right) , \qquad (5.11)$$

Equ. (5.9) thus simplifies to

$$\Psi_k(\underset{\sim}{\xi},t_n) = \sum_{p=1}^{n} \left[\sum_{q=1}^{p-1} \frac{\Delta t_p . \Delta t_q}{2} (D_q + D_{q-1}) + \Delta t_p^2 \left(\frac{D_p}{6} + \frac{D_{p-1}}{3} \right) \right] \qquad (5.12)$$

If we denote $\sum_{q=1}^{p-1} (.)$ by $\psi_k^*(\underset{\sim}{\xi}, t_{p-1})$, then

$$\psi_k(\underset{\sim}{\xi}, t_n) = \sum_{p=2}^{n} \left[\psi_k^*(\underset{\sim}{\xi}, t_{p-2}) + \frac{\Delta t_p . \Delta t_{p-1}}{2} (D_{p-1} + D_{p-2}) + \Delta t_p^2 \left(\frac{D_p}{6} + \frac{D_{p-1}}{3} \right) \right] \tag{5.13}$$

The first time derivative of $\psi_k(\underset{\sim}{\xi}, t_n)$, is obtained from equ. (5.6) and is given by

$$\dot{\psi}_k(\underset{\sim}{\xi}, t_n) = \int_0^{t_n} D_k(\underset{\sim}{\xi}, t'') \, dt'' \tag{5.14}$$

(The above follows from a basic theorem of differentiation which states that, if $F(x) = \int_a^x f(t)dt$, then $dF(x)/dx = f(x)$, where a = constant).

Discretising equ. (5.14) gives

$$\dot{\psi}_k(\underset{\sim}{\xi}, t_n) = \sum_{p=1}^{n} \int_{t_{p-1}}^{t_p} \left[D_p \left(\frac{t'' - t_{p-1}}{\Delta t_p} \right) + D_{p-1} \left(\frac{t_p - t''}{\Delta t_p} \right) \right] dt'' \tag{5.15}$$

Equ. (5.15) simplifies to

$$\dot{\Psi}_k(\underset{\sim}{\xi},t_n) = \sum_{p=1}^{n} \left[D_p + D_{p-1}\right] \frac{\Delta t_p}{2} \tag{5.16}$$

Differentiating equ. (5.6) twice with respect to time t, we obtain the second time derivative

$$\ddot{\Psi}_k(\underset{\sim}{\xi},t_n) = D_k(\underset{\sim}{\xi},t_n) = D_n \tag{5.17}$$

The third time derivative of equ. (5.6) is taken as a finite difference, using equ. (5.17), and is given by

$$\dddot{\Psi}_k(\underset{\sim}{\xi},t_n) = [D_n - D_{n-1}]/\Delta t_n \tag{5.18}$$

The solution at each time is obtained by updating the values of $\Psi_k(\underset{\sim}{\xi},t_n)$ and $\dot{\Psi}_k(\underset{\sim}{\xi},t_n)$ at each successive time, where t_n is the retarded time $n\Delta t - r/\alpha$ or $n\Delta t - r/\beta$, $n = 0,1,2,3,\ldots,N$.

Thus

$$\Psi_k(\underset{\sim}{\xi},t_n) = \Psi_k(\underset{\sim}{\xi},t_{n-1}) + \Psi_k^*(\underset{\sim}{\xi},t_{n-2}) + \frac{\Delta t_n . \Delta t_{n-1}}{2}\left(D_{n-1} + D_{n-2}\right) + \Delta t_n^2 \left(\frac{D_n}{6} + \frac{D_{n-1}}{3}\right) \tag{5.19}$$

$$\dot{\Psi}_k(\underset{\sim}{\xi},t_n) = \dot{\Psi}_k(\underset{\sim}{\xi},t_{n-1}) + \left[D_n + D_{n-1}\right] \frac{\Delta t_n}{2} \tag{5.20}$$

CHAPTER 6

COMPUTATIONAL ASPECTS

6.1 Introduction

Two separate computer codes exist for the fault propagation problem and the ground motion simulation problem. Each code is split up into modules that are controlled by driver units. Details of the layout of the coding can be found in Appendix E.

6.2 Fault Propagation Model with Prescribed Rupture Velocity

The primary modules involved in the fault propagation model with a prescribed rupture velocity criterion are GREEN, STRESS and DISPL.

GREEN calculates the values of the Green's functions $g_{11}(.)$ and $g_{12}(.)$ at the nodal points within the forward cone. (It is not necessary to calculate $g_{22}(.)$ since it exhibits 90° - rotational symmetry with $g_{11}(.)$). STRESS calculates the unknown incremental stresses ahead of the rupture front in part S_2 of cone S, using relevant stresses and Green's function values from all earlier times. DISPL calculates the displacements on the cracked part S_1 of cone S, using the stresses from STRESS as well as the known stresses on the cracked part of the fault surface.

Other minor modules perform secondary calculations (e.g. RAYL which calculates the Rayleigh cubic roots from the material properties of the medium). All the modules are documented in the coding and are thus easy to follow.

6.2.1 Data Storage

Dynamic boundary element methods require large amounts of dimensioned storage since data is needed from all previous times to obtain results at the current time. Storage arrays are needed to store $g_{11}(.)$, $g_{12}(.)$, $g_{22}(.)$, $\sigma_{23}(.)$, $\sigma_{13}(.)$, $u_1(.)$ and $u_2(.)$ including others.

Two basic alternatives exist for storing this data. Assume that (ixjxk) = (30x30x30) is needed, where (i,j,k) correspond to (x_1, x_2, t).

The first alternative is to use three arguments per array, e.g. G11 (30,30,30).

Thus we would require a total dimensioned storage of 5x30x30x30=135 K words to store the Green's function and stress values alone (assuming symmetry about the x_1 and x_2 axes for the stresses).

The second alternative is to use single-argument arrays. This would require extra arrays to keep control of the spatial and time positions of each Green's function and stress value calculated. The following arrays would be required for stresses and Green's functions.

G11(10 000) , G12(10 000) , G22(10 000), NGFLAG(30) , KEYG(10 000) , SIG13(10 000) , SIG23(10 000) , KEYSL(10 000) , KEYSM(10 000) , NSFLAG(30) ,

where KEYG(.) , KEYSL (.) and KEYSM(.) contain integer values denoting a particular (i,j) combination, and NGFLAG(.) , NSFLAG(.) are flags denoting the time level of a particular Green's function or stress value.

(An array size of 10 000 is needed since data is non-zero only within cone S, i.e. $10\,000 \simeq \frac{30x30x30}{3}$).

Thus we would need a total of (10 000 x 8) + (30 x 2) ≃ 80 K words, which is 60% of the storage needed for the first alternative.

However, the second alternative requires more CPU time, since the storage arrays must be searched through to obtain the data needed at each point and at each time level. In the development of the computer code, the second alternative had to be used to minimise the program size at the expense of CPU time.

6.2.2 Restart Option

A restart option is incorporated in the program to allow the user to restart the program just before STRESS. This eliminates having to recalculate the Green's function values if the material properties remain unchanged, but if one of the following is changed:

- the initial stress conditions
- the initial and/or final crack radius
- the symmetry conditions
- the coefficient of dynamic friction
- the total number of time steps to be solved for is less than that used when the Green's function values were calculated.

The user also has the option of stopping the program after calculation of the Green's functions, streses or displacements.

6.2.3 Symmetry Conditions

Besides the symmetry conditions that exist in the Green's functions, the user has the option of restricting the calculation of the stresses, displacements and velocities to certain quadrants of the (x_1, x_2) axis system, depending on the symmetry of the problem being solved.

In its present form, the program will always solve a problem with symmetry about the x_1 and x_2 axes (even though the user has the option of assuming no symmetry), but the program structure allows one to incorporate non-homogeneous initial stress conditions, which would result in a loss in symmetry.

6.2.4 Symmetry Properties of the Green's Functions

The various symmetry properties of the Green's functions mentioned in section (3.3.1) are explained below with respect to the discretised Green's functions that appear in the computer code.

We will introduce the following notation:

$$g(\underset{\sim}{x},t;\ \underset{\sim}{\xi},s) \equiv g(i,j,k;\ \ell,m,n)$$

where $\underset{\sim}{x} = (x_i,x_j) = (x_{1i},x_{2j})$ and $t = t_k$

and $\underset{\sim}{\xi} = (\xi_\ell,\xi_m) = (\xi_{1\ell},\xi_{2m})$ and $s = s_n$.

Thus, indices (i,j,k) define a particular receiver point and (ℓ,m,n) define a particular source point.

Also define notation $i\ell = i - \ell$, $jm = j - m$, $kn = k - n$.

6.2.4.1 Spatial Reciprocal Relation

For a regularly gridded mesh,

$$\begin{aligned} g(i,j,k;\ \ell,m,n) &= g(i+I,\ j+J,\ k;\ \ell+I,\ m+J,\ n) \\ &= g(i-\ell,\ j-m,\ k;\ 0,\ 0,\ n) \\ &= g(i\ell,\ jm,\ k;\ 0,\ 0,\ n) \end{aligned}$$

where I and J are arbitrary integers.

The spatial reciprocity is depicted pictorially in figure 8 for the first quadrant only.

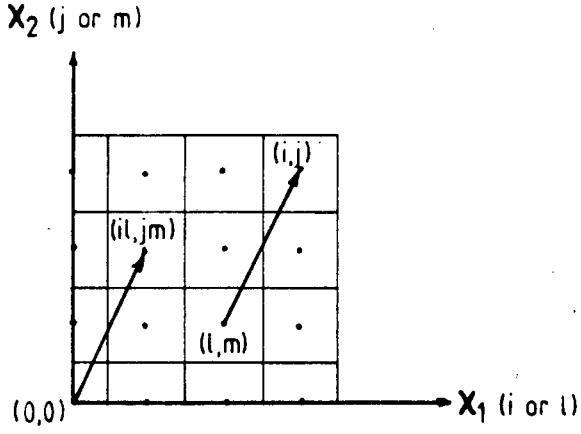

Figure 8 : Spatial reciprocal relation restricted to a single time level.

6.2.4.2 Time Reciprocal Relation

For a numerical scheme with regular time-stepping,

$$g(i,j,k;\ \ell,m,n) = g(i,j,k+K;\ \ell,m,n+K)$$
$$= g(i,j,k-n;\ \ell,m,0)$$
$$= g(i,j,kn;\ \ell,m,0)$$

where K is an arbitrary integer.

Note that the time and spatial reciprocal relations can be combined, and figure 8 thus merely shows a "two-dimensional" picture of the total reciprocity possibilities.

6.2.4.3 Rotational and 8-fold Symmetry

The 90° - rotational symmetry between $g_{11}(.)$ and $g_{22}(.)$, and part of the 8-fold symmetry of $g_{12}(.)$, is shown in Appendix E. Only a single quadrant is shown. The symmetry of $g_{11}(.)$ and $g_{22}(.)$ about the x_1 and x_2 axes can be imagined by extrapolating mirror images into the other quadrants. The inverse symmetry of $g_{12}(.)$ about these axes would be found by the same process, but including a sign change.

The above mentioned properties can be summarised as follows:

$$
\begin{aligned}
g_{11}(\pm i\ell,\pm jm,kn;0,0,0) &= g_{11}(\mp i\ell,\mp jm,kn;0,0,0) \\
&= g_{22}(\pm jm,\pm i\ell,kn;0,0,0) \\
g_{12}(\pm i\ell,\pm jm,kn;0,0,0) &= g_{21}(\pm i\ell,\pm jm,kn;0,0,0) \\
&= g_{12}(\pm jm,\pm i\ell,kn;0,0,0) \\
&= g_{12}(\mp jm,\mp i\ell,kn;0,0,0) \\
&= -g_{12}(\pm i\ell,\mp jm,kn;0,0,0) \\
&= -g_{12}(\mp i\ell,\pm jm,kn;0,0,0)
\end{aligned}
$$

6.2.5 Time-Step Choice

The user must choose a value for the time-step Δt as well as the dimensionless ratio $\alpha\Delta t/\Delta x$. The value of Δt chosen, does not affect the accuracy of the solution, but only defines the physical dimensions of the problem.

If for example, we choose $\Delta t = 0.0001$ seconds, and compare the solutions obtained with those for $\Delta t = 1.0$ second, then we find that the stresses are exactly the same for each time-step, but the values of the Green's functions, displacements and velocities differ by a factor of (1.0/0.001). Thus, it is possible to choose a time-step for a pre-required maximum fault size.

The value given to $\alpha\Delta t/\Delta x$ must be less than 1.0 to ensure that the compressional (P) wave does not travel faster than one element length in one time-step. If $\alpha\Delta t/\Delta x$ is greater or equal to unity, then a node immediately adjacent to the current node (at which results are being solved for) would also experience wave effects at the current time level. A value of $\alpha\Delta t/\Delta x$ less than 0.5 would ensure that the wave effects do not transmit beyond the boundaries of the current element during the current time-step. A smaller value of $\alpha\Delta t/\Delta x$ will produce a smaller time-step, and hence we would expect the results to be more accurate. However, a smaller time-step requires more computer storage and a longer run time. A value of $\alpha\Delta t/\Delta x$ equal to 0.5 was used by Das (1980) and produced accurate results.

6.3 Fault Propagation Model with Fracture Criterion

The modules STRESS, DISPL and VELOC in the fault propagation model with a prescribed rupture velocity criterion can be replaced by a single (more complex) module SDV, that includes a fracture criterion to determine when an element ruptures.

In this model, the position of the crack edge is governed by the state of stress near the crack edge. An element outside the crack ruptures when the maximum shear stress (averaged over the element) at the node is greater than the ultimate strength $\sigma_u(\underset{\sim}{\xi})$ of the material at nodal position $\underset{\sim}{\xi}$ on the fault plane. Thus fracture occurs when $\sigma_u(\underset{\sim}{\xi}) < \sqrt{\sigma_{13}^2(\underset{\sim}{\xi}) + \sigma_{23}^2(\underset{\sim}{\xi})}$ .It should be noted that the ultimate strength is grid-size dependent, since σ_{13} and σ_{23} are averaged at the node points of each element on the mesh.

An element along a pre-existing fault surface (one where rupture has already occurred and is currently not experiencing any slip) starts to slip as soon as the maximum static frictional stress at that element is exceeded.

Details of the theory involved in this model are documented in Das (1981). It involves simultaneously solving for the direction Ψ of the frictional force on the rupturing part of the crack plane and the velocity of slip $|\dot{\underset{\sim}{u}}|$ of each rupturing element. Having solved for these quantities, the incremental stresses are obtained from

$$\tau_{13} = \mu_d \, \sigma_{33}^{\,0} \cos\Psi - \sigma_{13}^{\,0}$$

$$\tau_{23} = \mu_d \, \sigma_{33}^{\,0} \sin\Psi - \sigma_{23}^{\,0}$$

The slip velocity $|\dot{\underset{\sim}{u}}|$ is needed to determine when an element stops slipping. Slip continues until $|\dot{\underset{\sim}{u}}|$ falls below a critical threshold value close to zero. As soon as the slip velocity is less than this threshold, the velocity is set to zero and the slip is stopped at this element. (A threshold value close to zero is needed to monitor the slip velocity since the slip velocity has two components on the fault plane, and thus the slip velocity vector can reverse direction without passing through zero).

As soon as the slip is halted at a particular element, the boundary conditions at the element immediately change. While the point is slipping, the stress is held at the dynamic frictional value and the unknown slip value is determined. When the slip stops, the slip value is known (and held constant) while the stress becomes unknown. An element can start slipping again as soon as the stress exceeds the static frictional stress at the element involved.

6.4 Ground Motion Simulation Model

The computer code for the simulation of the strong ground motion due to a seismic event has been restricted to the case of a planar rectangular fault surface.

Two basic dislocation functions are included, viz. linear and radial propagating ramp functions. A step function is also possible (by setting the rise time of the ramp function equal to zero).

In the case of the linear ramp function, the fault is assumed to originate as a line source, and propagates in the directions orthogonal to this. In the case of the radial function, the fault originates as a point source and grows radially, even though the discontinuity in displacement is assumed to be in one direction only (i.e. a self-similar crack as in Kostrov 1964).

CHAPTER 7

ANALYTICAL SOLUTION FOR SELF-SIMILAR SHEAR CRACK

The axisymmetric problem of a purely circular crack that grows at a uniform speed v_r radially in its own plane provides a check on our numerical results.

For a homogeneous, isotropic, elastic, infinite medium, with a single non-zero component of the initial stress tensor τ_{13}^{o} (applied in the x_1 direction), Kostrov (1964) solved for the displacements on the crack surface $x_3 = 0$. Dahlen (1974) provides a corrected and more convenient form of the solution given by Kostrov.

Assume that the crack forms at time $t = 0$, and spreads along the $x_3 = 0$ plane from the origin. The boundary conditions are given by:

$$\begin{aligned} \tau_{13} &= -\tau_{13}^{o} && \text{for} && x_3 = 0 \ , \ r \leq v_r.t \ , \\ \sigma_{33} &= 0 && \text{for} && x_3 = 0 \ , \ -\infty < r < \infty \ , \\ u_r &= 0 && \text{for} && x_3 = 0 \ , \ r > v_r.t \ , \end{aligned} \qquad (7.1)$$

where $r^2 = x_1^2 + x_2^2$

v_r = rupture speed.

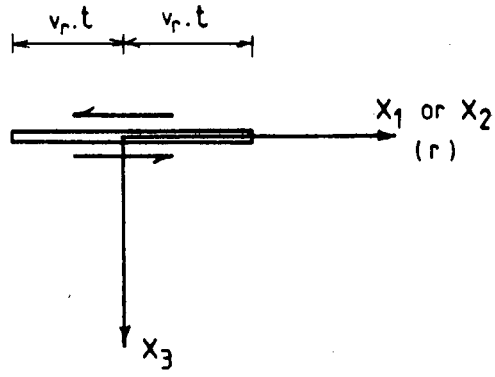

Figure 9 : Schematic representation of a self-similar shear crack

The solution for the displacements on the crack is given by

$$u_{x_1} = \frac{A}{2}\sqrt{\left(t^2 - \frac{r^2}{\alpha^2}\right)}\, H\left(t - \frac{r}{\alpha}\right) \quad .$$
$$u_{x_2} = 0 \qquad (7.2)$$

where $H(.)$ is the Heaviside step function,

A is a constant given by

$$A = C\left(\frac{v_r}{\beta}, \frac{\alpha}{\beta}\right).\tau_{13}{}^{0}.\beta/\mu \quad , \qquad (7.3)$$

where $C(.)$ is a dimensionless function given by

$$C(.) = (4\, v_r/\beta)\left[(v_r/\beta) + \left(1 - \frac{v_r^{\,2}}{\beta^2}\right)^{-1/2} \arccos(v_r/\beta) + \left(4\beta^2/v_r^{\,2}\right) \int_0^{\infty} I(s)\, ds\right]^{-1} \quad ,$$

$$\text{where } I(s) = \left[\frac{\left(s + \frac{v_r^{\,2}}{2\beta^2}\right)^2 - s\left(s + \frac{v_r^{\,2}}{\beta^2}\right)^{1/2}\left(s + \frac{v_r^{\,2}}{\alpha^2}\right)^{1/2}}{(s+1)^2\left(s + \frac{v_r^{\,2}}{\beta^2}\right)^{1/2}}\right] \qquad (7.4)$$

The dimensionless function $C(.)$ was integrated numerically by Dahlen for the case $\alpha^2 = 3\,\beta^2$ to give the function shown in figure 10.

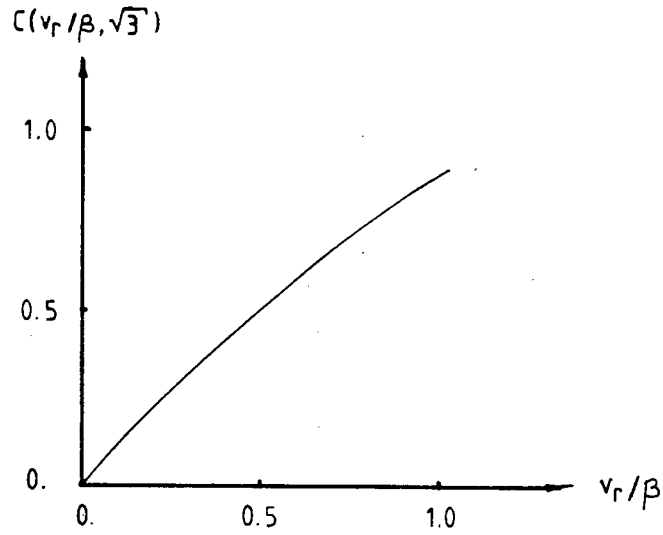

Figure 10 : Dimensionless function $C\left(\frac{v_r}{\beta}, \frac{\alpha}{\beta}\right)$ for a Poisson solid $\alpha^2 = 3\beta^2$

From the form of the above analytical solution, we expect azimuthal symmetry for the displacement fields. The stress fields should thus also exhibit symmetry about the centre of the crack. The fact that u_z (and hence τ_{zz}) is zero enables us to determine the amount of numerical "noise" due to the discretisations used in the numerical solution.

CHAPTER 8

RESULTS

The main results of the fault propagation model are those of the slip as a time-dependent function of position on the fault. Together with these, we show the discretised Green's functions and resulting stresses ahead of the crack tip. The ground motion simulation results are discussed in section 8.4. Appendix F contains two- and three-dimensional plots of the Green's functions, stresses, displacements and velocities on the plane of the fault. The ground motion simulation plots appear in appendix G.

8.1 Green's Function Results

The discretised Green's function values are calculated using Simpson's rule as well as a simple Romberg integration scheme (Davis and Rabinowitz 1975). The Simpson's rule results show larger magnitudes than the Romberg scheme results for the earlier times, but the results of each scheme have more similar magnitudes at later times (e.g. less than 10% different by the 35^{th} time-step). However, the Romberg scheme results show a deterioration in the wave form of the Rayleigh and shear wave front at later times, whereas the Simpson's rule results do not show any deterioration.

We do not have any direct check on the magnitude of the Green's function results. (The only way to check results is by comparing our displacement results with those for the analytical solution to the problem of a self-similar shear crack). Das (1980) does present a three-dimensional plot

at the 35^{th} time-step. We present the equivalent plot obtained from our model and the wave forms are exactly as expected. The P-wave tends to zero amplitude towards the x_2-axis, where it is zero, and the combined S- and R-wave fronts exhibit an azimuthal type symmetry. The Green's function plots for the earlier times are not as smooth as at later times.

8.2 Stress, Displacement and Velocity Results for a Self-Similar Shear Crack Problem

The analytical solution for a self-similar shear crack provides the simplest way of checking the accuracy of the results on the fault plane. The details of this problem are available in chapter 7.

We tested two different material property sets: the first set is for realistic material properties of ρ = 2700 kg/m^3, ν = 0.25, E = 75.0 x 10^9 Pa; the second set is for the case where the P-wave velocity α = 1 (ρ = 2700 kg/m^3, ν = 0.25, E = 2375 Pa). The α = 1 case was presented by Das (1980) to validate her numerical results. The results for each material set show reasonable agreement with the analytical solution curves.

It is evident from the displacement time-histories that the numerical results are not smooth. This can be directly traced to the stress results. At certain times, the stress peaks ahead of the rupture front are much higher than at other times. This erratic behaviour may be due to the inaccuracy in the numerical integration of the Green's functions. A more accurate numerical integration scheme may smooth out the stress and displacement results.

The negative slope in the displacement results means that the fault slip is in fact reversing direction at certain times. This is clearly not physically realistic. Das (1980) notes that the slip at a point inside the crack is stopped when the slip velocity at that point tends to reverse sign. However this physical constraint on the slip does not directly deal with the problem of the abovementioned erratic stress peaks.

It is also evident from the plots in appendix F that the displacement results obtained via Simpson's rule are very close to the analytical results, whereas those obtained from a Romberg integration of the Green's functions are much less than the analytical solution results for the case $\alpha\Delta t/\Delta x = 0.5$. It is important to note that decreasing the error tolerances (by a factor of 1000) for the Romberg scheme does not alter the results at all.

The velocity plots should show a decrease in the velocity magnitudes with time. The erratic behaviour in the displacement results prevents this from occurring as the velocities are simply obtained from a finite difference scheme, using the displacement results.

Results have also been included of displacements obtained using a ratio of $\alpha\Delta t/\Delta x = 0.25$ instead of 0.5. The Romberg-based results are still significantly less than the analytical results. The Simpson-based results are not as smooth as those obtained using a ratio of 0.5.

For a value of $\alpha\Delta t/\Delta x = 1.0$, the Simpson-based results are smoother than the results based on a ratio of 0.5 or 0.25.

formulation over the fault plane, the term in r^{-n} will be smooth over a grid interval if $n\Delta x/r_{min} << 1$, where r_{min} is the minimum distance from an observation point $\underset{\sim}{x}$ to the fault plane $d\Sigma(\underset{\sim}{\xi})$. Also, since the dislocation function $D_k(\underset{\sim}{\xi}, t - \frac{r}{\alpha})$ or $D_k(\underset{\sim}{\xi}, t - \frac{r}{\beta})$ can rapidly change over a time interval $\Delta x/\alpha$ or $\Delta x/\beta$ respectively, $\Delta x/\alpha$ or $\Delta x/\beta$ must be much smaller than the minimum period contained in the slip function. (For a ramp dislocation function, the minimum period is the rise time). This is demonstrated in one of the plots at station 4 where a course mesh of 10 elements in the x_1-direction and 5 elements in the x_2-direction is used.

Other essential parameters used are:

fault width	=	1032 m (in the x_2-direction)
fault length	=	968 m (in the x_1-direction)
maximum dislocation	=	1.0 cm (in the x_1-direction)
P-wave velocity	=	6 km/sec
S-wave velocity	=	3.4 km/sec
ramp function rise time	=	0.12 sec
rupture velocity	=	3 km/sec

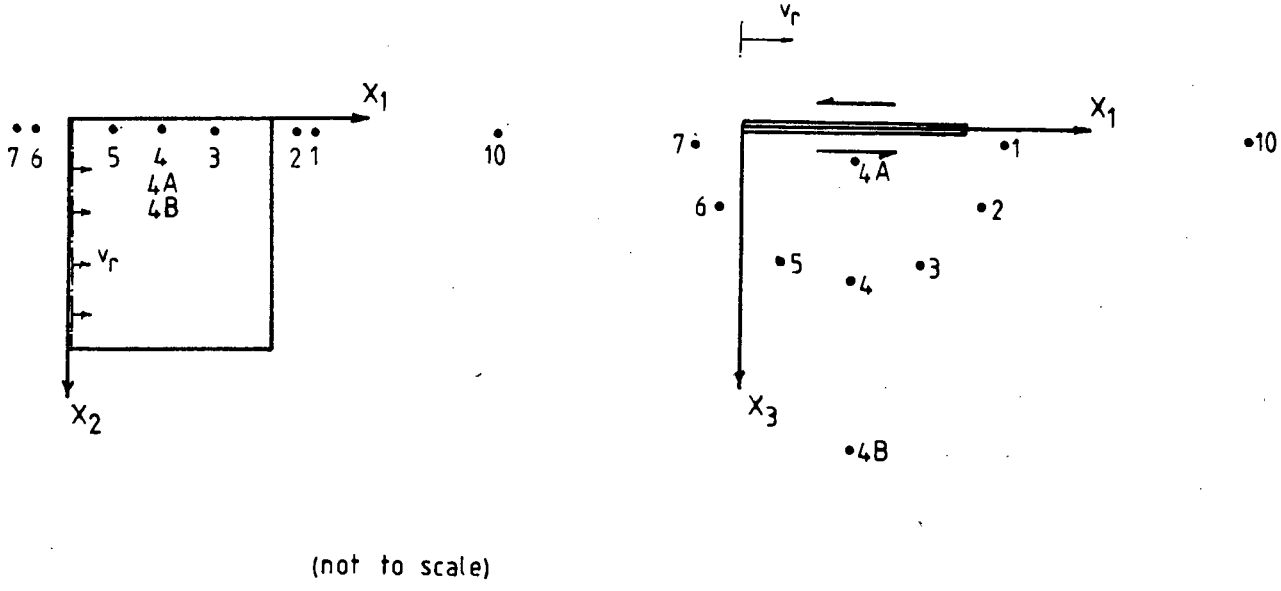

(not to scale)

Figure 11 : Schematic representation of fault surface and field stations

The field locations (as in Anderson and Richards 1975) are given by:

Station	x_1(m)	x_2(m)	x_3(m)
nearfield			
1	1377.	16.	75.0
2	1234.	16.	433.
3	917.	16.	750.
4	484.	16.	866.
4A	484.	16.	108.25
5	51.	16.	750.
6	-266.	16.	433.
7	-379.	16.	75.0
far field			
10	4438.	16.	346.
4B	484.	16.	3464.

Our results, for both the near-field and the far-field stations, compare extremely well with those of Anderson and Richards (1975). It is evident from the station 2 results that the ground motion due to the radial and line source dislocation functions are very similar. Anderson and Richards mention that different source functions often give very similar results and that it would be advantageous to study the acceleration record instead of the displacement record since near-field data is usually gathered in terms of accelerations. However, in the mining industry, near-field data is gathered in terms of velocities in the form of seismograms. We present velocity plots in appendix G obtained by a simple central difference of the displacements. It is also possible to directly differentiate the Maruyama formula to obtain the velocity equation.

CHAPTER 9

CONCLUSIONS AND RECOMMENDATIONS

A BEM for dynamic shear fracture propagation in an infinite continuum has been implemented along with a ground motion simulation model which takes an arbitrary slip function as input. These provide a basis for further studies of slip and fracture criteria, stopping mechanisms of rupture, and the interpretation of seismic records.

The BIEM fault propagation model has been tested for the simple case for which analytical results are available and is shown to be satisfactory. The major shortcoming of the fault propagation model is the amount of computing time needed to run an example with a large number of time-steps (say 40). In its present form, to calculate the stresses, displacements and velocities on the fault plane, the program requires 1 minute computing time on a SPERRY UNIVAC 1100 for a mesh of (ixjxk) = (5x5x10), 35 minutes for a mesh of (10x10x20), and in excess of 5 hours for a mesh of (20x20x40). The bulk of the computing time is CPU time, and there is minimal I/O time. Das (1980) notes that her program requires only 15 minutes of CPU time on an IBM 360/75 for a (25x25x50) mesh. It is possible that the CPU time is only a small part of the total computing time if a different programming structure is used. Storage limitations in the present work necessitate the use of one-dimensional storage arrays. (The present fault propagation code has a total size of 207 K words for a maximum mesh size of (20x20x40)). As a result, the calculation of an unknown stress value requires that the Green's function and stress values must be searched through continuously to obtain the desired data.

A further shortcoming is the non-smoothness of the Green's function values at earlier times, and hence in the displacement and stress results. The negative slope in the displacement results means that the fault slip reverses direction at certain times, which is not physically realistic. An improvement of the numerical integration used in determining the Green's functions may produce the desired smoothness, although this requires further study. The BIEM code thus needs to be improved to reduce overall computing times and to obtain the desired efficiency.

An advantage of the BIEM is that it can easily incorporate a fracture criterion model so as to allow the study of spontaneous crack growth. This has been demonstrated without studying the variety of possible criteria available.

The ground motion simulation model uses a linear interpolation in time of the slip function to integrate, in a stepwise manner, the Maruyama equations for displacement due to a dynamic dislocation. Excellent results have been obtained for the case of a linearly propagating ramp function and for a self-similar (radially propagating) crack.

The synthesis of seismic waves due to slip on the fault is an important feature of this simulation model, as it aids the interpretation of real seismograms.

However, no results have been shown of the ground motion due to the slip produced by the fracture propagation model. The code has this capability, but because one can only obtain results for a small number of time steps due to the reasons mentioned above, only the P-wave effect would be felt at

the receiver point. The S-wave effect would not be felt by the time that the slip data for the P-wave influence was exhausted. Thus, only the first part of a ground motion displacement curve can be obtained, using the present code.

It appears worthwhile, because of the easy physical interpretation, to investigate the possibility of using the Maruyama formulation to obtain the fault slip history as well as the resulting ground motion. This requires that only the cracked part of the fault plane is discretised since Maruyama's formula is essentially a Green's function for an impulsive point slip. The slip on the fault is written as the integral (sum) of the elemental slips and the Maruyama form of the Green's function. One would however, have to overcome the 3^{rd}-order singularity in $|\underset{\sim}{x} - \underset{\sim}{\xi}|$, either analytically or numerically, before implementing such a method.

The above recommendation, together with the "fine-tuning" of the present model, provides the basis for future work in the field of fracture propagation leading to the interpretation of seismic records.

Appendix A

The constants appearing in the dimensionless functions $I_1(T)$ and $I_2(T)$ in section 3.8 are given below.

Define
$$a^{-1} = 16(A-1)(R_1-R_2)(R_3-R_1)$$
$$b^{-1} = 16(A-1)(R_1-R_2)(R_2-R_3)$$
$$c^{-1} = 16(A-1)(R_3-R_1)(R_2-R_3) \qquad (A.1)$$

where
$$A = \alpha^2/\beta^2 \qquad (A.2)$$

Then
$$c_1 = -2aA(A-R_1)(1-R_1)^{1/2}$$
$$c_2 = 2bA(A-R_2)(1-R_2)^{1/2}$$
$$c_3 = -2cA(R_3-A)(R_3-1)^{1/2}$$
$$c_4 = A/(8A-8) \qquad (A.3)$$

and
$$C_1 = 4bA(A-R_2)(1-R_2)$$
$$C_2 = 4bA(A-R_2) \qquad (A.4)$$

Appendix B

Rayleigh Cubic Equation: Procedure to find roots R_1, R_2, R_3

The Rayleigh cubic equation in P^2 is given by Richards (1979) as :

$$(A-2P^2)^4 - 16\,X^2\,Y^2\,P^4 = 0 \qquad (B.1)$$

or, $$16(1-A)(P^2-R_1)(P^2-R_2)(P^2-R_3) = 0$$

where P = dimensionless slowness

R_i = Rayleigh roots (i=1 to 3)

$X^2 = 1 - P^2$

$Y^2 = A - P^2$

$$A = \alpha^2/\beta^2 = \frac{2-2\nu}{1-2\nu} \qquad (B.2)$$

However, $R_3^{1/2} = \frac{\alpha}{\gamma}$, where γ = Rayleigh wave speed. Thus, if we know the value of γ , we can reduce the cubic equation to a quadratic equation and solve for R_1 and R_2 .

Achenbach (1973) gives an approximation to the Rayleigh wave speed, in terms of Poisson's ratio, as

$$\gamma \simeq \left[\frac{0.862 + 1.14\nu}{1 + \nu}\right]\beta \quad \text{for } 0 \leq \nu < 0.5 \qquad (B.3)$$

Combining equations (B.1) and (B.2) gives :

$$-\left[\frac{24A^2 - 16A}{16(1 - A)}\right] = R_1 + R_2 + R_3 \qquad (B.4)$$

$$-\frac{8\,A^3}{16(1 - A)} = R_1\,R_2 + R_1\,R_3 + R_2\,R_3 \qquad (B.5)$$

$$- \frac{A^4}{16(1 - A)} = R_1 R_2 R_3 \qquad (B.6)$$

Substituting in the known value for R_3 into equations (B.4) and (B.6), we obtain :

$$- \left[\frac{24A^2 - 16A}{16(1 - A)}\right] - \left(\frac{\alpha}{\gamma}\right)^2 = R_1 + R_2 \qquad (B.7)$$

$$- \frac{A^4}{16(1-A)\left(\frac{\alpha}{\gamma}\right)^2} = R_1 R_2 \qquad (B.8)$$

Substituting equation (B.8) into (B.7) gives

$$R_2^2 + R_2 \left[\frac{24A^2 - 16A}{16(1 - A)} + \left(\frac{\alpha}{\gamma}\right)^2\right] - \left[\frac{A^4}{16(1-A)\left(\frac{\alpha}{\gamma}\right)^2}\right] = 0 \quad . \qquad (B.9)$$

Equation (B.9) gives two real roots R_2 (the lesser of the two is R_1), provided $\nu \leq 0.25$.

Richards (1979) notes that the critical value for real roots is $\nu = 0.263$, but our value differs (by 1%) due to the approximation to R_3 used in equation (B.3).

Figure (B.1) below shows the Rayleigh roots, as in Richards (1979), where, since T is regarded as a value of P, the roots are shown in the complex P-plane.

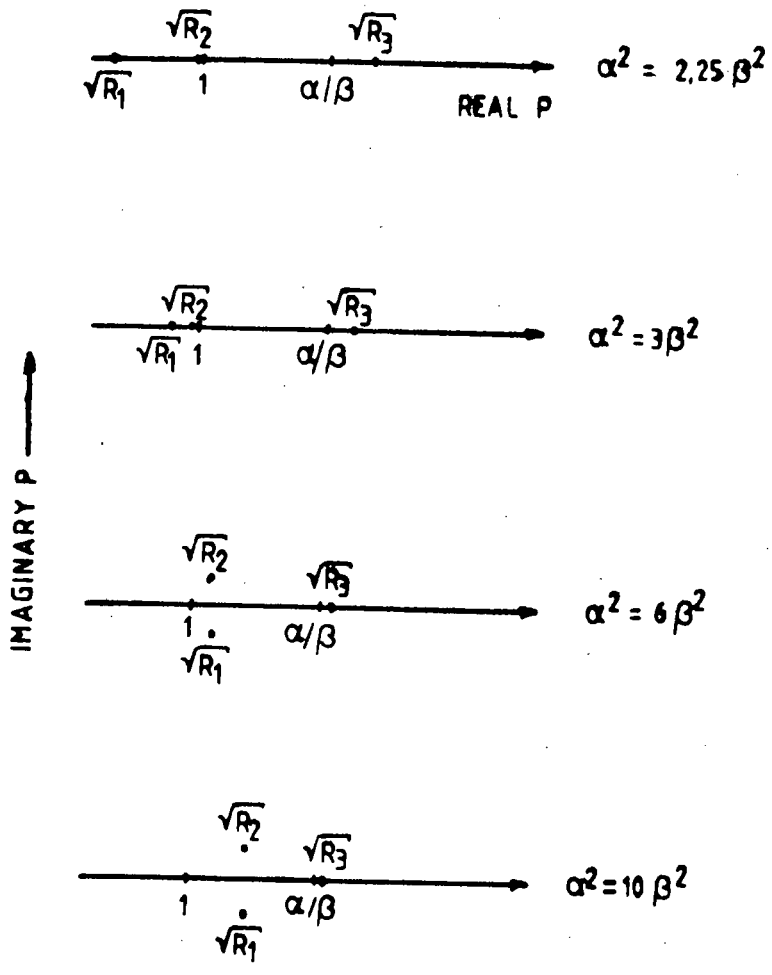

Figure B.1 : Rayleigh roots for various ratios of α^2/β^2

Appendix C

In order to integrate the integral equations (3.32) analytically, it is necessary to transform the variables of integration from Cartesian to polar coordinates. It then is possible to integrate over r analytically. Details are given in this appendix and also in Appendix D. The integration over ϕ is done numerically, using either Romberg numerical integration or Simpson's rule. Results for both integration schemes are presented in Appendix F.

C.1 Coordinate transformation from (x_1 , x_2) to (r , ϕ) system

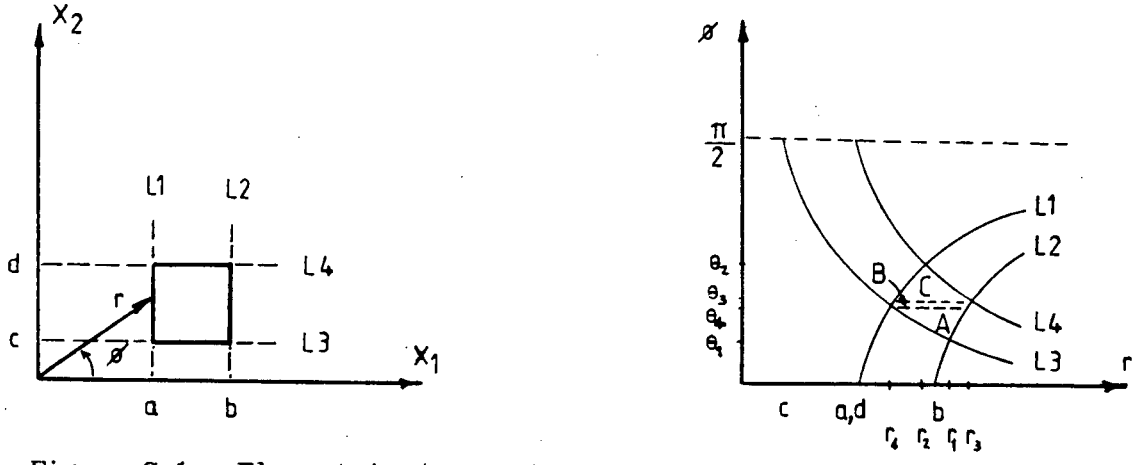

Figure C.1 : Element in (x_1, x_2) system and corresponding element in (r, ϕ) system

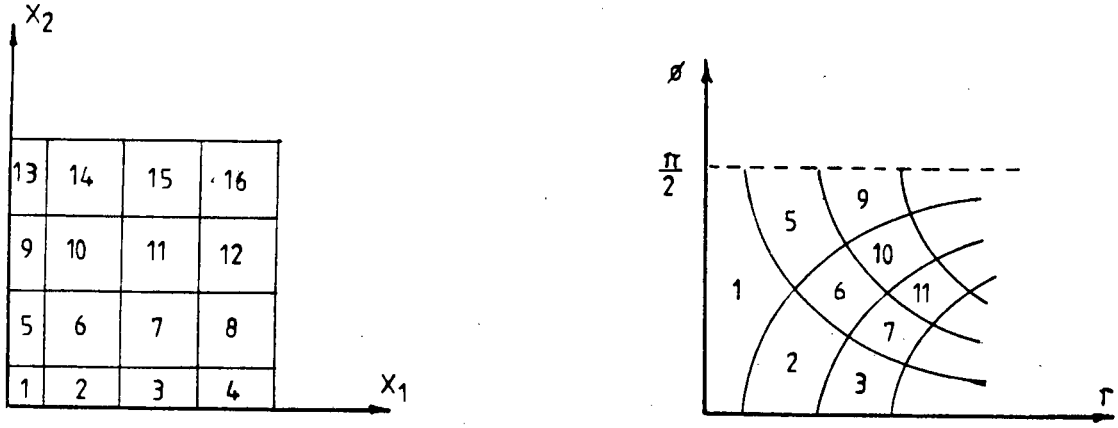

Figure C.2 : (x_1,x_2) and (r,ϕ) systems for a number of elements

The transformation equations are $x_1 = r \cos \phi$, and

$$x_2 = r \sin \phi \ .$$

The transformation introduces a Jacobian factor r since,

$$\iint_{S(x_1,x_2)} f(x_1, x_2)\, dx_1\, dx_2 = \iint_{S(r,\phi)} f(r,\phi)\, \frac{\partial(x_1,x_2)}{\partial(r,\phi)}\, dr\, d\phi \quad ,$$

where $\dfrac{\partial(x_1,x_2)}{\partial(r,\phi)}$ = Jacobian = $\begin{bmatrix} \dfrac{\partial x_1}{\partial r} & \dfrac{\partial x_1}{\partial \phi} \\ \dfrac{\partial x_2}{\partial r} & \dfrac{\partial x_2}{\partial \phi} \end{bmatrix} = \begin{bmatrix} \cos\phi & -r\sin\phi \\ \sin\phi & r\cos\phi \end{bmatrix}$

$$= r \cos^2\phi + r \sin^2\phi$$

$$= r \quad .$$

For a particular element (see Figure C.1) :

$$r = \frac{a}{\cos\phi} = L1 \quad ,$$

$$= \frac{b}{\cos\phi} = L2 \quad ,$$

$$= \frac{c}{\sin\phi} = L3 \quad ,$$

$$= \frac{d}{\sin\phi} = L4 \quad .$$

θ_1 is given by L3 = L2 , or $\dfrac{b}{\cos\phi} = \dfrac{c}{\sin\phi}$.

$$\therefore \quad \tan\phi = \frac{c}{b} \quad \therefore \ \theta_1 = \arctan\left(\frac{c}{b}\right)$$

$$\therefore \ r_1 = \frac{b}{\cos\theta_1} = \frac{c}{\sin\theta_1}$$

θ_2 is given by L1 = L4 , or $\dfrac{a}{\cos\phi} = \dfrac{b}{\sin\phi}$

$$\therefore \quad \tan\phi = \frac{d}{a} \quad \therefore \ \theta_2 = \arctan\left(\frac{d}{a}\right)$$

$$\therefore \ r_2 = \frac{a}{\cos\theta_2} = \frac{d}{\sin\theta_2}$$

θ_3 is given by L3 = L1 , or $\dfrac{a}{\cos\phi} = \dfrac{c}{\sin\phi}$

$\therefore \quad \tan\phi = \dfrac{c}{a} \qquad \therefore \ \phi_3 = \arctan\left(\dfrac{c}{a}\right)$

$$\therefore \ r_3 = \frac{a}{\cos\theta_3} = \frac{c}{\sin\theta_3}$$

θ_4 is given by L4 = L2 , or $\dfrac{b}{\cos\phi} = \dfrac{d}{\sin\phi}$

$\therefore \ \tan\phi = \dfrac{d}{b} \qquad \therefore \ \theta_4 = \arctan\left(\dfrac{d}{b}\right)$

$$\therefore \ r_4 = \frac{d}{\sin\theta_4} = \frac{b}{\cos\theta_4}$$

If $\theta_4 > \theta_3$, then

$$\int_a^b \int_c^d f(x_1,x_2)\, dx_2 dx_1 = \int_{\theta_1}^{\theta_3} \int_{\frac{c}{\sin\phi}}^{\frac{b}{\cos\phi}} f(r,\phi) r\, dr\, d\phi + \int_{\theta_3}^{\theta_4} \int_{\frac{a}{\cos\phi}}^{\frac{b}{\cos\phi}} f(r,\phi) r\, dr\, d\phi$$

$$+ \int_{\theta_4}^{\theta_2} \int_{\frac{a}{\cos\phi}}^{\frac{d}{\sin\phi}} f(r,\phi)\ r\, dr\, d\phi \quad .$$

If $\theta_4 < \theta_3$, then

$$\int_a^b \int_c^d f(x_1,x_2)\, dx_2 dx_1 = \int_{\theta_1}^{\theta_4} \int_{\frac{c}{\sin\phi}}^{\frac{b}{\cos\phi}} f(r,\phi) r\, dr\, d\phi + \int_{\theta_4}^{\theta_3} \int_{\frac{c}{\sin\phi}}^{\frac{d}{\sin\phi}} f(r,\phi) r\, dr\, d\phi$$

$$+ \int_{\theta_3}^{\theta_2} \int_{\frac{a}{\cos\phi}}^{\frac{d}{\sin\phi}} f(r,\phi)\ r\, dr\, d\phi \quad .$$

If $\theta_4 = \theta_3$, then

$$\int_a^b \int_c^d f(x_1,x_2)\, dx_2 dx_1 = \int_{\theta_1}^{\theta_4} \int_{\frac{c}{\sin\phi}}^{\frac{b}{\cos\phi}} f(r,\phi) r\, dr\, d\phi + \int_{\theta_4}^{\theta_2} \int_{\frac{a}{\cos\phi}}^{\frac{d}{\sin\phi}} f(r,\phi) r\, dr\, d\phi$$

C.2 Transformed integral limits : special cases

For the elements running along the x_1 or x_2 axes, one of the transformed integrals drops out of the transformed equations.

For elements along the x_1-axis , $c = 0$. Thus $\theta_1 = \theta_3 = 0$, and $r_1 = b$, $r_3 = a$.

For elements along the x_2-axis , $a = 0$. Thus $\theta_2 = \theta_3 = \pi/2$, and $r_2 = \frac{d}{\sin\theta_2} = d$, $r_3 = \frac{c}{\sin\theta_3} = c$.

Appendix D

D.1 Analytical integration of non-singular Green's functions (with respect to r)

There are only 5 different types of functions to be integrated with respect to r, as can be seen from the Green's functions :

(note: - the Jacobian factor r is included below

- dots on the integral signs indicate integration limits).

$$\int_{\cdot}^{\cdot} r^{-1}.r\,dr = \int_{\cdot}^{\cdot} 1.dr = [r]_{\cdot}^{\cdot} \qquad (D.1)$$

$$\int_{\cdot}^{\cdot} r^{-3}(b^2 r^{-2} - a^2)^{-\frac{1}{2}} r\,dr = \int_{\cdot}^{\cdot} r^{-2}(b^2 r^{-2} - a^2)^{-\frac{1}{2}} dr \qquad (D.2)$$

$$\int_{\cdot}^{\cdot} r^{-3}(a^2 - b^2 r^{-2})^{-\frac{1}{2}} r\,dr = \int_{\cdot}^{\cdot} r^{-2}(a^2 - b^2 r^{-2})^{-\frac{1}{2}} dr \qquad (D.3)$$

$$\int_{\cdot}^{\cdot} r^{-1}(b^2 r^{-2} - a^2)^{\frac{1}{2}} r\,dr = \int_{\cdot}^{\cdot} (b^2 r^{-2} - a^2)^{\frac{1}{2}} dr \qquad (D.4)$$

$$\int_{\cdot}^{\cdot} r^{-1}(a^2 - b^2 r^{-2})^{\frac{1}{2}} r\,dr = \int_{\cdot}^{\cdot} (a^2 - b^2 r^{-2})^{\frac{1}{2}} dr \qquad (D.5)$$

Integrals (D.2) to (D.5) are given below, and were taken from Gradshteyn and Ryzhik (1965) :

$$\int^{\cdot} r^{-2}(b^2\, r^{-2} - a^2)^{-\frac{1}{2}}\, dr = \frac{1}{a} \int^{\cdot} r^{-1} \left(\frac{b^2}{a^2} - r^2 \right)^{-\frac{1}{2}} dr$$

$$= \frac{1}{2b}\, \ell n \left[\frac{b/a - \sqrt{\frac{b^2}{a^2} - r^2}}{b/a + \sqrt{\frac{b^2}{a^2} - r^2}} \right]^{\cdot}$$

$$= \frac{1}{b}\, \ell n \left[\frac{b/a - \sqrt{\frac{b^2}{a^2} - r^2}}{r} \right]^{\cdot} \qquad \text{(D.6)}$$

$$\int^{\cdot} r^{-2}(a^2 - b^2\, r^{-2})^{-\frac{1}{2}}\, dr = \frac{1}{a} \int^{\cdot} r^{-1} \left(r^2 - \frac{b^2}{a^2} \right)^{-\frac{1}{2}} dr$$

$$= \frac{1}{b} \arccos \left(\frac{b}{ar} \right)^{\cdot} \qquad \text{(D.7)}$$

$$\int_{\cdot}^{\cdot} (b^2\, r^{-2} - a^2)^{1/2}\, dr = a \int_{\cdot}^{\cdot} r^{-1} \left(\frac{b^2}{a^2} - r^2 \right)^{1/2} dr$$

$$= \left[\frac{1}{2}\, b\, \ell n \left[\frac{b/a - \sqrt{\left(\frac{b}{a}\right)^2 - r^2}}{b/a + \sqrt{\left(\frac{b}{a}\right)^2 - r^2}} \right] + a \sqrt{\left(\frac{b}{a}\right)^2 - r^2} \right]_{\cdot}^{\cdot}$$

$$= \left[b\, \ell n \left[\frac{b/a - \sqrt{\left(\frac{b}{a}\right)^2 - r^2}}{r} \right] + a \sqrt{\left(\frac{b}{a}\right)^2 - r^2} \right]_{\cdot}^{\cdot}$$

$$\int_{\cdot}^{\cdot} (a^2 - b^2\, r^{-2})^{1/2}\, dr = a \int_{\cdot}^{\cdot} r^{-1} \left(r^2 - \frac{b^2}{a^2} \right)^{1/2} dr \qquad (D.8)$$

$$= \left[- b \arccos \left(\frac{b}{ar} \right) + a \sqrt{r^2 - \frac{b^2}{a^2}} \right]_{\cdot}^{\cdot} \qquad (D.9)$$

D.2 Calculation of Green's functions $\iint g_{11}(\cdot) d\underset{\sim}{\xi}$ and $\iint g_{22}(\cdot)\, d\underset{\sim}{\xi}$

For $T \leq 1$: $\left(t \leq \frac{r}{\alpha} \right)$

$g_{11}^H = g_{12}^H = 0 \quad \therefore \quad F_{11} = F_{12} = 0$.

For $T \geq T_3$: $\left(t \geq \frac{r}{\gamma}\right)$

$$g^H_{11} = \left(\frac{\cos^2\phi}{2\mu\pi r}\right) - \left(\frac{-2c_4 \sin^2\phi}{\mu\pi r}\right) = \left(\frac{1}{\mu\pi r}\right)\left(\frac{\cos^2\phi}{2} + 2\, c_4 \sin^2\phi\right)$$

$$g^H_{12} = \left(\frac{\cos\phi \sin\phi}{2\mu\pi r}\right) + \left(\frac{-2c_4 \cos\phi \sin\phi}{\mu\pi r}\right) = \left(\frac{\cos\phi \sin\phi}{\mu\pi r}\right)\left(\tfrac{1}{2} - 2\, c_4\right)$$

For $\alpha/\beta \leq T < T_3$: $\left(\frac{r}{\beta} \leq t < \frac{r}{\gamma}\right)$

$$g^H_{11} = \left[\left(\frac{\cos^2\phi}{2\mu\pi r}\right) - \left(\frac{2\alpha^2 t^2 c_3 \cos^2\phi}{\mu\pi\, r^3 (T_3^2 - \alpha^2 t^2 r^{-2})^{1/2}}\right)\right] -$$

$$\left[\left(\frac{-2c_4 \sin^2\phi}{\mu\pi r}\right) + \left(\frac{2c_3 \sin^2\phi\, (T_3^2 - \alpha^2 t^2 r^{-2})^{1/2}}{\mu\pi r}\right)\right] .$$

$$g^H_{12} = \left[\left(\frac{\cos\phi \sin\phi}{2\mu\pi r}\right) - \left(\frac{2\alpha^2 t^2 c_3 \cos\phi \sin\phi}{\mu\pi r^3 (T_3^2 - \alpha^2 t^2 r^{-2})^{1/2}}\right)\right] +$$

$$\left[\left(\frac{-2c_4 \sin\phi \cos\phi}{\mu\pi r}\right) + \left(\frac{2c_3 \cos\phi \sin\phi\, (T_3^2 - \alpha^2 t^2 r^{-2})^{1/2}}{\mu\pi r}\right)\right] .$$

For $1 < T < \alpha/\beta$: $\left(\frac{r}{\alpha} < t < \frac{r}{\beta}\right)$

$$g^H_{11} = \left[\left(\frac{\alpha^2 t^2 c_1 \cos^2\phi}{\mu\pi r^3 (\alpha^2 t^2 r^{-2} - T_1^2)^{1/2}}\right) - \left(\frac{\alpha^2 t^2 c_2 \cos^2\phi}{\mu\pi r^3 (\alpha^2 t^2 r^{-2} - T_2^2)^{1/2}}\right) -\right.$$

$$\left.\left(\frac{\alpha^2 t^2 c_3 \cos^2\phi}{\mu\pi r^3 (T_3^2 - \alpha^2 t^2 - r^{-2})^{1/2}}\right)\right]$$

$$- \left[\left(\frac{-c_4 \sin^2\phi}{\mu\pi r}\right) + \left(\frac{c_1 \sin^2\phi(\alpha^2t^2r^{-2} - T_1^2)^{1/2}}{\mu\pi r}\right) - \left(\frac{c_2 \sin^2\phi(\alpha^2t^2r^{-2} - T_2^2)^{1/2}}{\mu\pi r}\right)\right.$$

$$\left. + \left(\frac{c_3 \sin^2\phi(T_3^2 - \alpha^2t^2 r^{-2})^{1/2}}{\mu\pi r}\right)\right] \quad .$$

$$g^H_{12} = \left[\left(\frac{\alpha^2t^2c_1 \cos\phi \sin\phi}{\mu\pi r^3(\alpha^2t^2r^{-2} - T_1^2)^{1/2}}\right) - \left(\frac{\alpha^2t^2c_2 \cos\phi \sin\phi}{\mu\pi r^3(\alpha^2t^2r^{-2} - T_2^2)^{1/2}}\right)\right.$$

$$\left. - \left(\frac{\alpha^2t^2c_3 \cos\phi \sin\phi}{\mu\pi r^3(T_3^2 - \alpha^2 t^2 r^{-2})^{1/2}}\right)\right]$$

$$+ \left[\left(\frac{-c_4 \cos\phi \sin\phi}{\mu\pi r}\right) + \left(\frac{c_1 \cos\phi \sin\phi(\alpha^2t^2 r^{-2} - T_1^2)^{1/2}}{\mu\pi r}\right) -\right.$$

$$\left.\left(\frac{c_2 \cos\phi \sin\phi(\alpha^2t^2 r^{-2} - T_1^2)^{1/2}}{\mu\pi r}\right) + \left(\frac{c_3 \cos\phi \sin\phi(T_3^2 - \alpha^2t^2 r^{-2})^{1/2}}{\mu\pi r}\right)\right]$$

Now define $F^{\pm} = \int\int_{\Omega} g^H(t \pm \frac{\Delta t}{2}) \, d\Omega$

and $\left[\cdot \right]_{\cdot}^{\cdot} a \equiv g^H(.)$ integrated with respect to r ,

where a = index indicating integral type as in the numbered list of integrals at start of this Appendix.

Thus,

For $T \leq 1$: $F^{\pm}_{11} = 0$.

$F^{\pm}_{12} = 0$.

For $T \geq T_3$: $F_{11}^{\pm} = \int_{\phi} \left(\frac{\frac{1}{2}\cos^2\phi + 2c_4\sin^2\phi}{\mu\pi} \right) \left[r \right]_{\cdot}^{\cdot 1} d\phi$

$$F_{12}^{\pm} = \int_{\phi} \left(\frac{\cos\phi \sin\phi}{\mu\pi} \right) \left(\frac{1}{2} - 2c_4 \right) \left[r \right]_{\cdot}^{\cdot 1} d\phi$$

For $\alpha/\beta \leq T < T_3$

$F_{11}^{\pm} =$

$$\int_{\phi} \left\{ \left(\frac{\frac{1}{2}\cos^2\phi + 2\, c_4 \sin^2\phi}{\mu\pi} \right) \left[r \right]_{\cdot}^{\cdot 1} - \left(\frac{2\alpha^2 t^2 c_3 \cos^2\phi}{\mu\pi} \right) \left[\frac{1}{\alpha t} \arccos\left(\frac{\alpha t}{T_3 r} \right) \right]_{\cdot}^{\cdot 3} \right.$$

$$\left. - \left(\frac{2c_3 \sin^2\phi}{\mu\pi} \right) \left[- \alpha t \arccos\left(\frac{\alpha t}{T_3 r} \right) + T_3 \sqrt{r^2 - \frac{\alpha^2 t^2}{T_3^2}} \right]_{\cdot}^{\cdot 5} \right\} d\phi$$

$F_{12}^{\pm} =$

$$\int_{\phi} \left\{ \left(\frac{\cos\phi \sin\phi}{\mu\pi} \right) \left(\frac{1}{2} - 2c_4 \right) \left[r \right]_{\cdot}^{\cdot 1} - \left(\frac{2\alpha^2 t^2 c_3 \cos\phi \sin\phi}{\mu\pi} \right) \left[\frac{1}{\alpha t} \arccos\left(\frac{\alpha t}{T_3 r} \right) \right]_{\cdot}^{\cdot 3} \right.$$

$$\left. + \left(\frac{2c_3 \cos\phi \sin\phi}{\mu\pi} \right) \left[- \alpha t \arccos\left(\frac{\alpha t}{T_3 r} \right) + T_3 \sqrt{r^2 - \frac{\alpha^2 t^2}{T_3^2}} \right]_{\cdot}^{\cdot 5} \right\} d\phi$$

For $1 < T < \alpha/\beta$:

$$F_{11}^{\pm} =$$

$$\int_{\phi} \left\{ \left(\frac{\alpha^2 t^2 \, c_1 \cos^2\phi}{\mu\pi} \right) \left[\frac{1}{\alpha t} \cdot \ell n \left| \frac{\frac{\alpha t}{T_1} - \sqrt{\left(\frac{\alpha t}{T_1}\right)^2 - r^2}}{r} \right| \right]_{\cdot}^{\cdot} 2 \quad -$$

$$\left(\frac{\alpha^2 t^2 \, c_2 \cos^2\phi}{\mu\pi} \right) \left[\frac{1}{\alpha t} \cdot \ell n \left| \frac{\frac{\alpha t}{T_2} - \sqrt{\left(\frac{\alpha t}{T_2}\right)^2 - r^2}}{r} \right| \right]_{\cdot}^{\cdot} 2 \quad -$$

$$\left(\frac{\alpha^2 t^2 \, c_3 \cos^2\phi}{\mu\pi} \right) \left[\frac{1}{\alpha t} \cdot \arccos\left(\frac{\alpha t}{T_3 r}\right) \right]_{\cdot}^{\cdot} 3 + \left(\frac{c_4 \sin^2\phi}{\mu\pi} \right) \left[r \right]_{\cdot}^{\cdot} 1 \quad -$$

$$\left(\frac{c_1 \sin^2\phi}{\mu\pi} \right) \left[\alpha t \, \ell n \left| \frac{\frac{\alpha t}{T_1} - \sqrt{\left(\frac{\alpha t}{T_1}\right)^2 - r^2}}{r} \right| + T_1 \sqrt{\left(\frac{\alpha t}{T_1}\right)^2 - r^2} \right]_{\cdot}^{\cdot} 4 \quad +$$

$$\left(\frac{c_2 \sin^2\phi}{\mu\pi} \right) \left[\alpha t \, \ell n \left| \frac{\frac{\alpha t}{T_2} - \sqrt{\left(\frac{\alpha t}{T_2}\right)^2 - r^2}}{r} \right| + T_2 \sqrt{\left(\frac{\alpha t}{T_2}\right)^2 - r^2} \right]_{\cdot}^{\cdot} 4 \quad -$$

$$\left(\frac{c_3 \sin^2\phi}{\mu\pi} \right) \left[- \alpha t \arccos\left(\frac{\alpha t}{T_3 r}\right) + T_3 \sqrt{r^2 - \left(\frac{\alpha t}{T_3}\right)^2} \right]_{\cdot}^{\cdot} 5 \quad \Big\} \, d\phi$$

$$F_{12}^{\pm} =$$

$$\int_{\phi} \left\{ \left(\frac{\alpha t \, c_1 \cos\phi \sin\phi}{\mu\pi} \right) \left[\ell n \left| \frac{\frac{\alpha t}{T_1} - \sqrt{\left(\frac{\alpha t}{T_1}\right)^2 - r^2}}{r} \right| \right]_{\cdot}^{\cdot 2} - \right.$$

$$\left(\frac{\alpha t \, c_2 \cos\phi \sin\phi}{\mu\pi} \right) \left[\ell n \left| \frac{\frac{\alpha t}{T_2} - \sqrt{\left(\frac{\alpha t}{T_2}\right)^2 - r^2}}{r} \right| \right]_{\cdot}^{\cdot 2} -$$

$$\left(\frac{\alpha t \, c_3 \cos\phi \sin\phi}{\mu \pi} \right) \left[\arccos \left(\frac{\alpha t}{T_3 r} \right) \right]_{\cdot}^{\cdot 3} - \left(\frac{c_4 \cos\phi \sin\phi}{\mu \pi} \right) \left[r \right]_{\cdot}^{\cdot 1} +$$

$$\left(\frac{c_1 \cos\phi \sin\phi}{\mu\pi} \right) \left[\ell n \left| \frac{\frac{\alpha t}{T_1} - \sqrt{\left(\frac{\alpha t}{T_1}\right)^2 - r^2}}{r} \right| + T_1 \sqrt{\left(\frac{\alpha t}{T_1}\right)^2 - r^2} \right]_{\cdot}^{\cdot 4} -$$

$$\left(\frac{c_2 \cos\phi \sin\phi}{\mu\pi} \right) \left[\alpha t \, \ell n \left| \frac{\frac{\alpha t}{T_2} - \sqrt{\left(\frac{\alpha t}{T_2}\right)^2 - r^2}}{r} \right| + T_2 \sqrt{\left(\frac{\alpha t}{T_2}\right)^2 - r^2} \right]_{\cdot}^{\cdot 4} +$$

$$\left. \left(\frac{c_3 \cos\phi \sin\phi}{\mu\pi} \right) \left[- \alpha t \arccos \left(\frac{\alpha t}{T_3 r} \right) + T_3 \sqrt{r^2 - \left(\frac{\alpha t}{T_3}\right)^2} \right]_{\cdot}^{\cdot 5} \right\} d\phi$$

Simplifying for $\alpha/\beta \leq T < T_3$,

$$F_{11}^{\pm} =$$

$$\int_{\phi} \left(\frac{-2c_3}{\mu\pi}\right)\left[\left(\cos^2\phi - \sin^2\phi\right)\left(\alpha t \arccos\left(\frac{\alpha t}{T_3 r}\right)\right) + \sin^2\phi \;\; T_3 \sqrt{r^2 - \left(\frac{\alpha t}{T_3}\right)^2}\right]_{\cdot}^{\cdot} d\phi$$

$$F_{12}^{\pm} =$$

$$\int_{\phi} \left(\frac{-2c_3 \cos\phi \sin\phi}{\mu\pi}\right) \left[2\alpha t \arccos\left(\frac{\alpha t}{T_3 r}\right) + T_3 \sqrt{r^2 - \left(\frac{\alpha t}{T_3}\right)^2}\right]_{\cdot}^{\cdot} d\phi$$

Simplifying for $1 < T < \alpha/\beta$,

$$F_{11}^{\pm} =$$

$$\int_{\phi} \left\{ \frac{\alpha t}{\mu\pi} \left(\cos^2\phi - \sin^2\phi\right)\left[c_1 \ell n \left|\frac{\frac{\alpha t}{T_1} - \sqrt{\left(\frac{\alpha t}{T_1}\right)^2 - r^2}}{r}\right| - c_2 \ell n \left|\frac{\frac{\alpha t}{T_2} - \sqrt{\left(\frac{\alpha t}{T_2}\right)^2 - r^2}}{r}\right| \right.\right.$$

$$\left. - c_3 \arccos\left(\frac{\alpha t}{T_3 r}\right)\right]_{\cdot}^{\cdot}$$

$$\left. - \frac{\sin^2\phi}{\mu\pi}\left[c_1 T_1 \sqrt{\left(\frac{\alpha t}{T_1}\right)^2 - r^2} - c_2 T_2 \sqrt{\left(\frac{\alpha t}{T_2}\right)^2 - r^2} + c_3 T_3 \sqrt{r^2 - \left(\frac{\alpha t}{T_3}\right)^2}\right]_{\cdot}^{\cdot}\right\} d\phi$$

and $F^{\pm}_{12} =$

$$\int_{\phi} \left\{ \left(\frac{2\alpha t \cos\phi \sin\phi}{\mu\pi} \right) \left[c_1 \ell n \left| \frac{\frac{\alpha t}{T_1} - \sqrt{\left(\frac{\alpha t}{T_1}\right)^2 - r^2}}{r} \right| - c_2 \ell n \left| \frac{\frac{\alpha t}{T_2} - \sqrt{\left(\frac{\alpha t}{T_2}\right)^2 - r^2}}{r} \right| \right.\right.$$

$$\left.\left. - c_3 \arccos\left(\frac{\alpha t}{T_3 r}\right) \right]_{\cdot}^{\cdot} \right.$$

$$\left. + \left(\frac{\cos\phi \sin\phi}{\mu \pi} \right) \left[c_1 T_1 \sqrt{\left(\frac{\alpha t}{T_1}\right)^2 - r^2} - c_2 T_2 \sqrt{\left(\frac{\alpha t}{T_2}\right)^2 - r^2} + c_3 T_3 \sqrt{r^2 - \left(\frac{\alpha t}{T_3}\right)^2} \right]_{\cdot}^{\cdot} \right\} d\phi$$

To do the numerical integration over ϕ , each $\int_{\phi} \ldots d\phi$ integral must be written as

$$\int_{\theta_1}^{\theta_3} \ldots d\phi + \int_{\theta_3}^{\theta_4} \ldots d\phi + \int_{\theta_4}^{\theta_2} \ldots d\phi \quad \text{if} \quad \theta_4 > \theta_3 \quad ,$$

$$\int_{\theta_1}^{\theta_4} \ldots d\phi + \int_{\theta_4}^{\theta_3} \ldots d\phi + \int_{\theta_3}^{\theta_2} \ldots d\phi \quad \text{if} \quad \theta_4 < \theta_3 \quad ,$$

$$\int_{\theta_1}^{\theta_3} \ldots d\phi + \int_{\theta_3}^{\theta_2} \ldots d\phi \quad \text{if} \quad \theta_4 = \theta_3 \quad ,$$

where θ_1 , θ_2 , θ_3 are given in Appendix C.

Also, when substituting in the limits of r, the integrals must be further sub-divided according to whether $\gamma t < r \leq \beta t < r < \alpha t$,

$r \geq \alpha t$ or $r \leq \gamma t$

Appendix E

E.1 Structure of fracture propagation programs

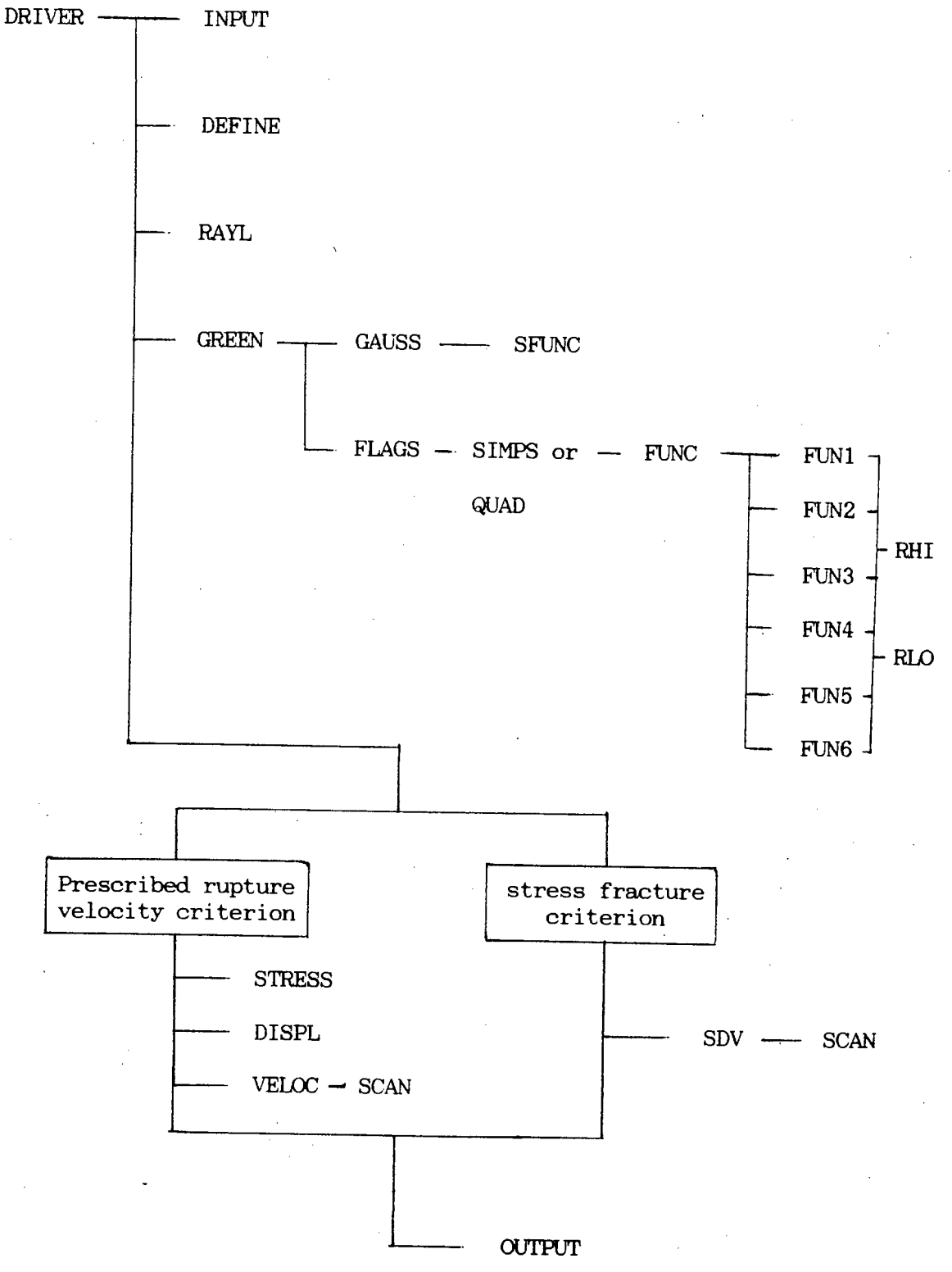

E.2 Structure of ground motion simulation program

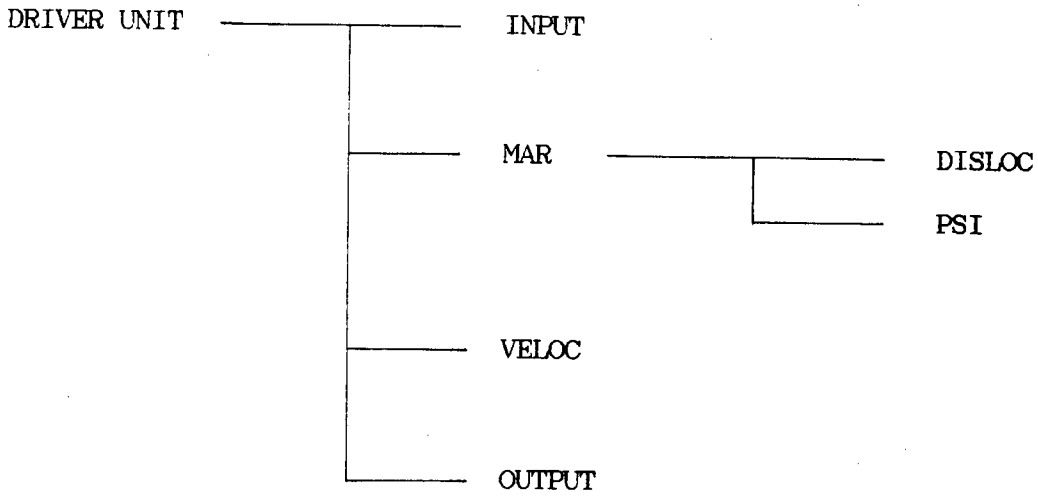

Appendix F

Fracture Propagation Model Results

The plots appearing in this appendix are identified according to a plotfile number appearing at the base of each plot (e.g. EDPGO3, EDPSDVO5, etc.). The letters "SDV" mean that the plot is a stress, displacement or velocity plot, and the letter "G" means that the plot is a Green's function plot. Spatial (i,j) and temporal (k) mesh positions are indicated on each plot in capital letters. (Standard S.I. units are used throughout).

The plotfile numbers are given by :

03 : SIM, MAT1, $\alpha\Delta t/\Delta x = 0.5$, $\tau^{o}_{13} = 0.5 \times 10^{7}$ Pa, SS

04 : ROM, MAT1, $\alpha\Delta t/\Delta x = 0.5$, $\tau^{o}_{13} = 0.5 \times 10^{7}$, fracture criterion

05 : ROM, MAT1, $\alpha\Delta t/\Delta x = 0.5$, $\tau^{o}_{13} = 0.5 \times 10^{7}$, SS

06 : SIM, MAT1, $\alpha\Delta t/\Delta x = 0.5$, $\tau^{o}_{13} = 0.5 \times 10^{7}$, $r_{min} = 0.$, $r_{max} = 3\Delta x$

08 : SIM, MAT2, $\alpha\Delta t/\Delta x = 0.5$, $\tau^{o}_{13} = 90.43$ Pa, SS

10 : ROM, MAT2, $\alpha\Delta t/\Delta x = 0.5$, $\tau^{o}_{13} = 90.43$, SS

11 : ROM, MAT2, $\alpha\Delta t/\Delta x = 0.25$, $\tau^{o}_{13} = 90.43$, SS

12 : SIM, MAT2, $\alpha\Delta t/\Delta x = 0.25$, $\tau^{o}_{13} = 90.43$, SS

13 : SIM, MAT2, $\alpha\Delta t/\Delta x = 1.0$, $\tau^{o}_{13} = 90.43$, SS

where SIM = Simpson's rule numerical integration of the Green's functions

ROM = Romberg scheme numerical integration of the Green's functions

MAT1 = material set 1 (ρ = 2700. kg/m^3, E = 75 x 10^9 Pa, ν = 0.25)

MAT2 = material set 2 (ρ = 2700. kg/m^3, E = 2375 Pa, ν = 0.25)

SS = self-similar crack (prescribed rupture velocity).

The continuous curves on the displacement time-histories are the analytical solution curves.

The two-dimensional plots each contain two curves denoting the x_1- and x_2-directions as follows :

x_1 :

x_2 :

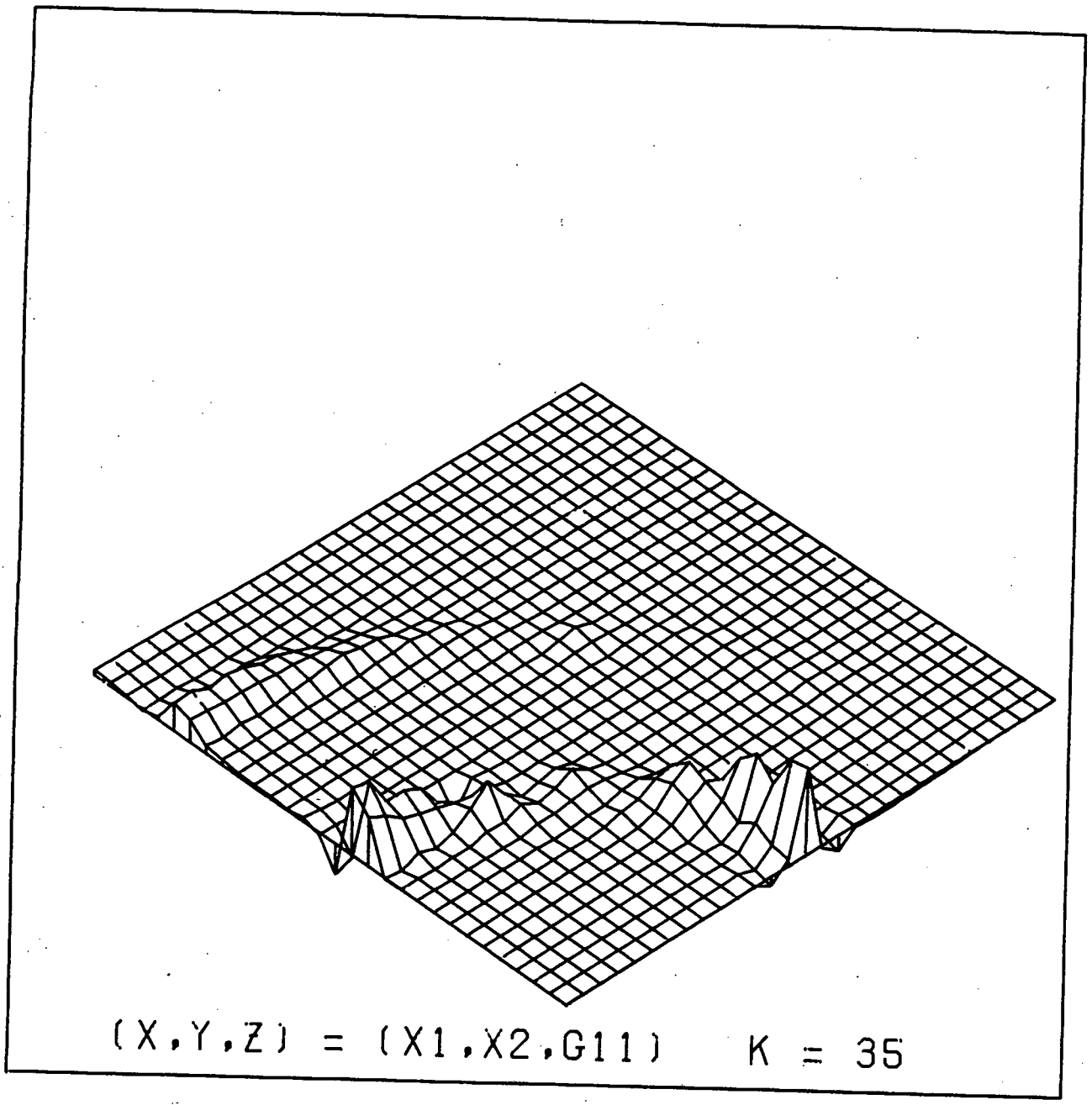

EDPG05

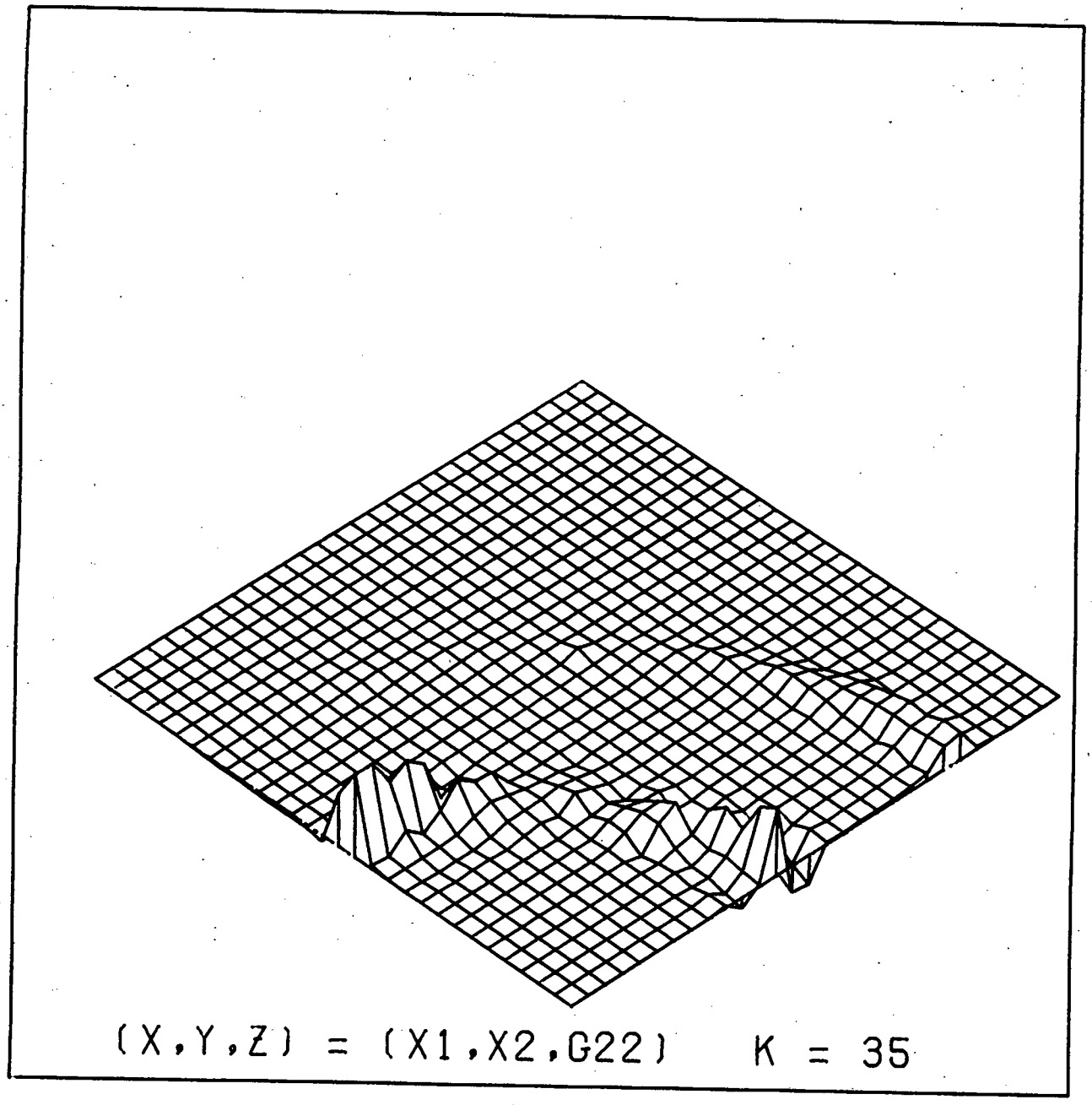

EDPG05

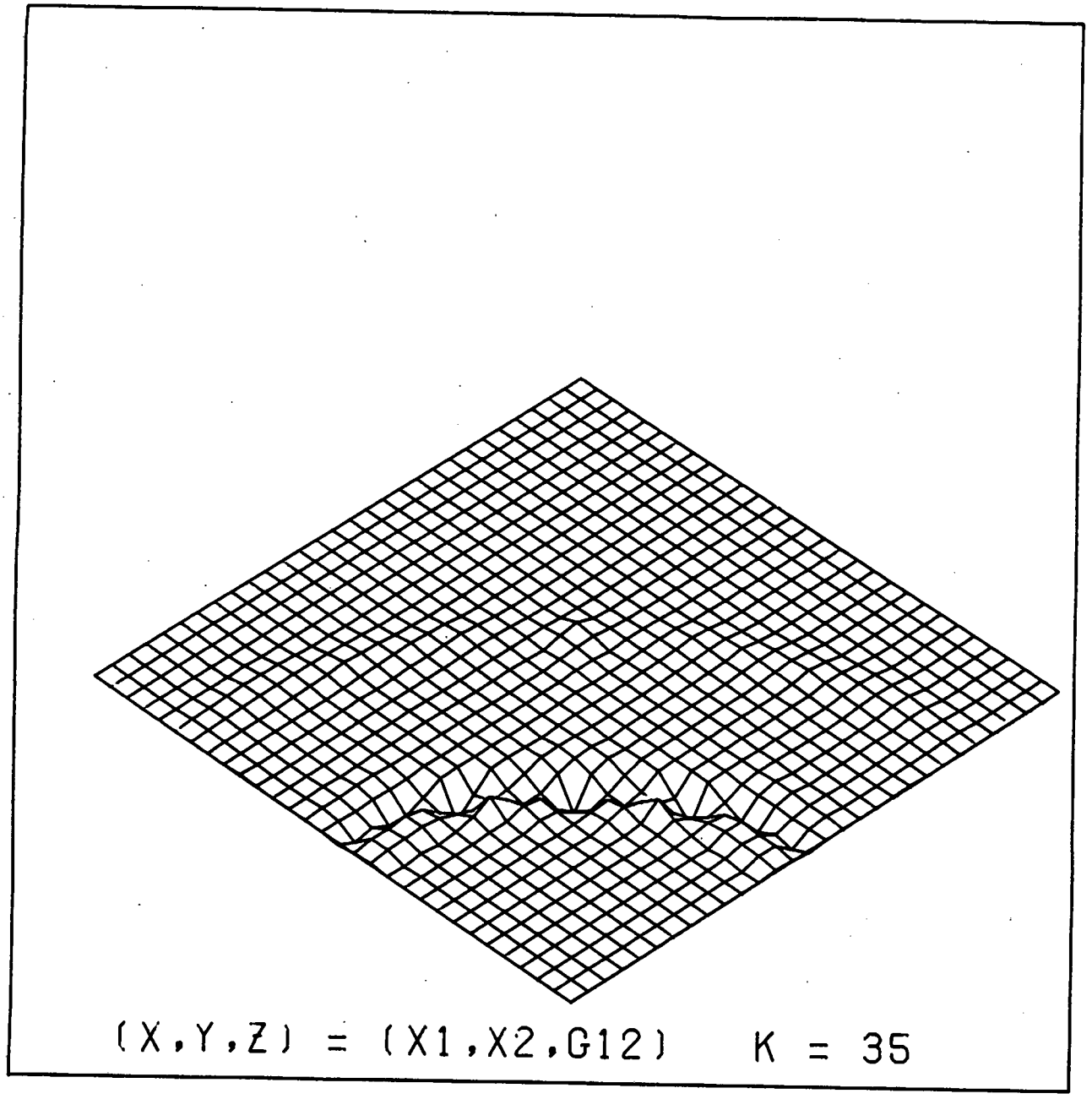

EDPG05

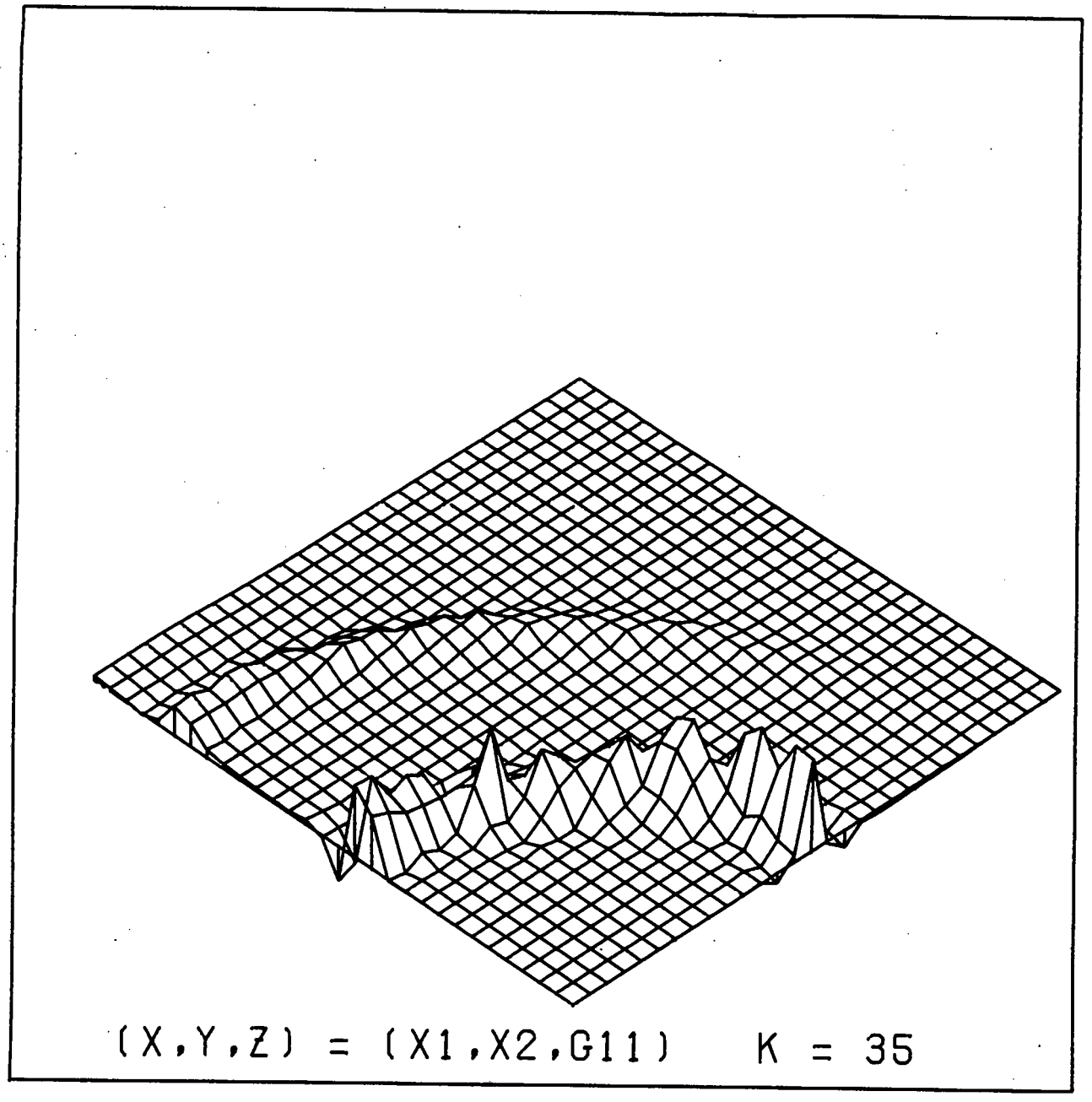

EDPG03

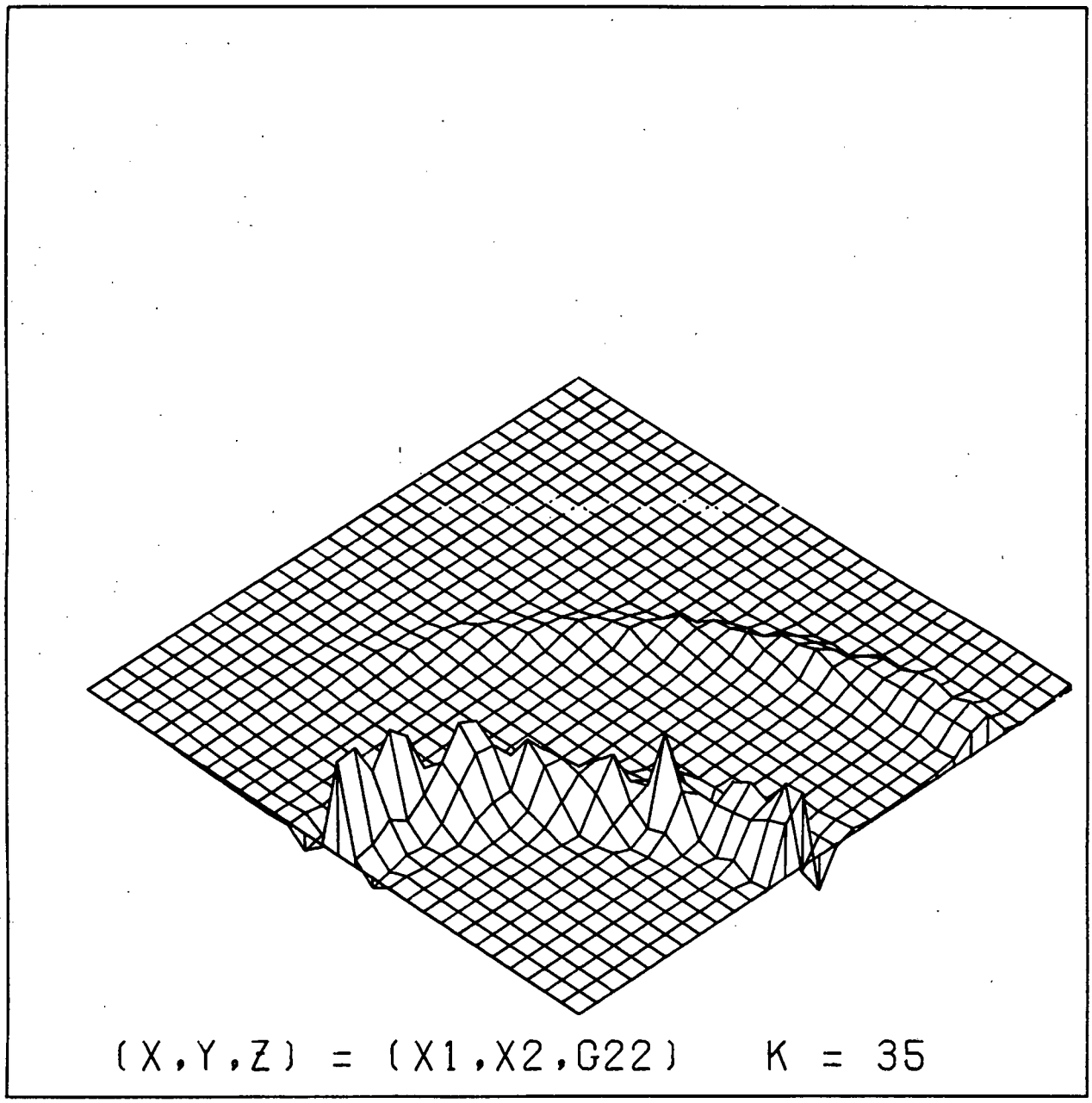

EDPG03

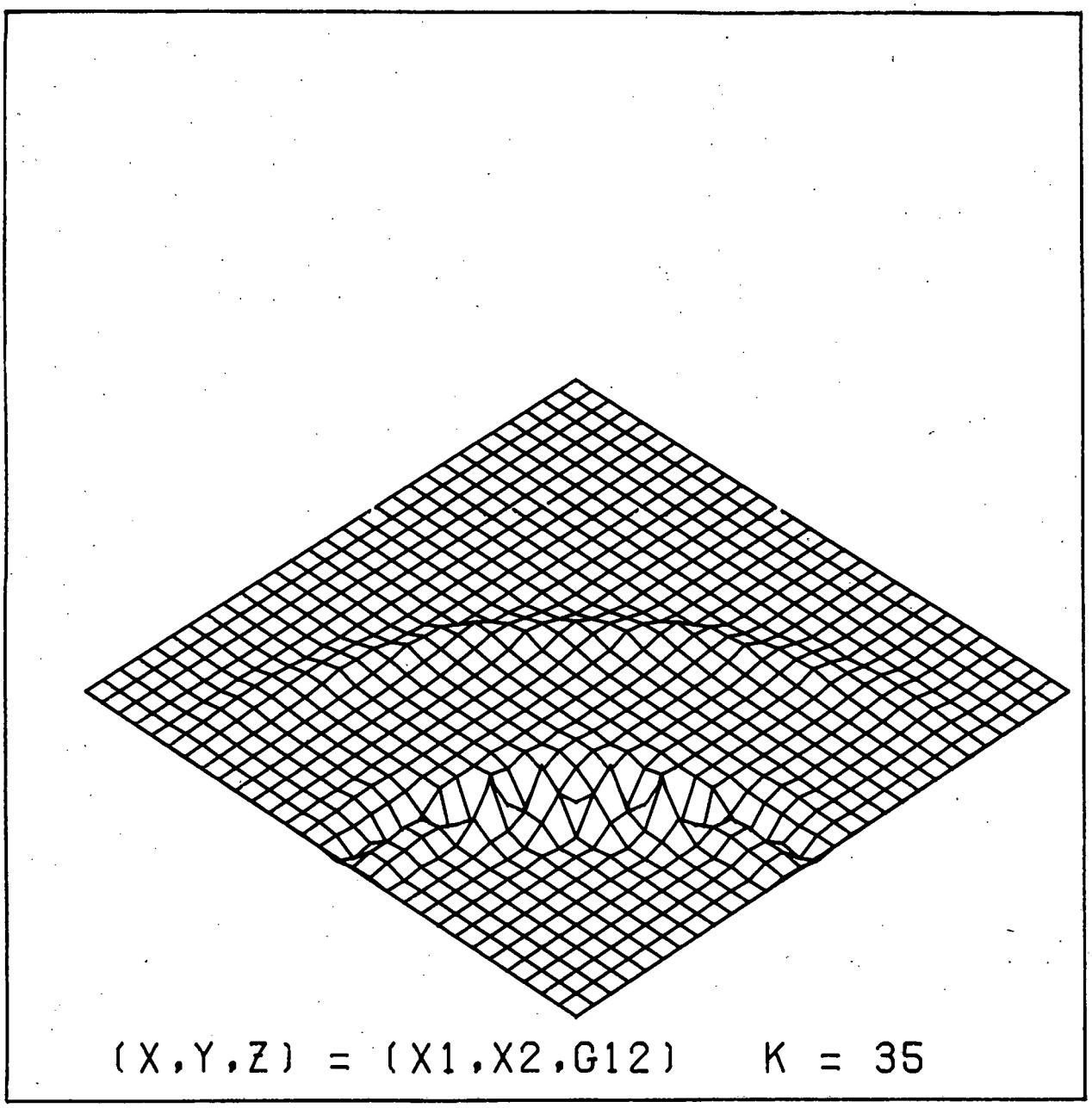

EDPG03

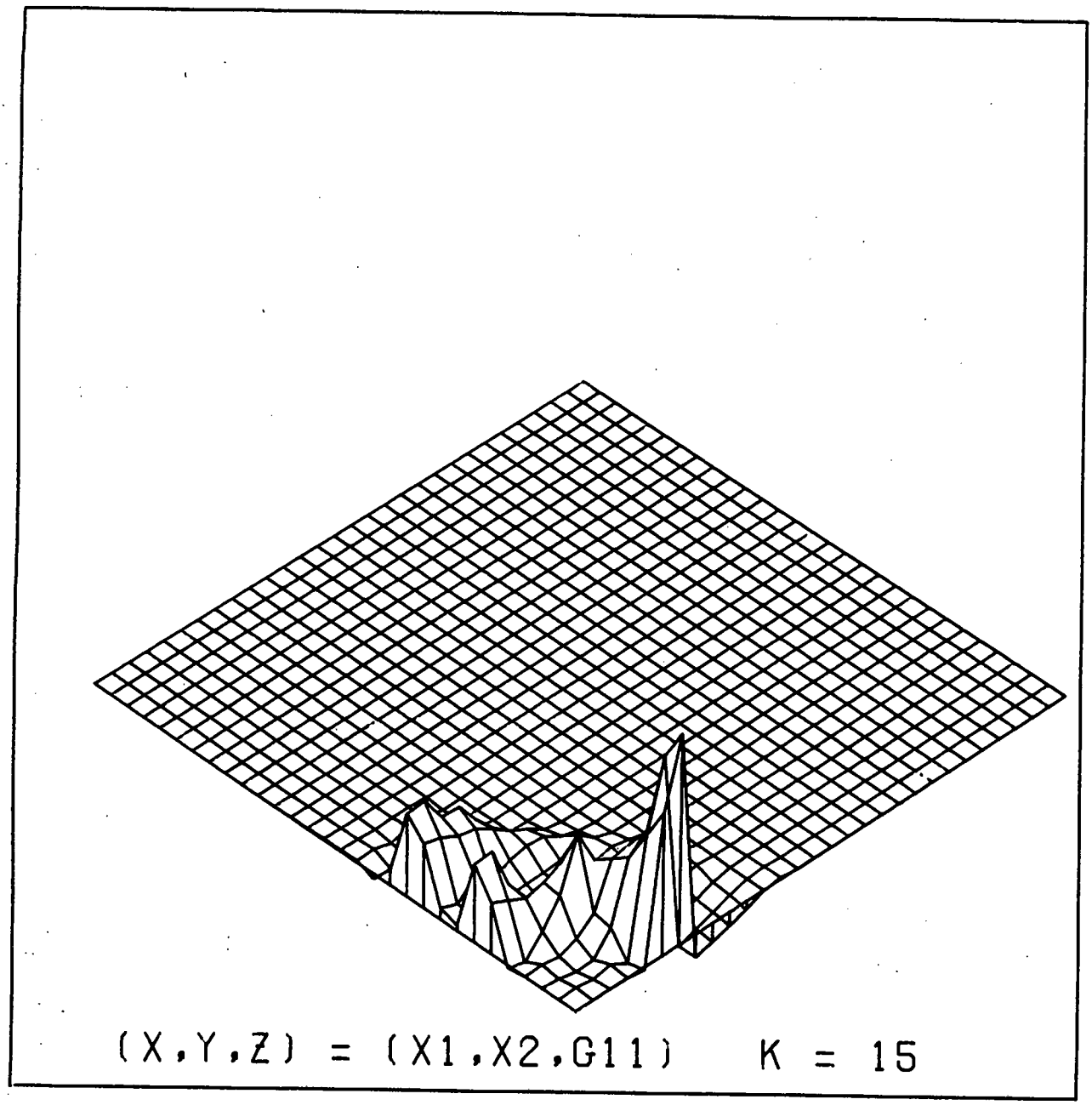

EDPG03

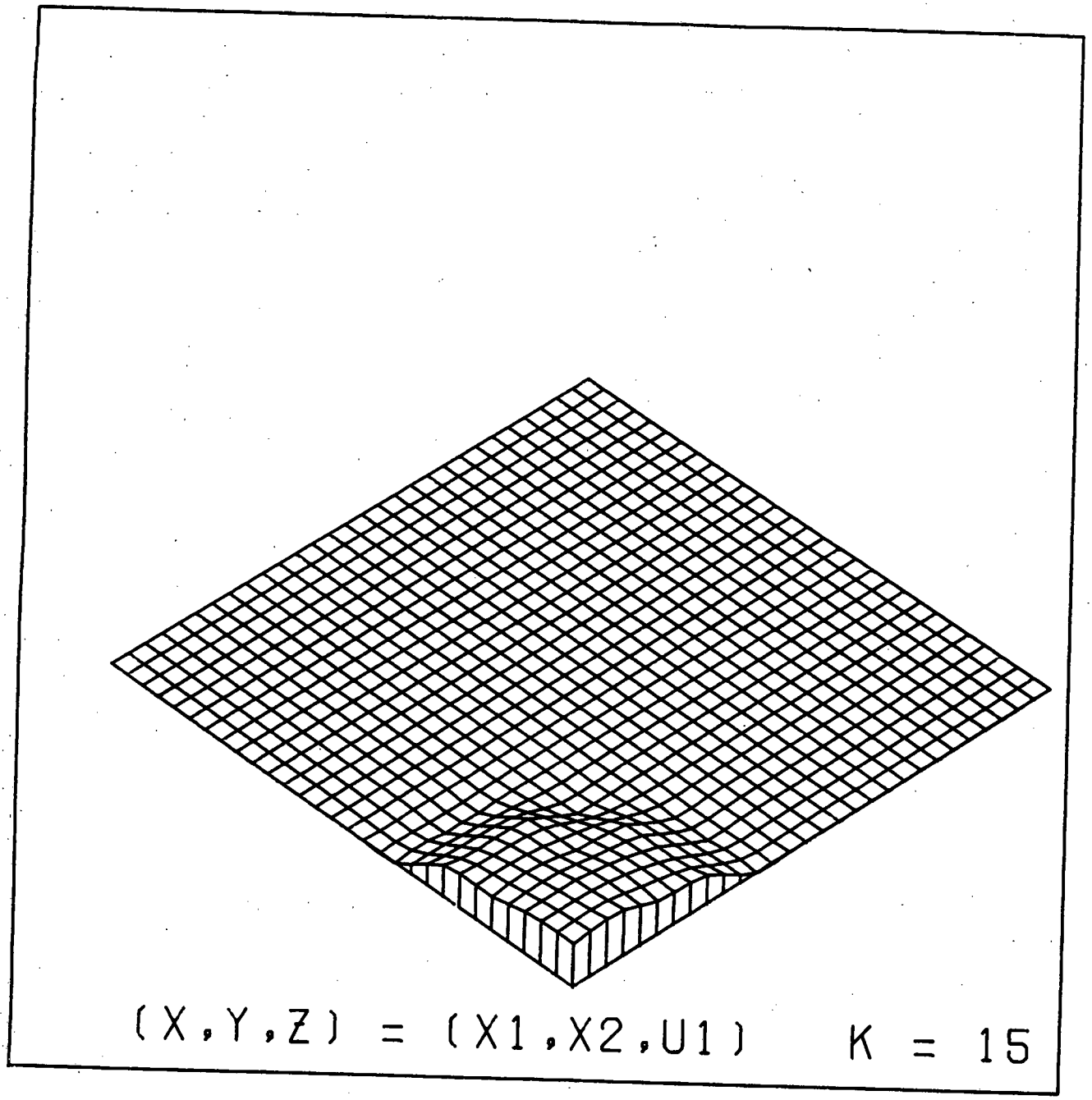

EDPSDV08

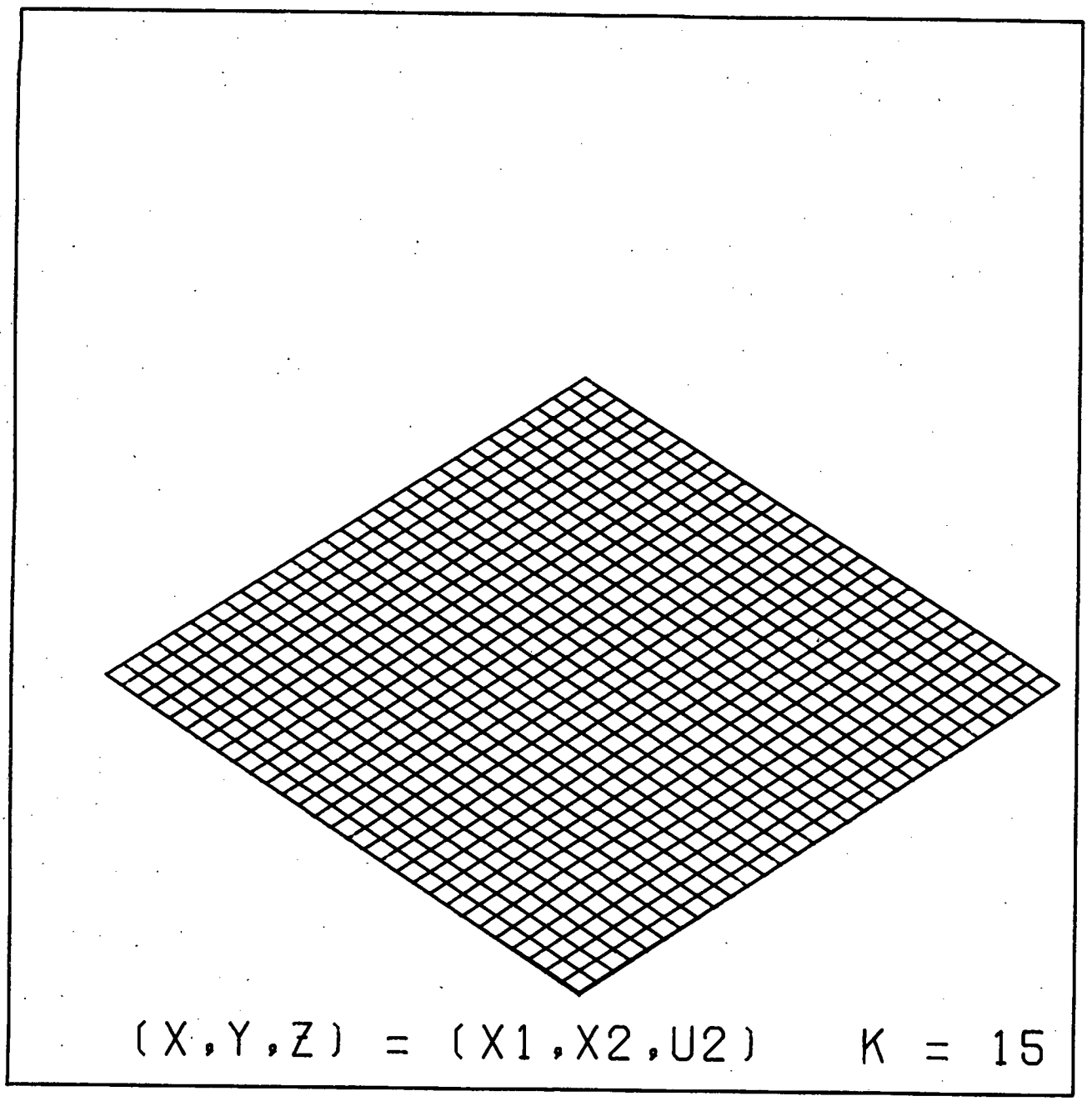

EDPSDV08

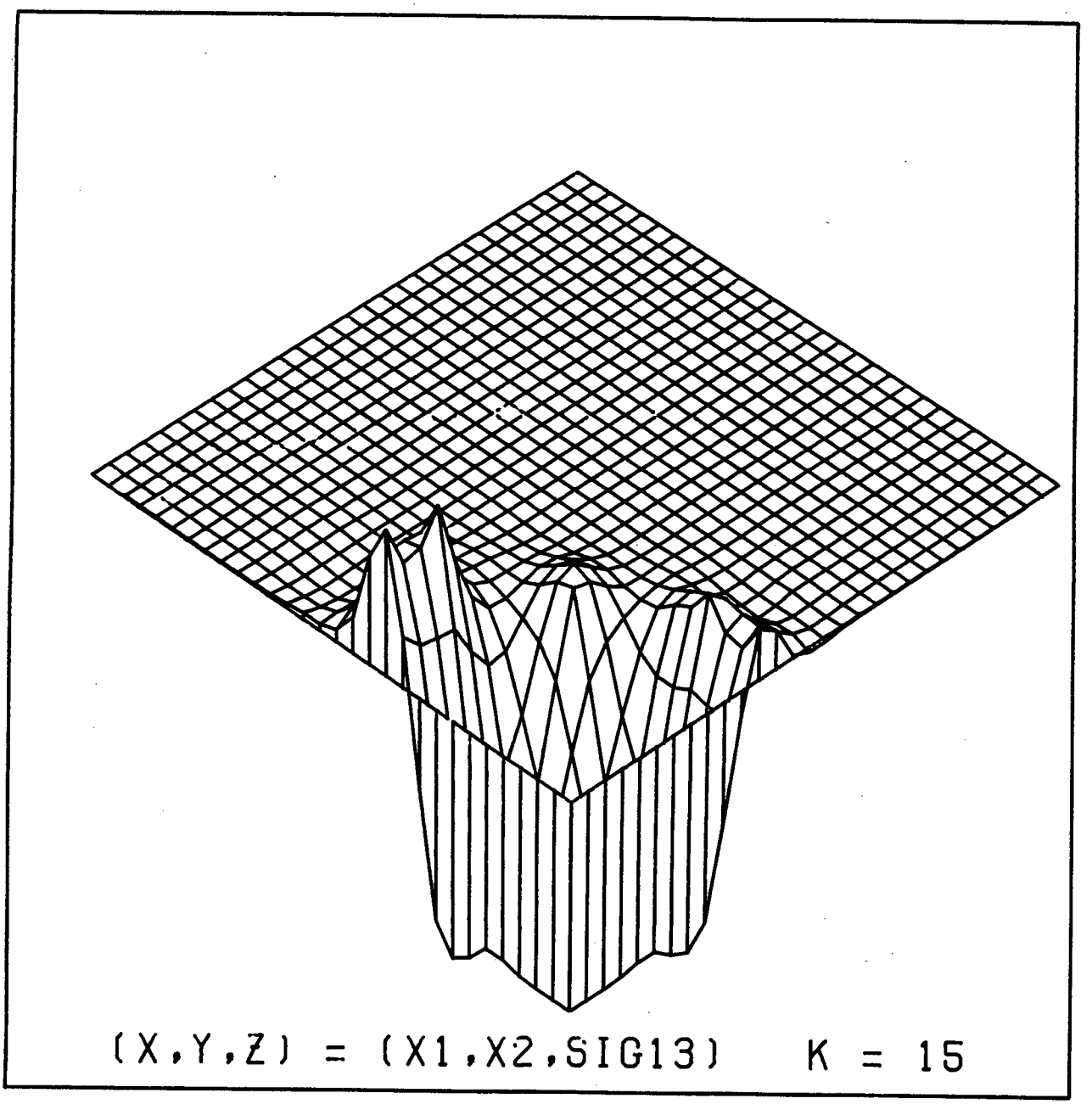

EDPSDV08

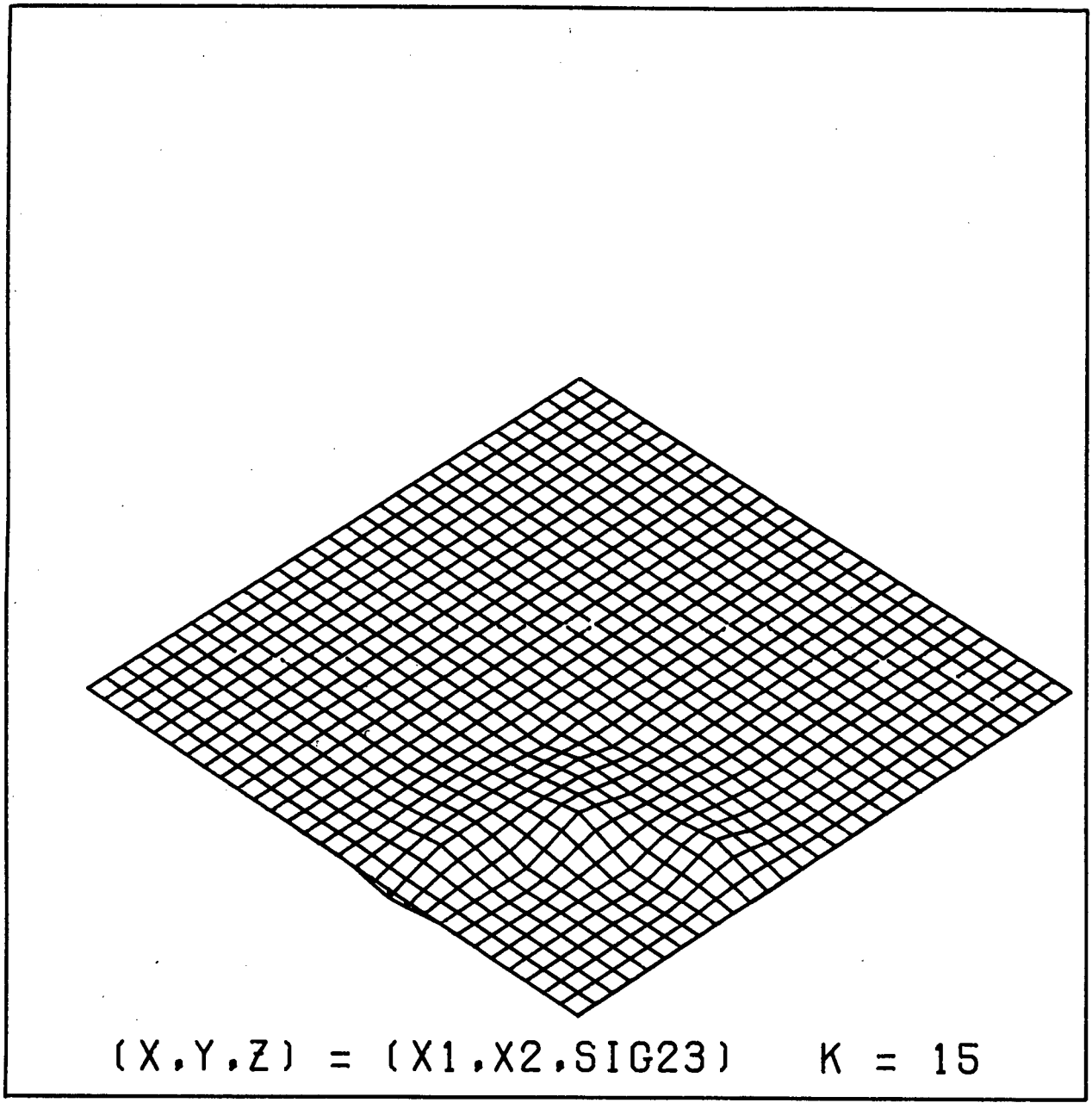

EDPSDV08

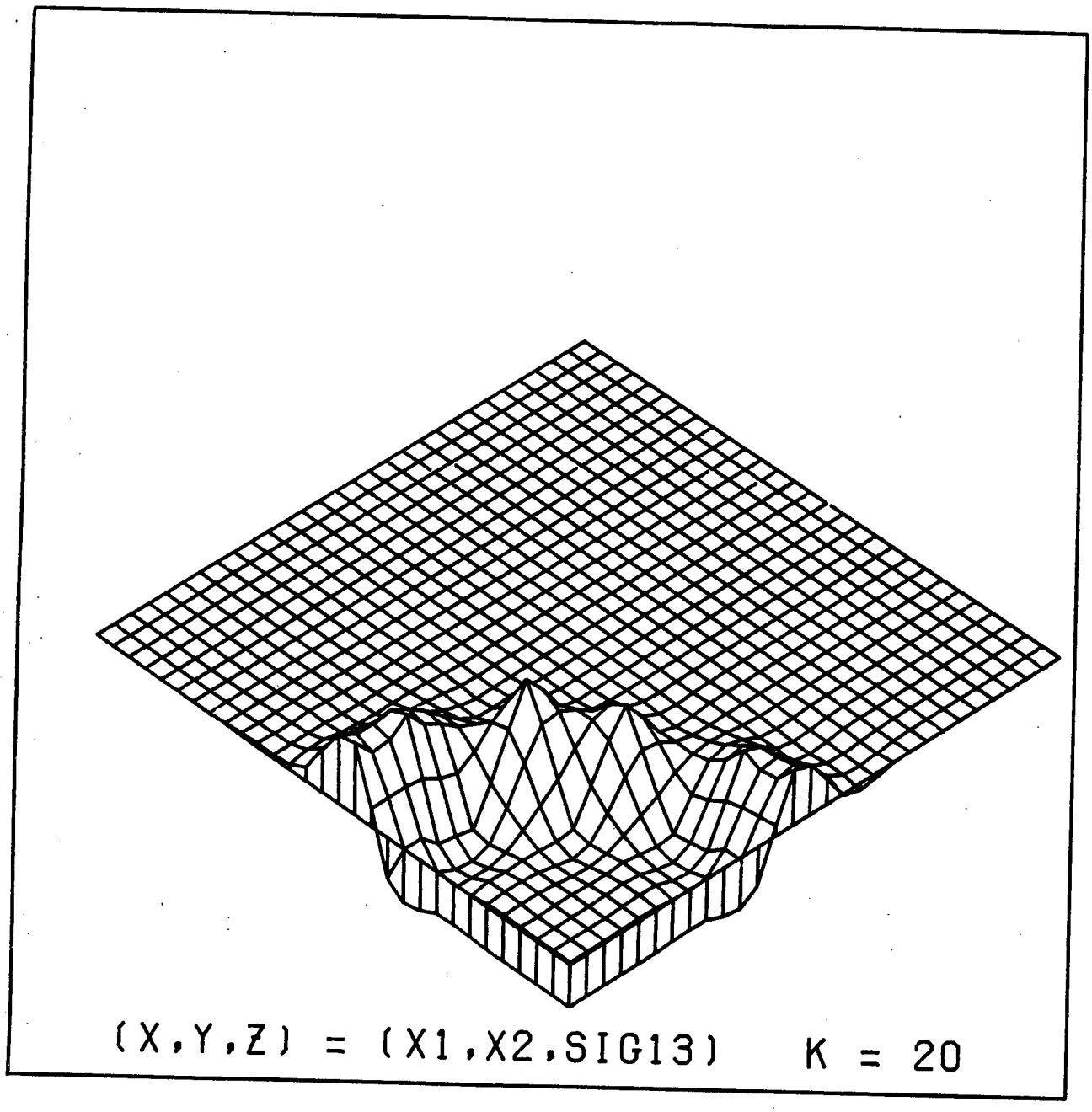

EDPSDV08

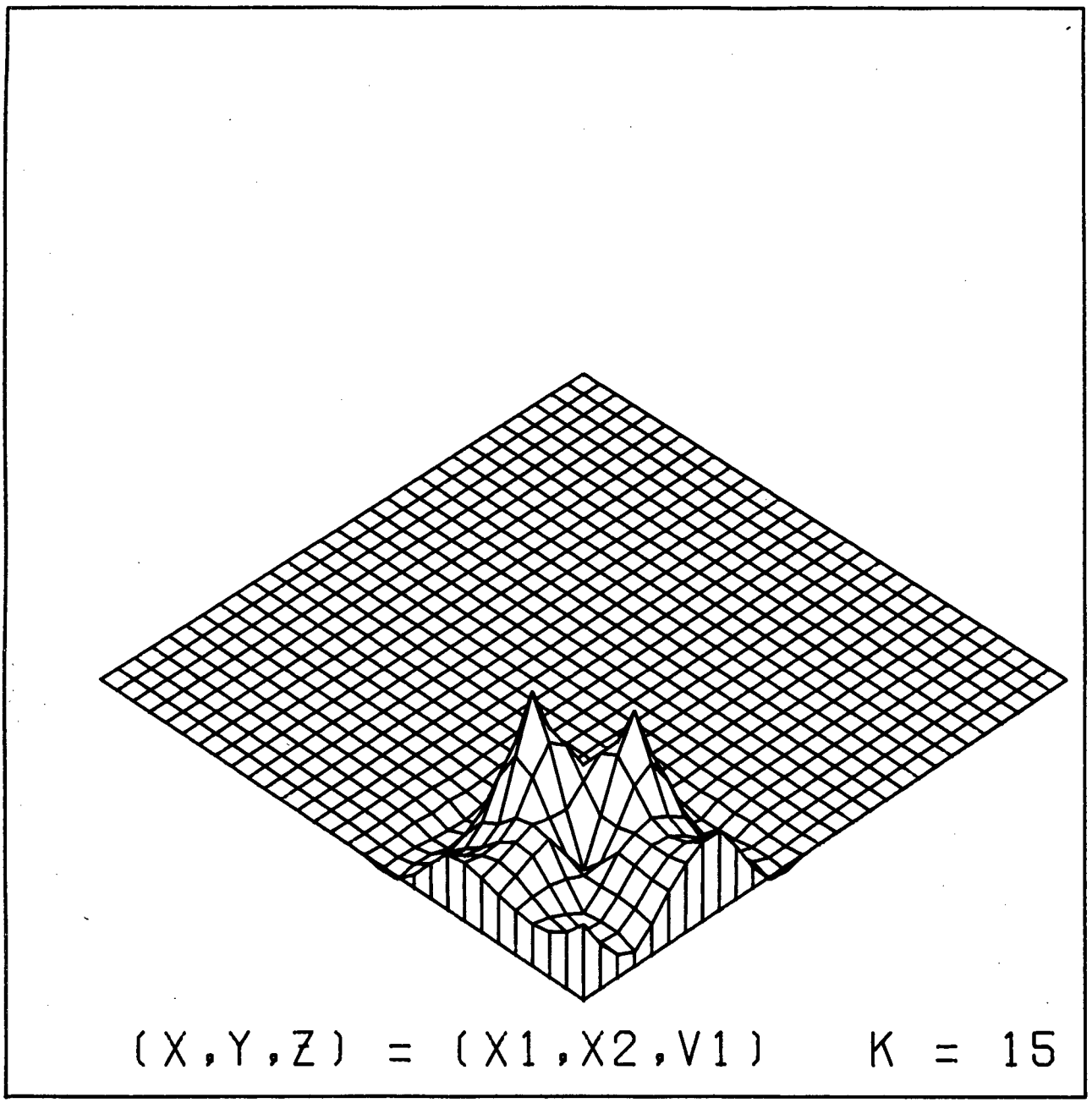

EDPSDV08

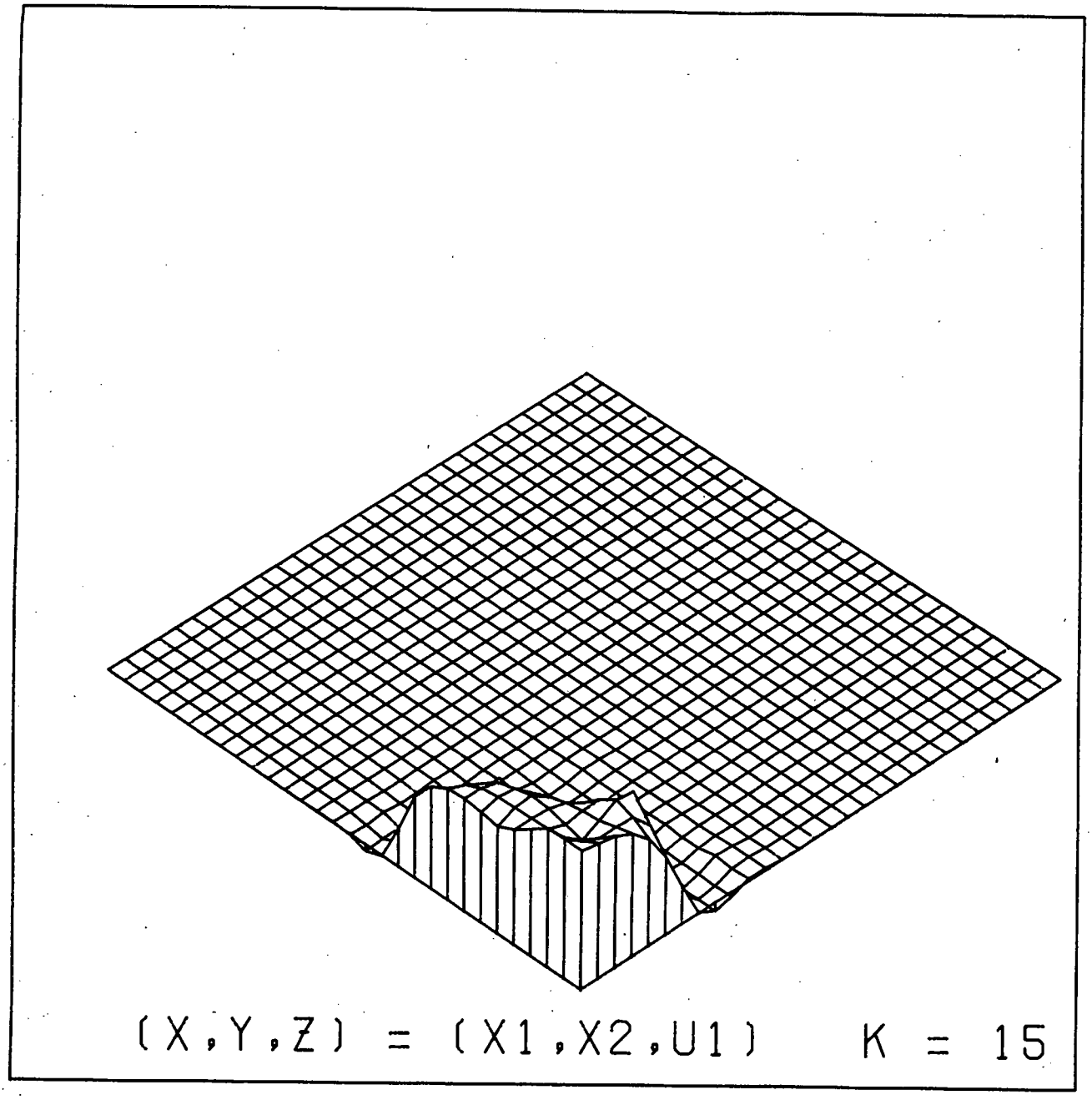

EDPSDV04

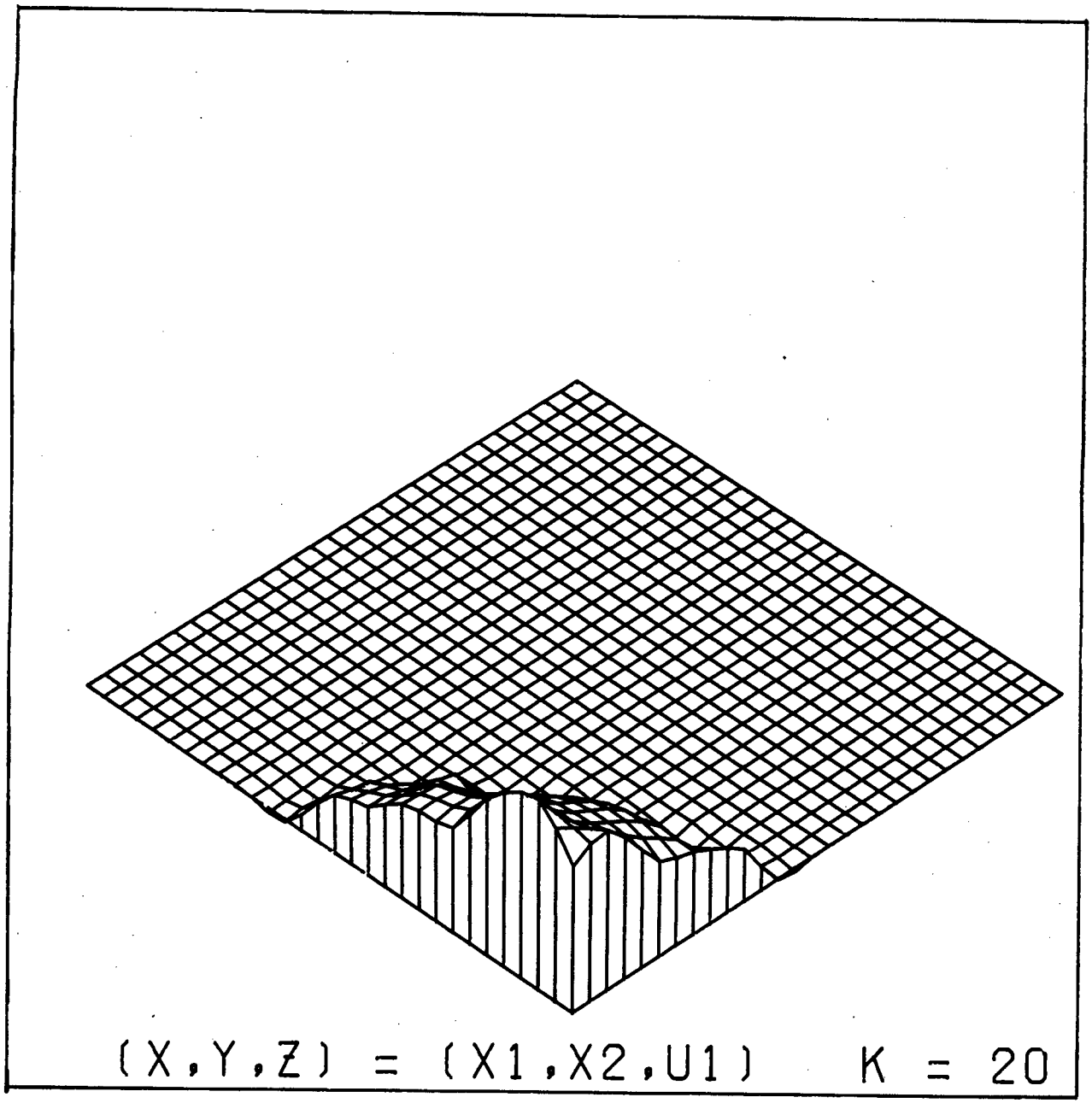

EDPSDV04

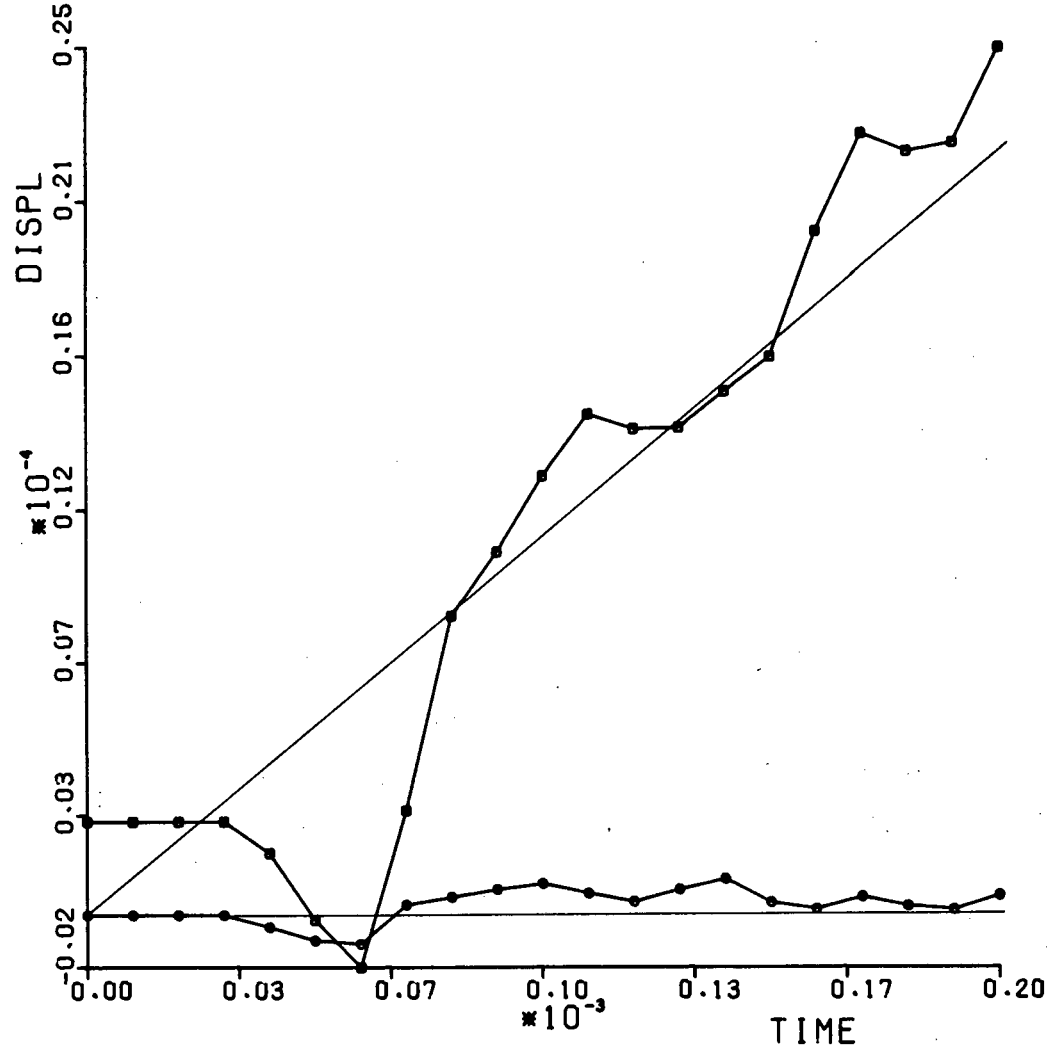

(I,J) = (0,0) EDPSDV03

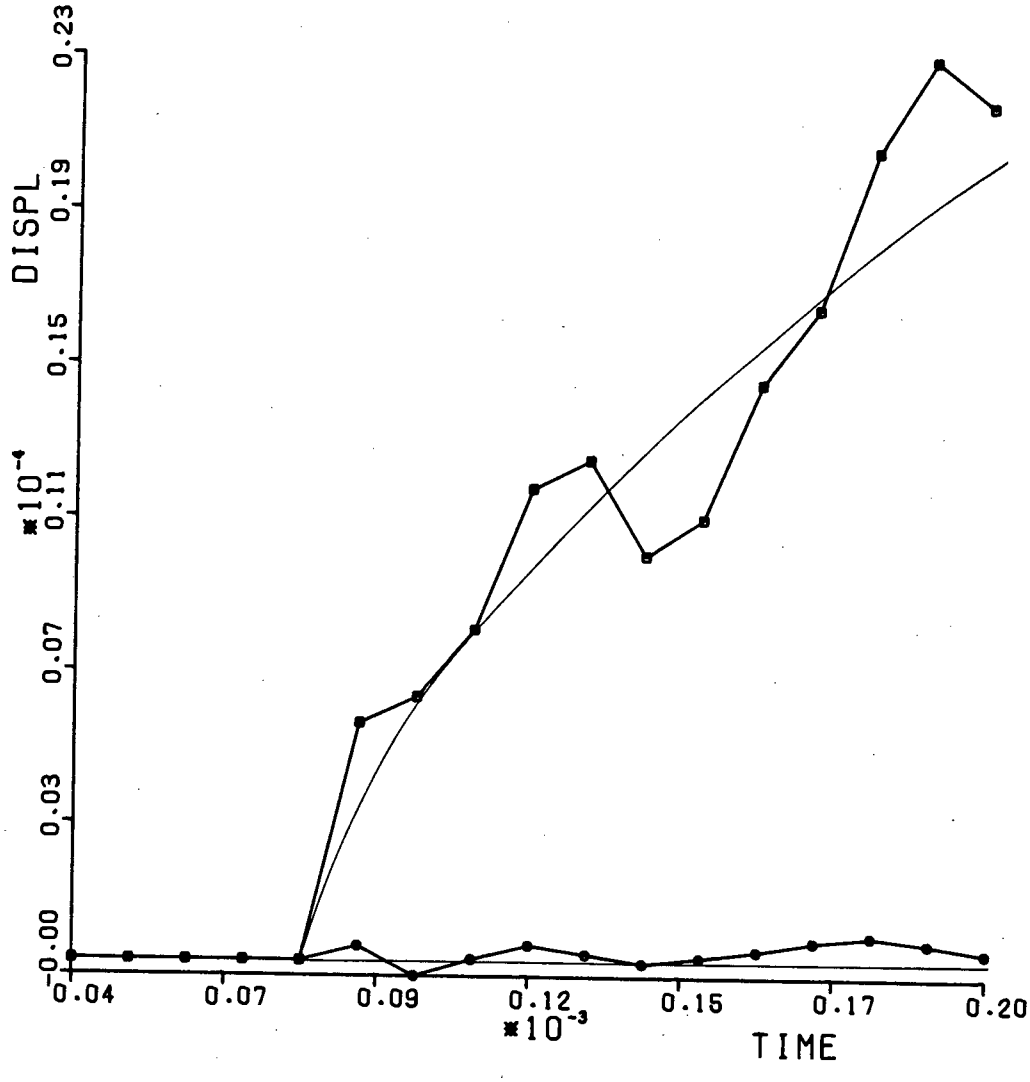

(I,J) = (2,0) EDPSDV03

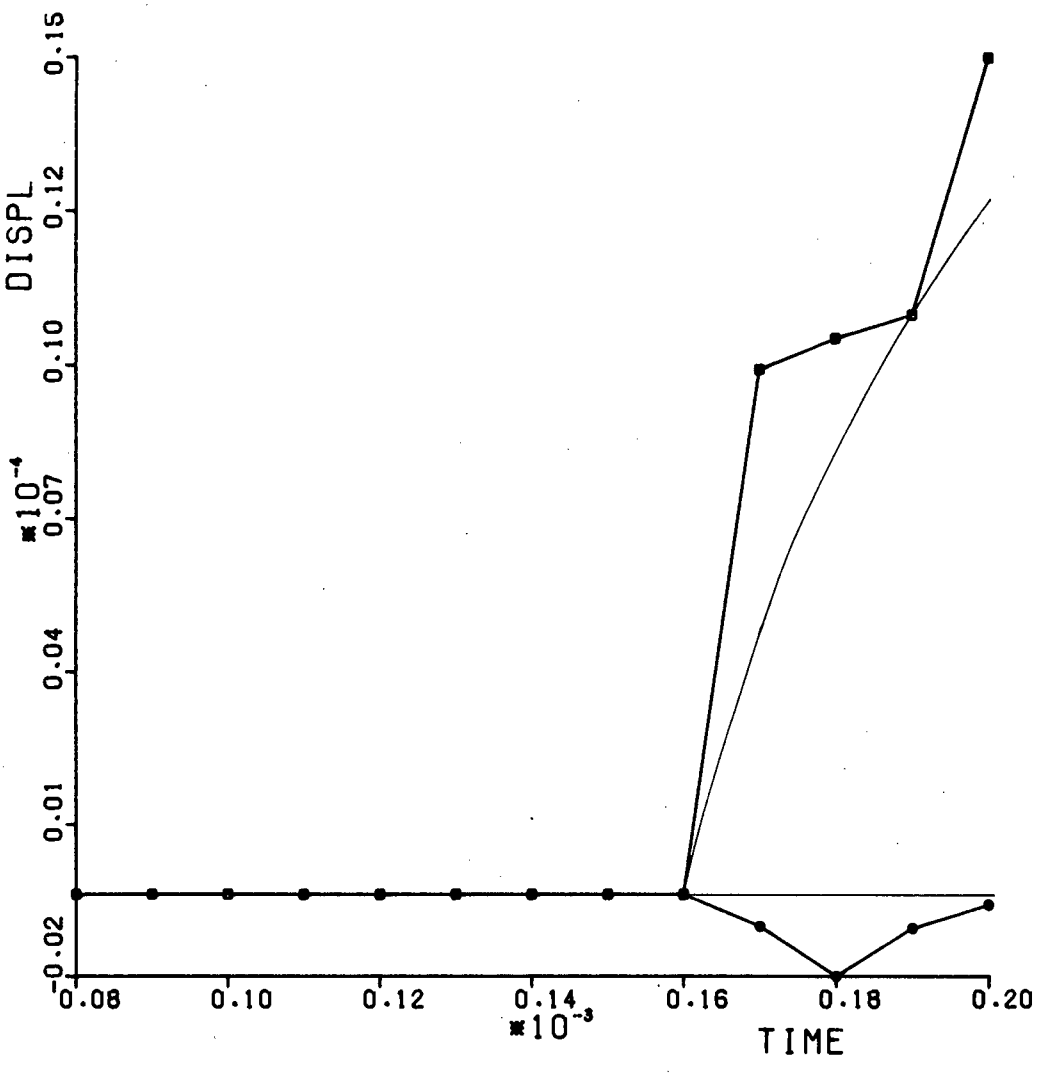

(I,J) = (4,0) EDPSDV03

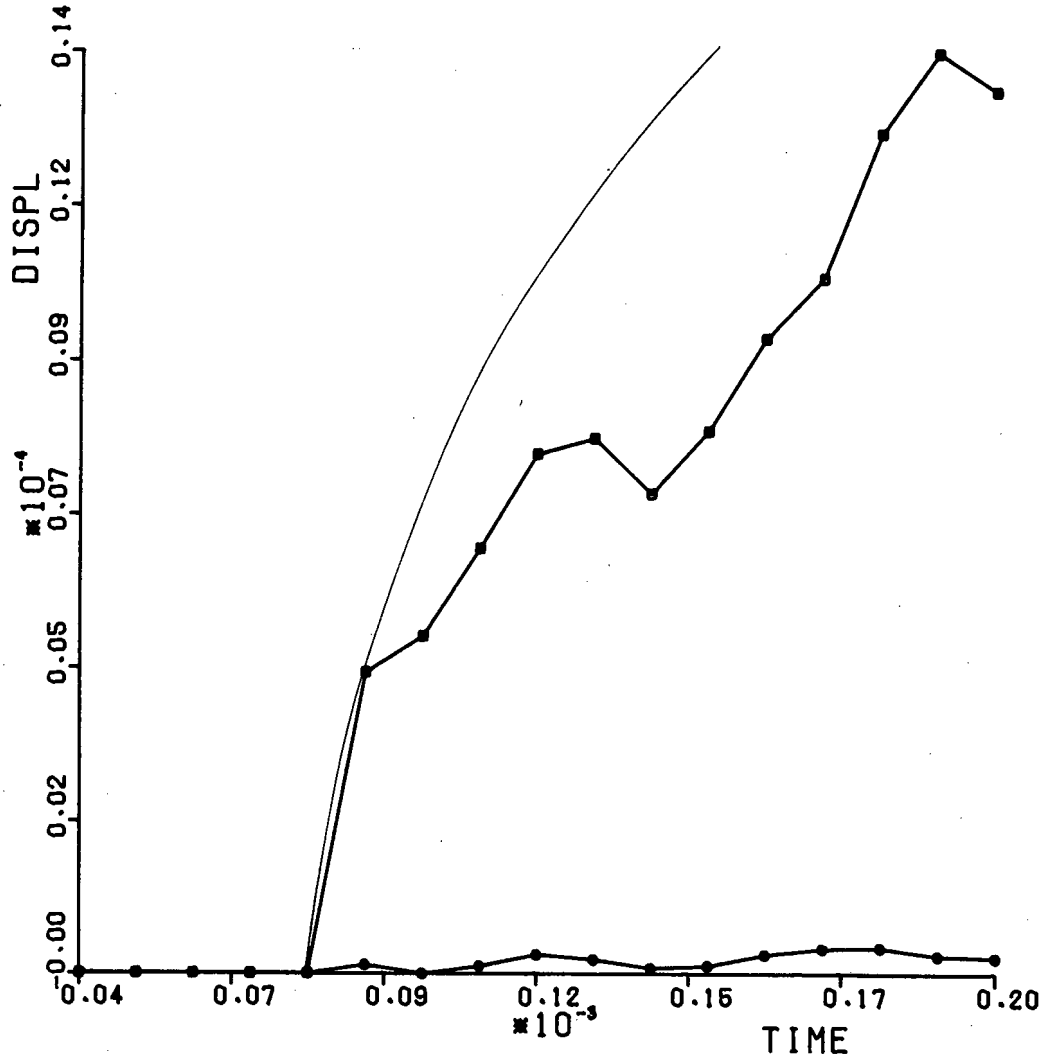

(I,J) = (2,0) EDPSDV05

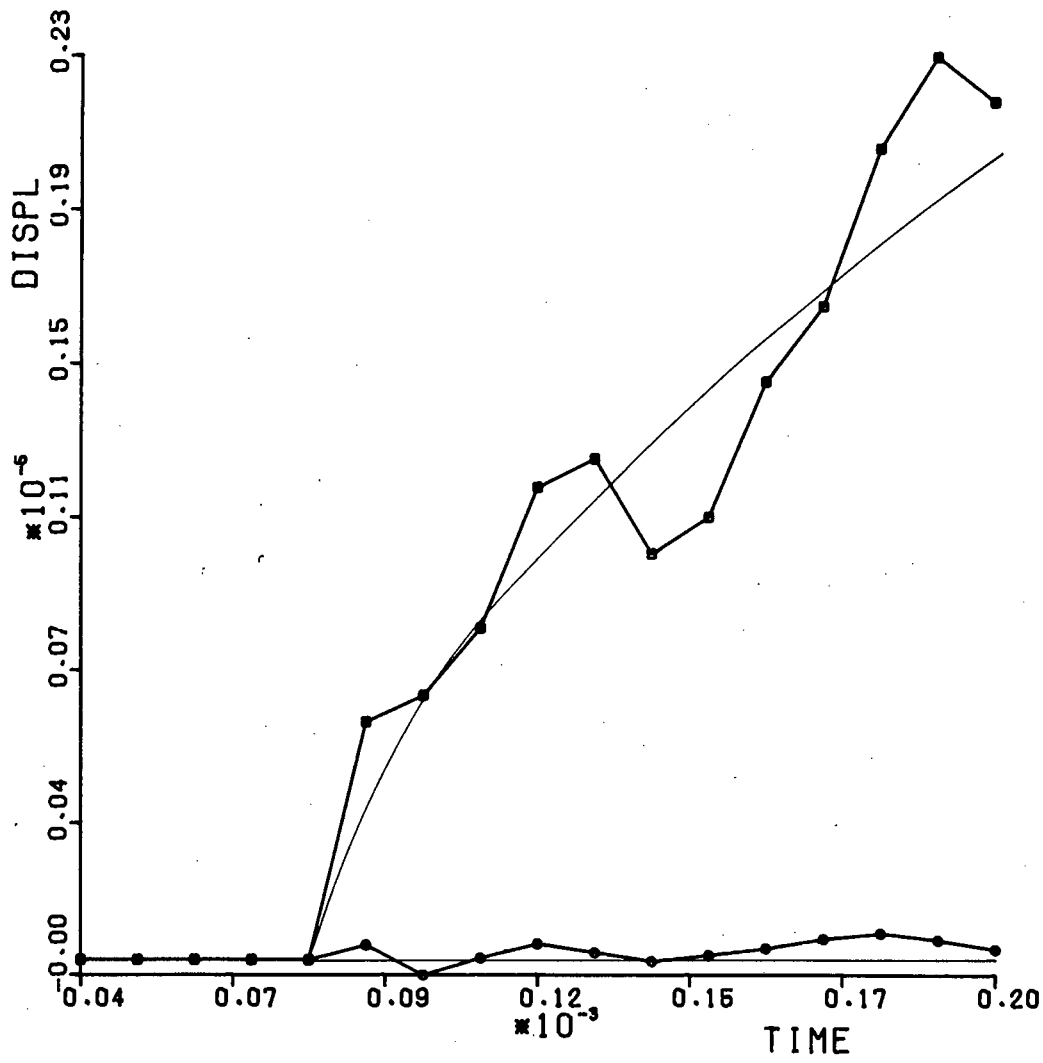

(I,J) = (2,0) EDPSDV08

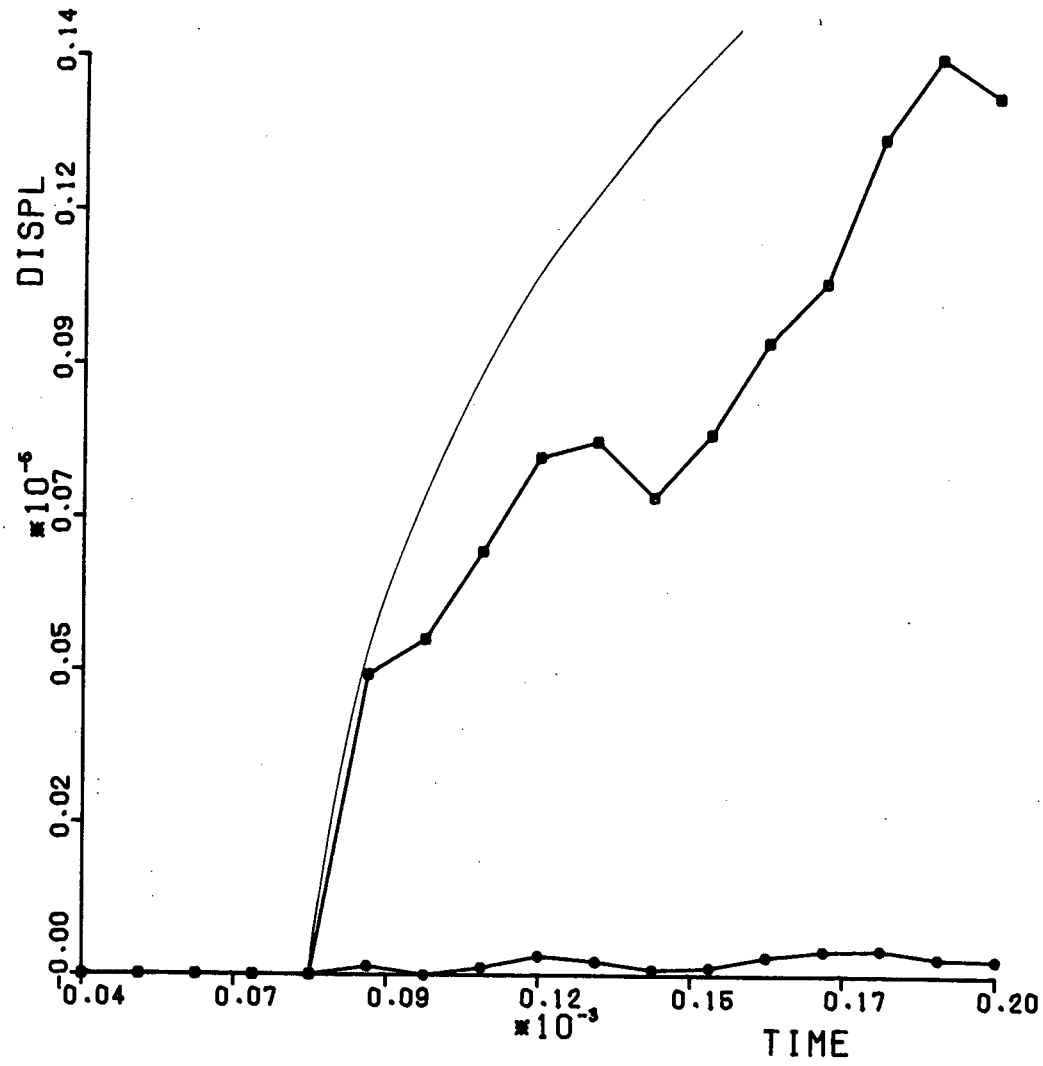

(I,J) = (2,0) EDPSDV10

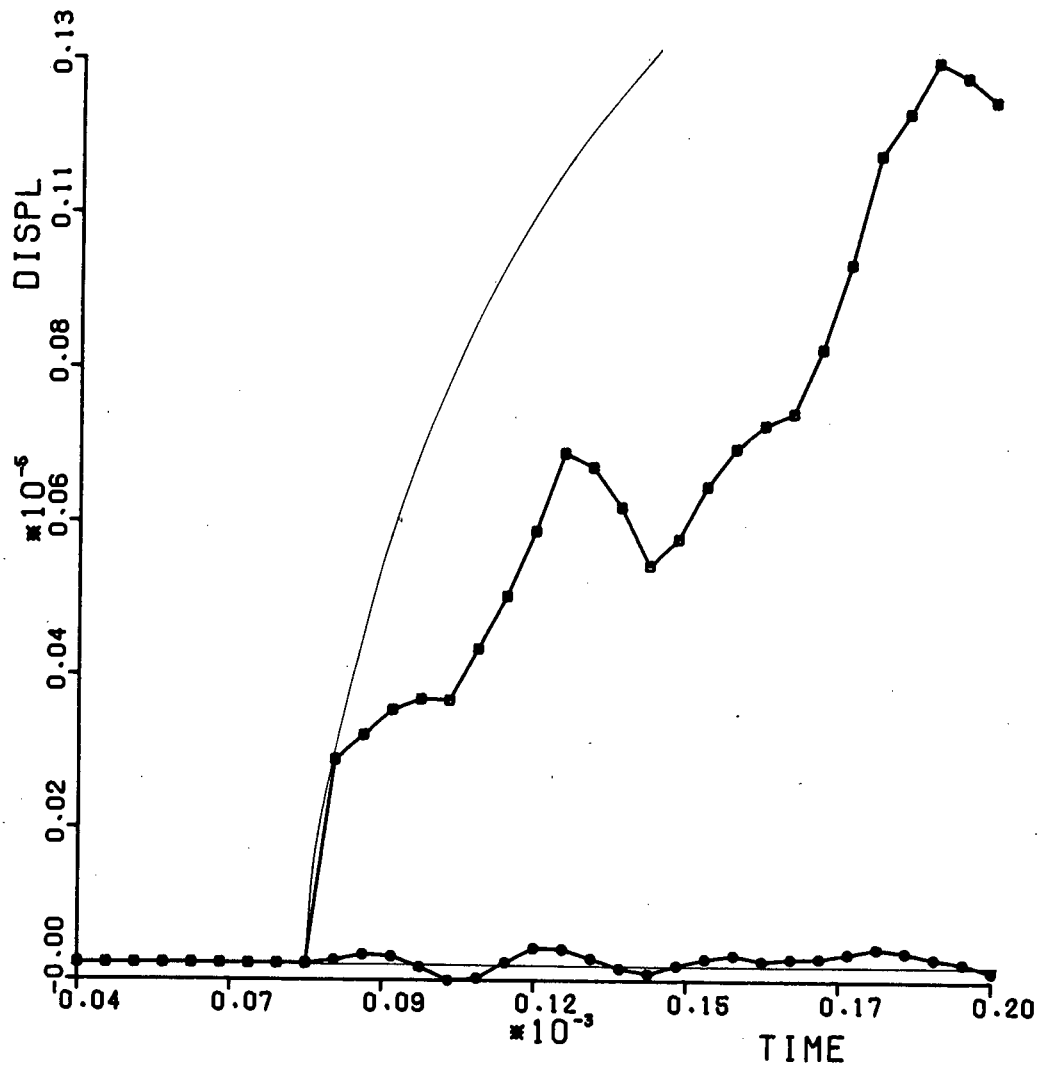

(I,J) = (2,0) EDPSDV11

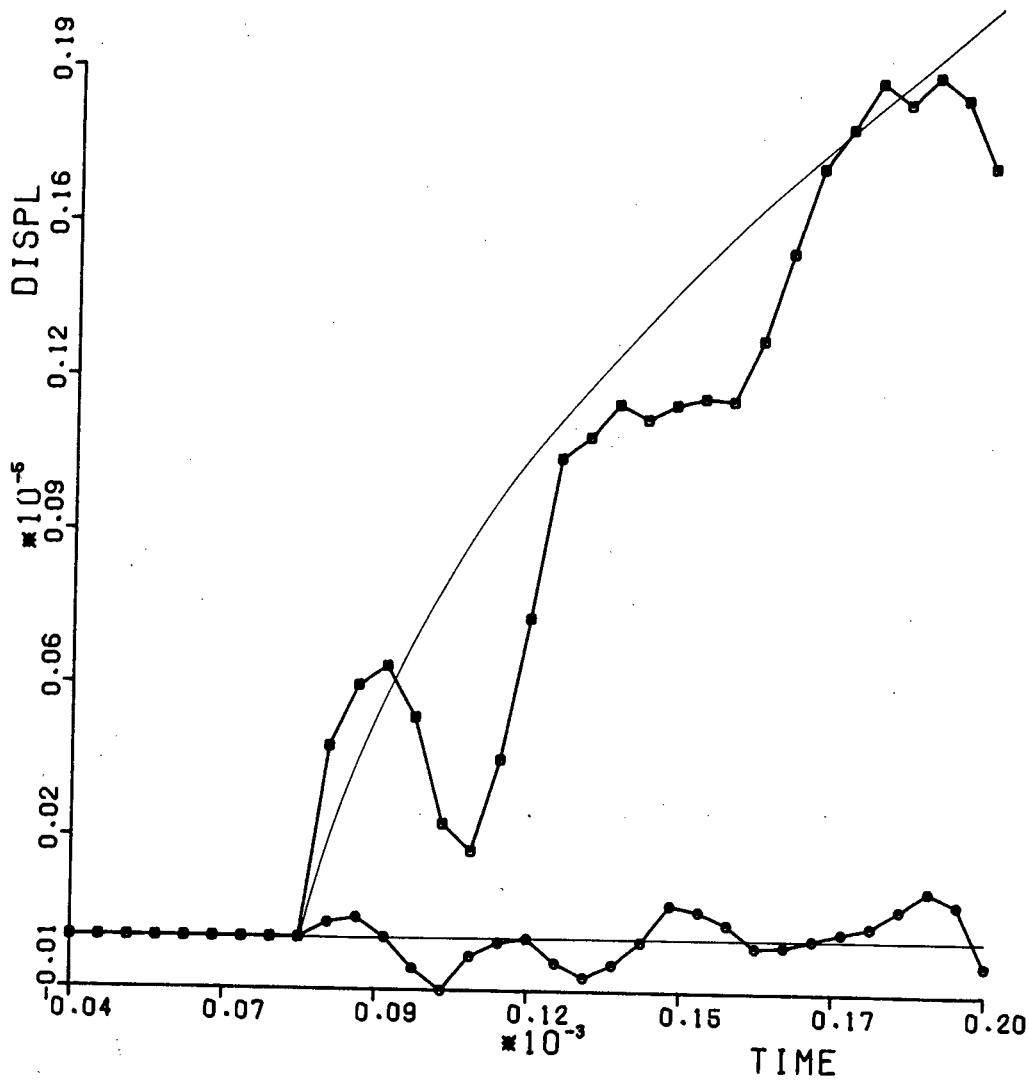

(I,J) = (2,0) EDPSDV12

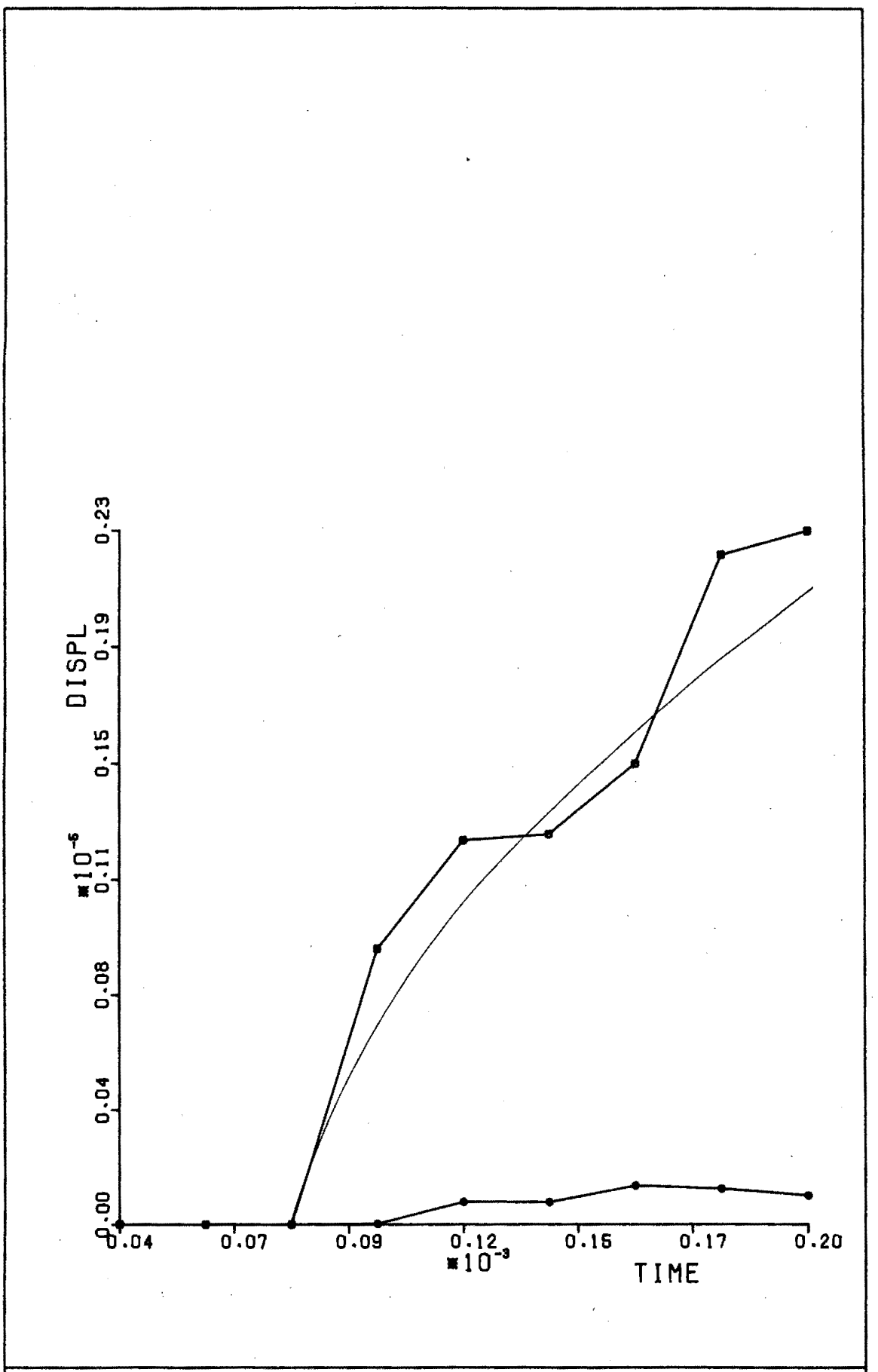

(I,J) = (2,0) EDPSDV13

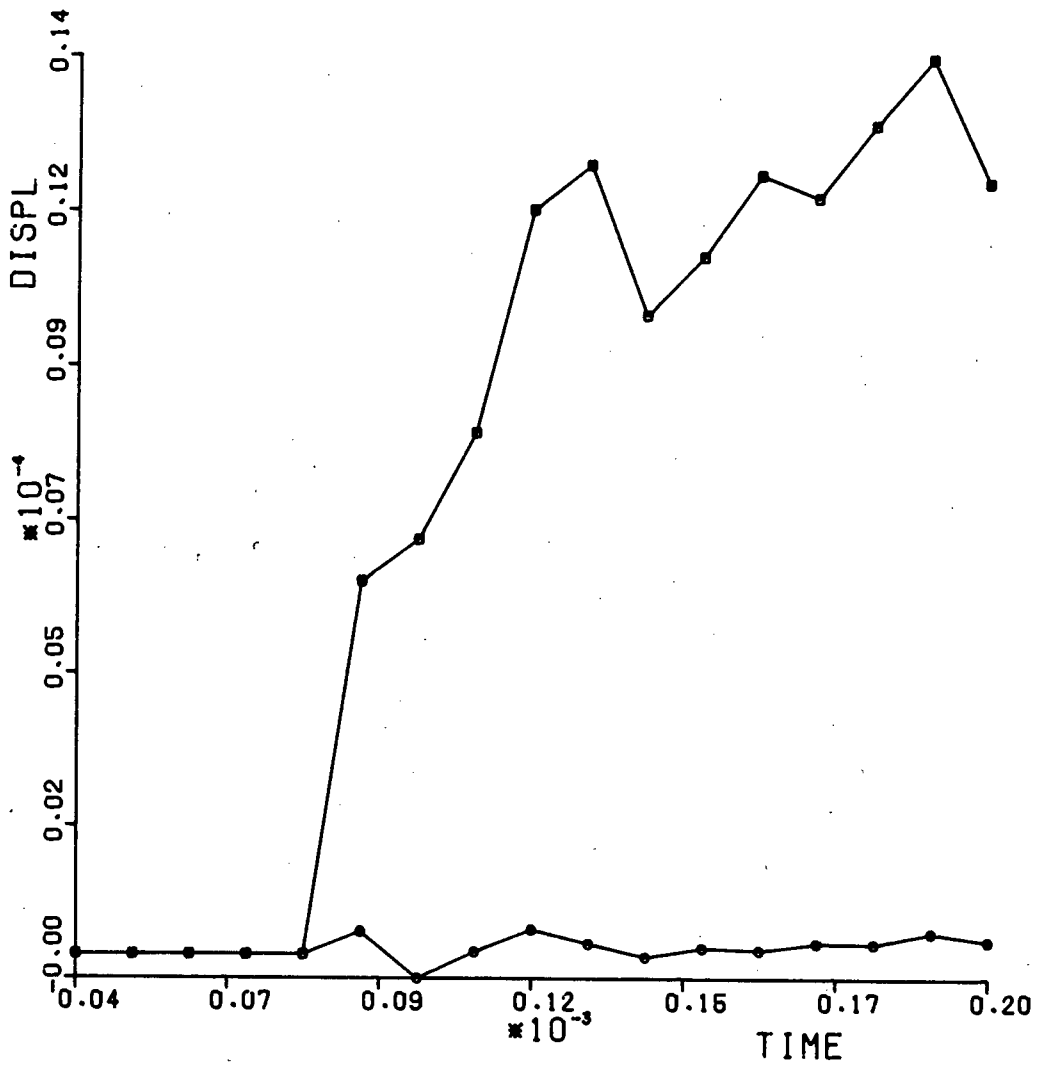

(I,J) = (2,0) EDPSDV06

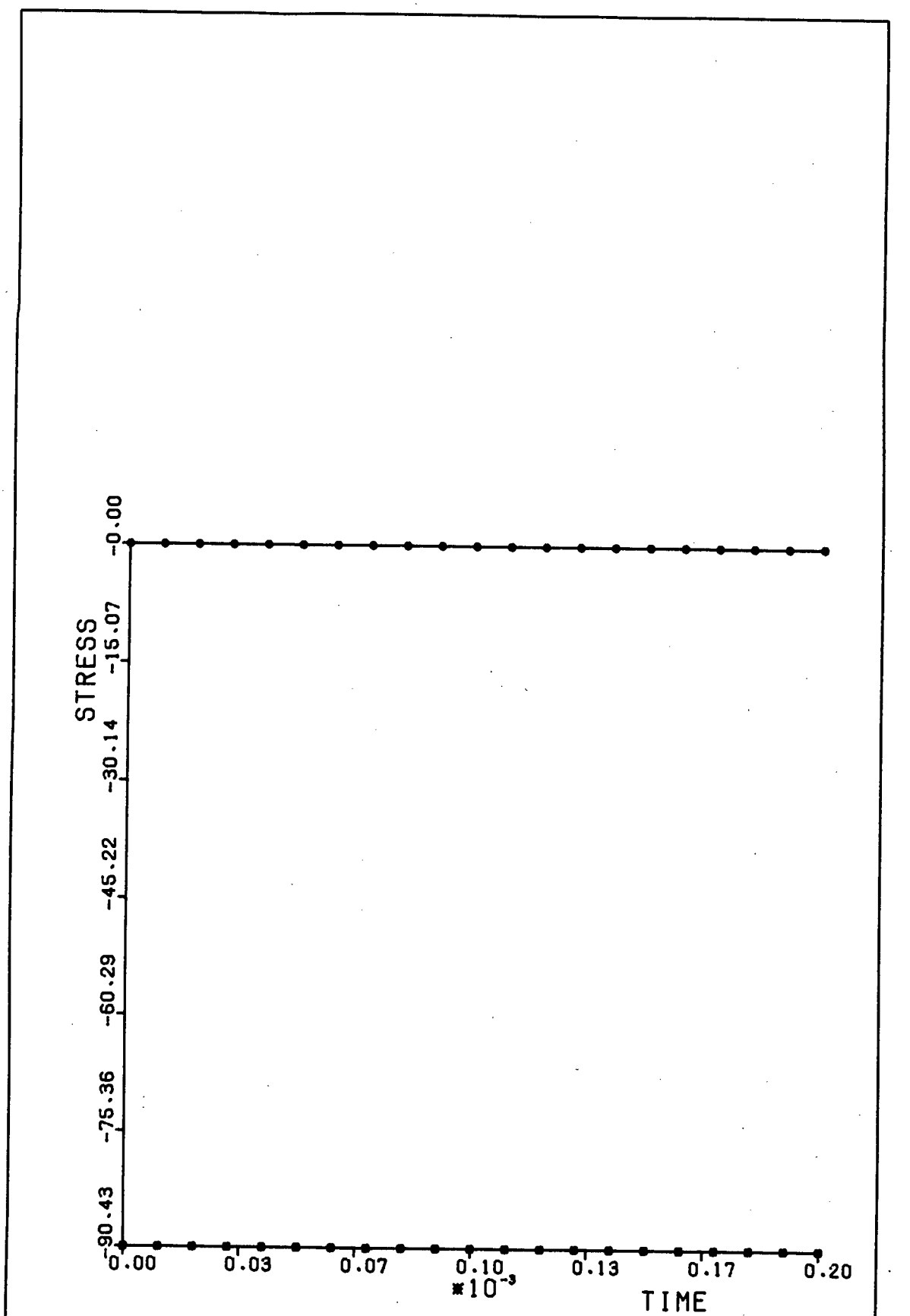

(I,J) = (0,0) EDPSDV08

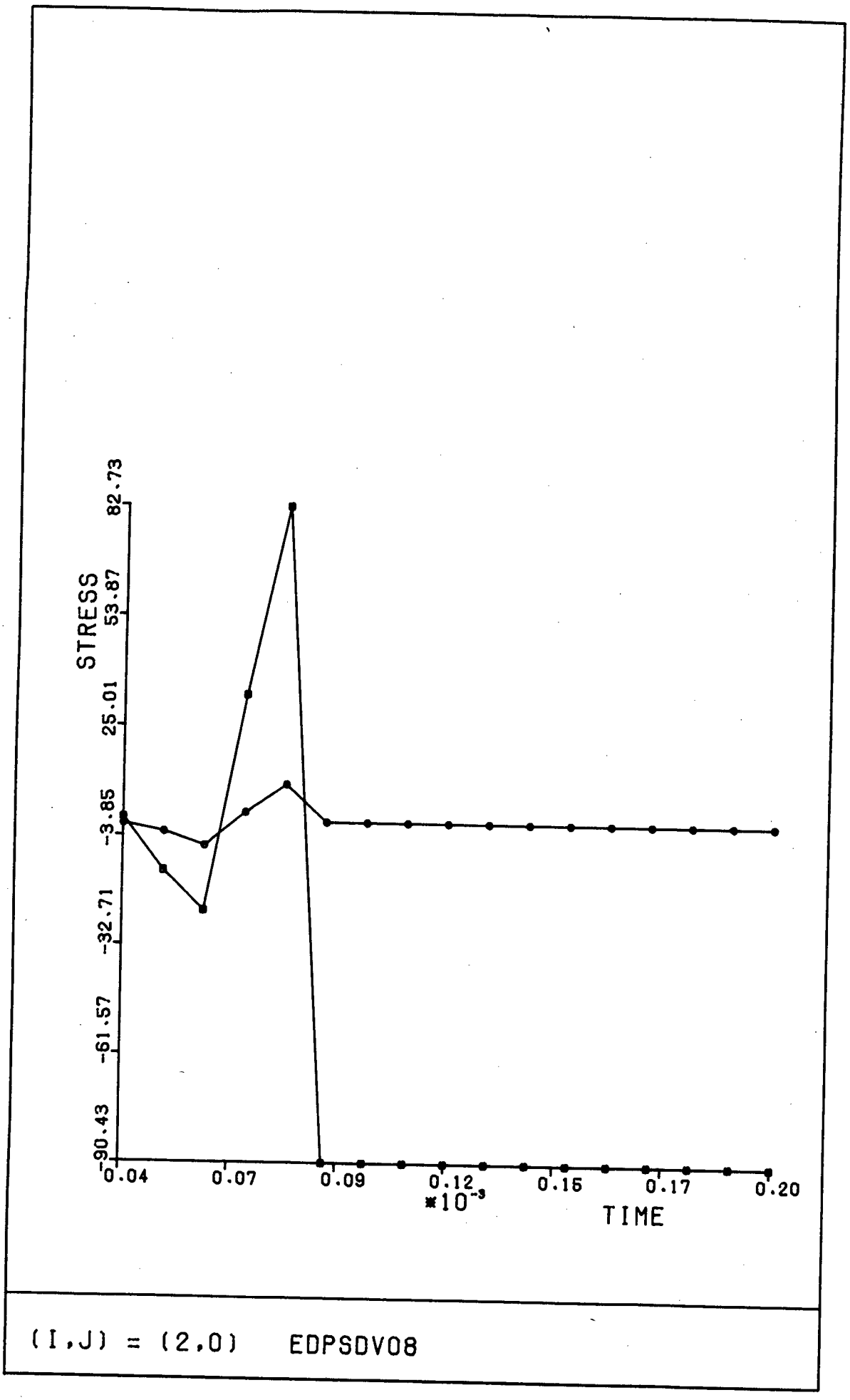
STRESS
82.73
53.87
25.01
-3.85
-32.71
-61.57
-90.43
0.04
0.07
0.09
0.12
0.15
0.17
0.20
*10^-3
TIME
(I,J) = (2,0) EDPSDV08

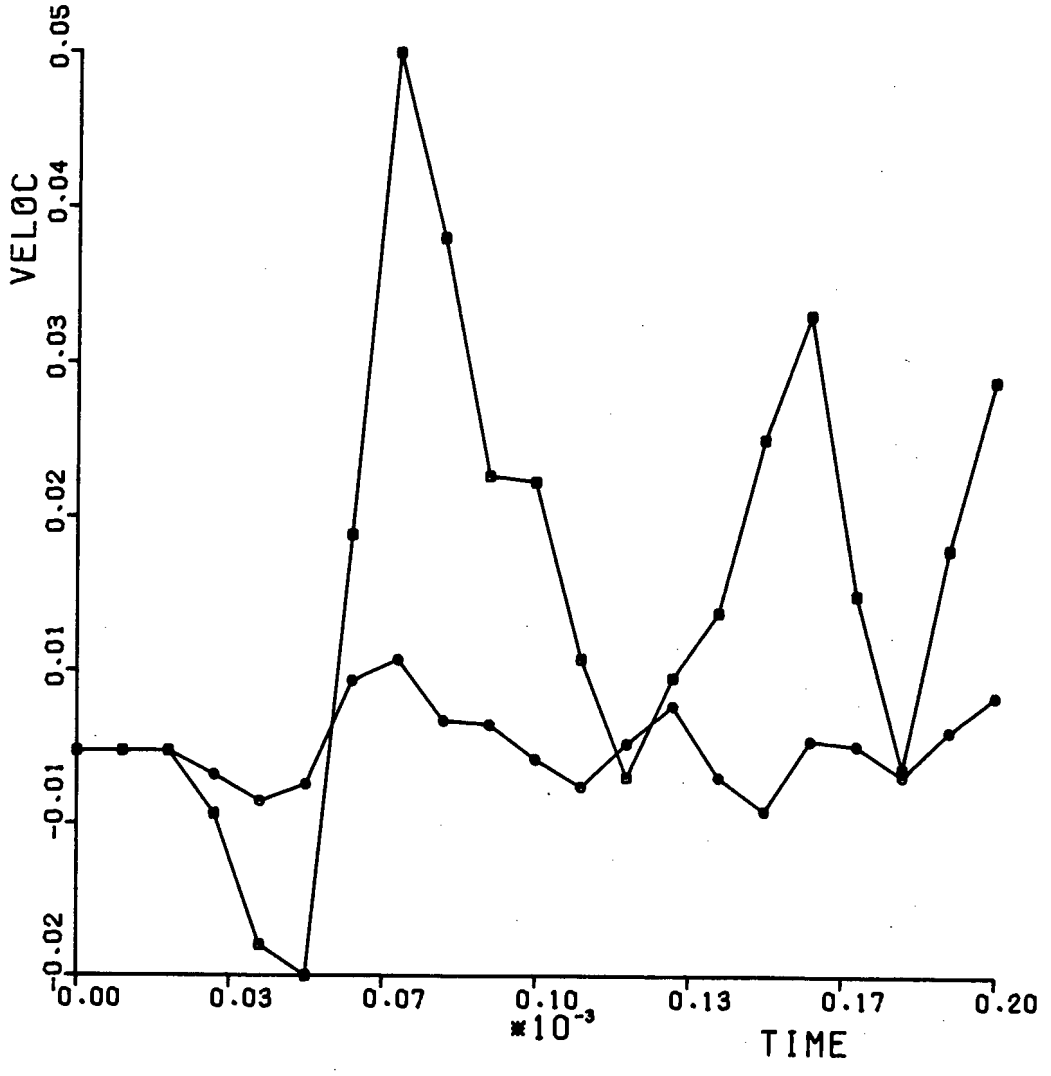

(I,J) = (0,0) EDPSDV08

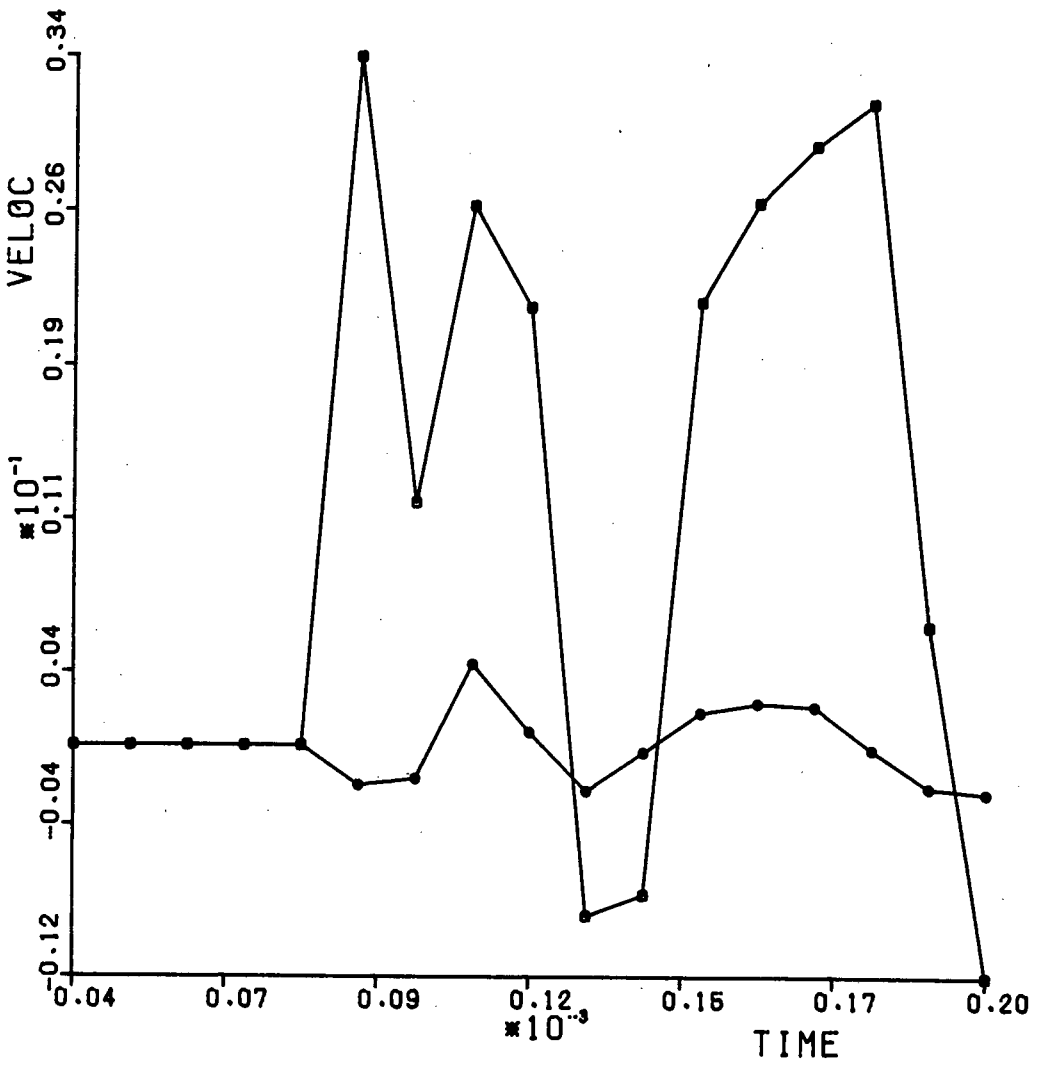

(I,J) = (2,0) EDPSDV08

Appendix G

Ground Motion Simulation Plots

The plots appearing in this appendix are obtained using a linear ramp dislocation function of rise-time 0.12 seconds, a fault mesh of 20 elements in the x_1-direction and 10 elements in the x_2-direction, and a time-step of 0.01 seconds, unless otherwise indicated. The remaining input data is available in section 8.4. Station numbers are indicated at the base of each plot.

Three curves appear on each plot, corresponding to the x_1, x_2 and x_3 directions. The following symbols identify the three directions.

x_1 :

x_2 :

x_3 :

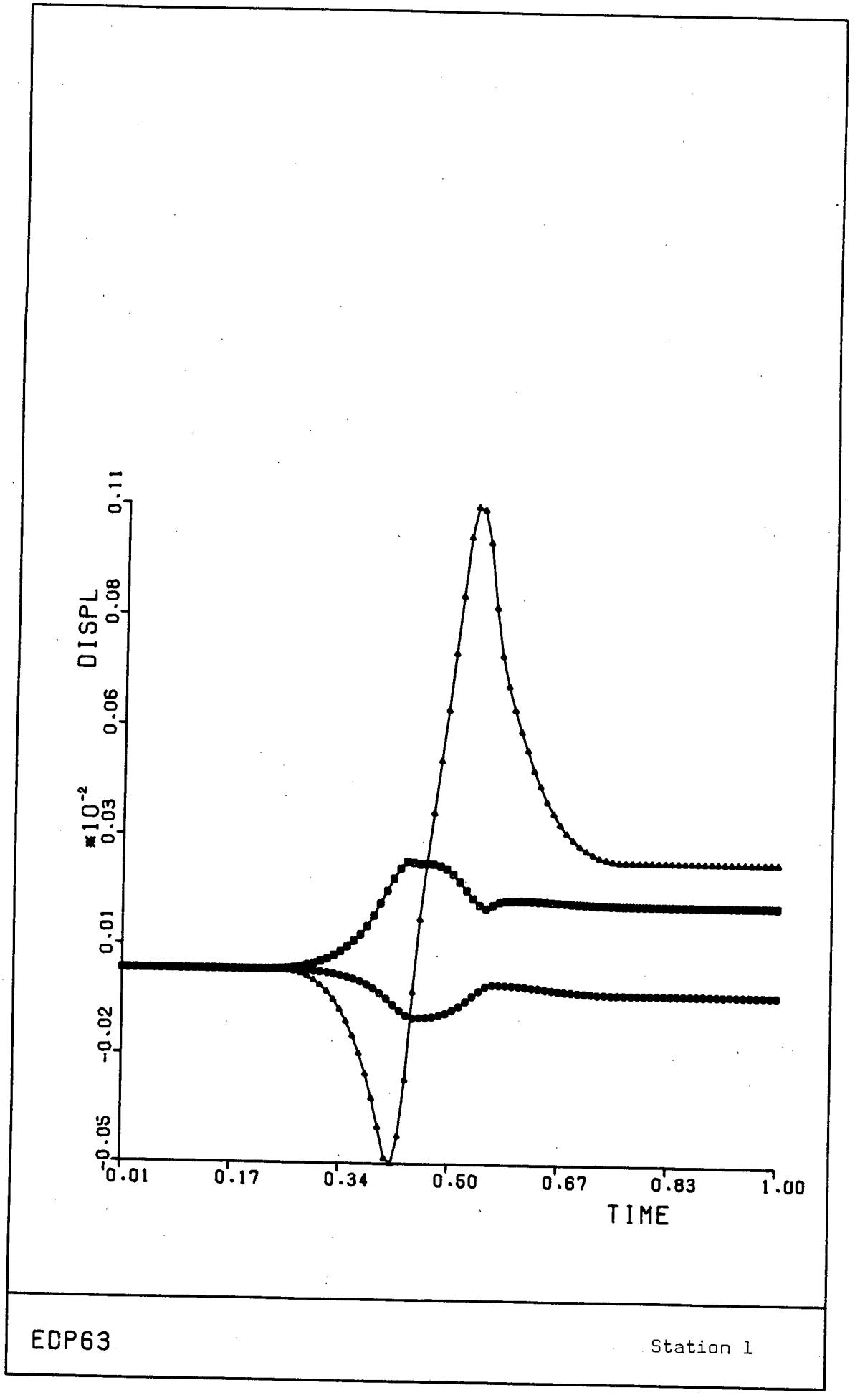
DISPL
*10⁻²
0.11
0.08
0.06
0.03
0.01
-0.02
-0.05
0.01
0.17
0.34
0.50
0.67
0.83
1.00
TIME
EDP63
Station 1

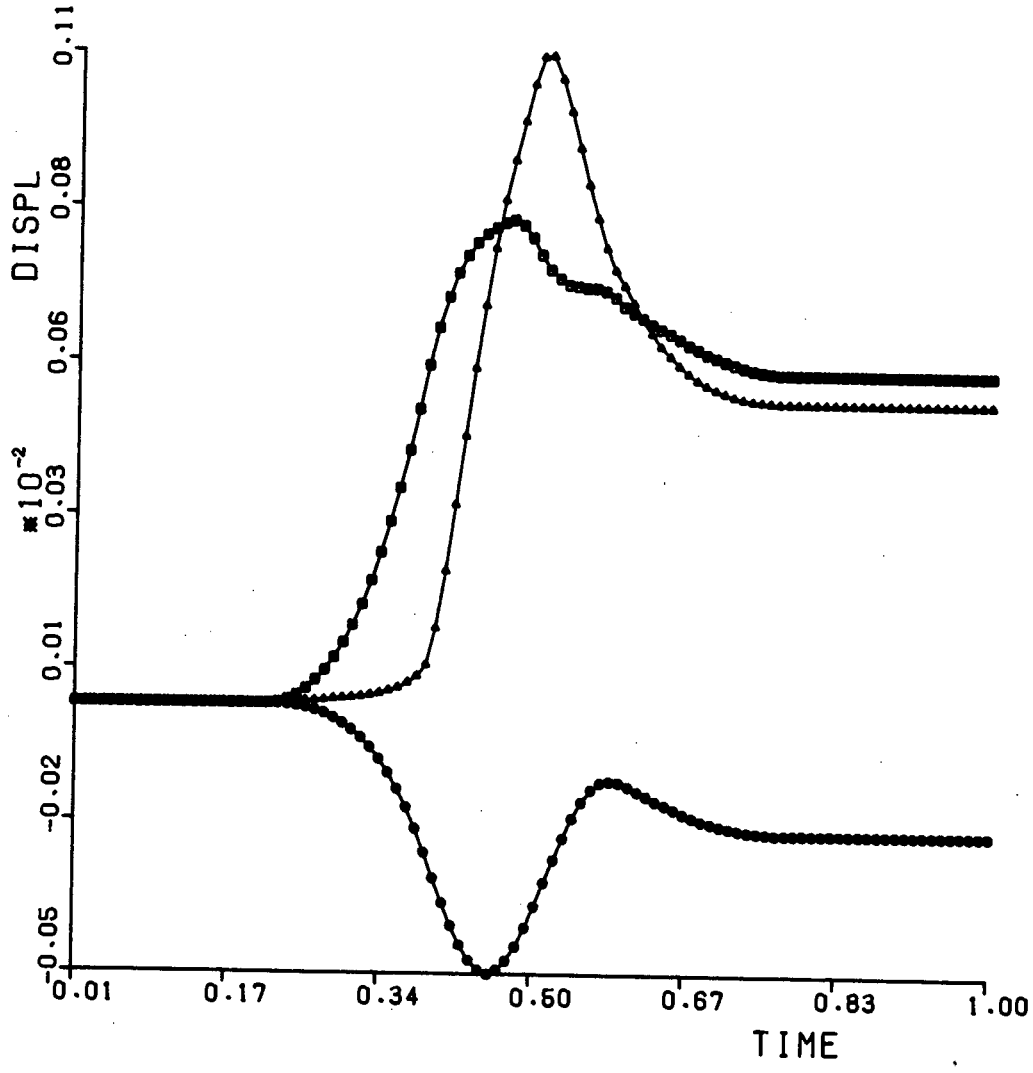

EDP51

Station 2

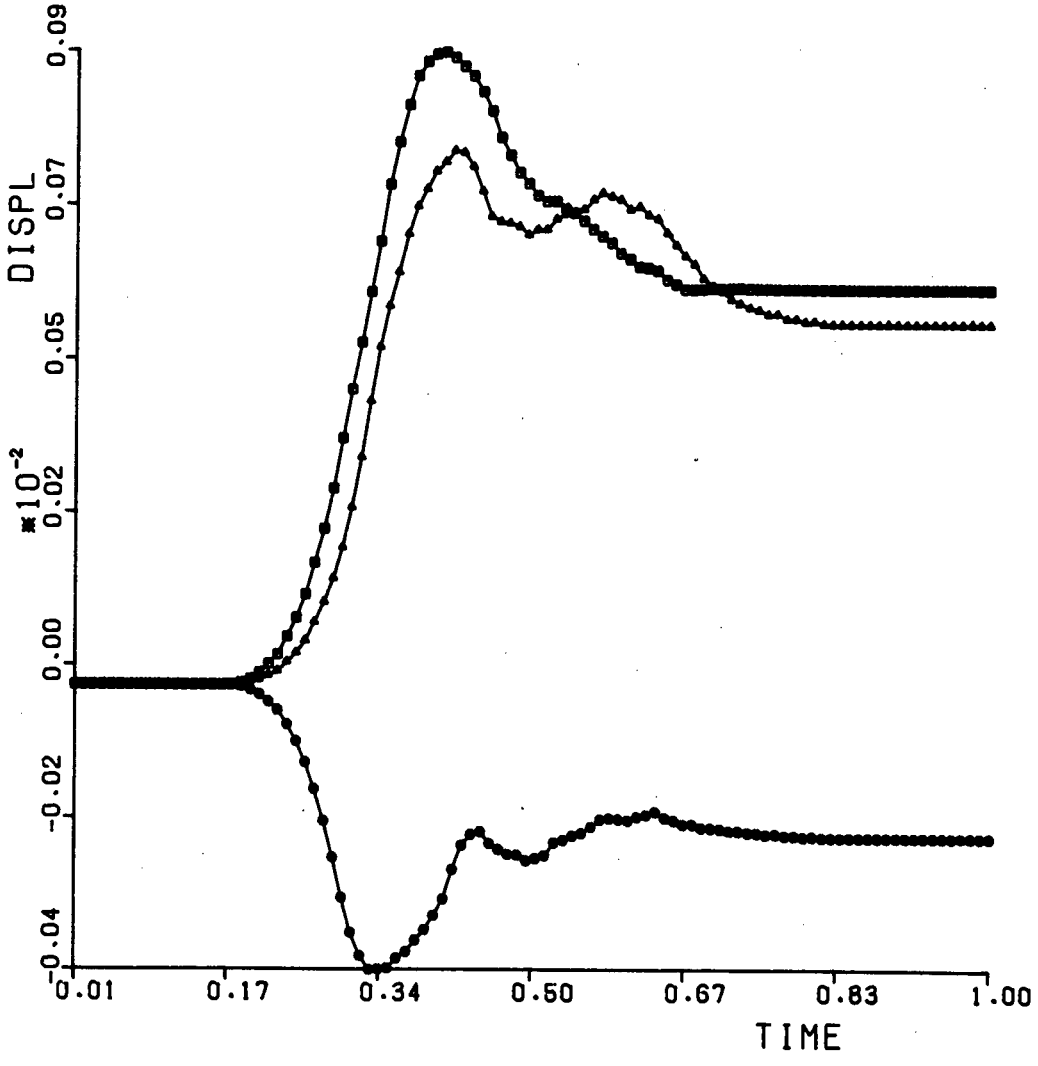

EDP50 Station 2 : Self-similar (radially propagating) crack

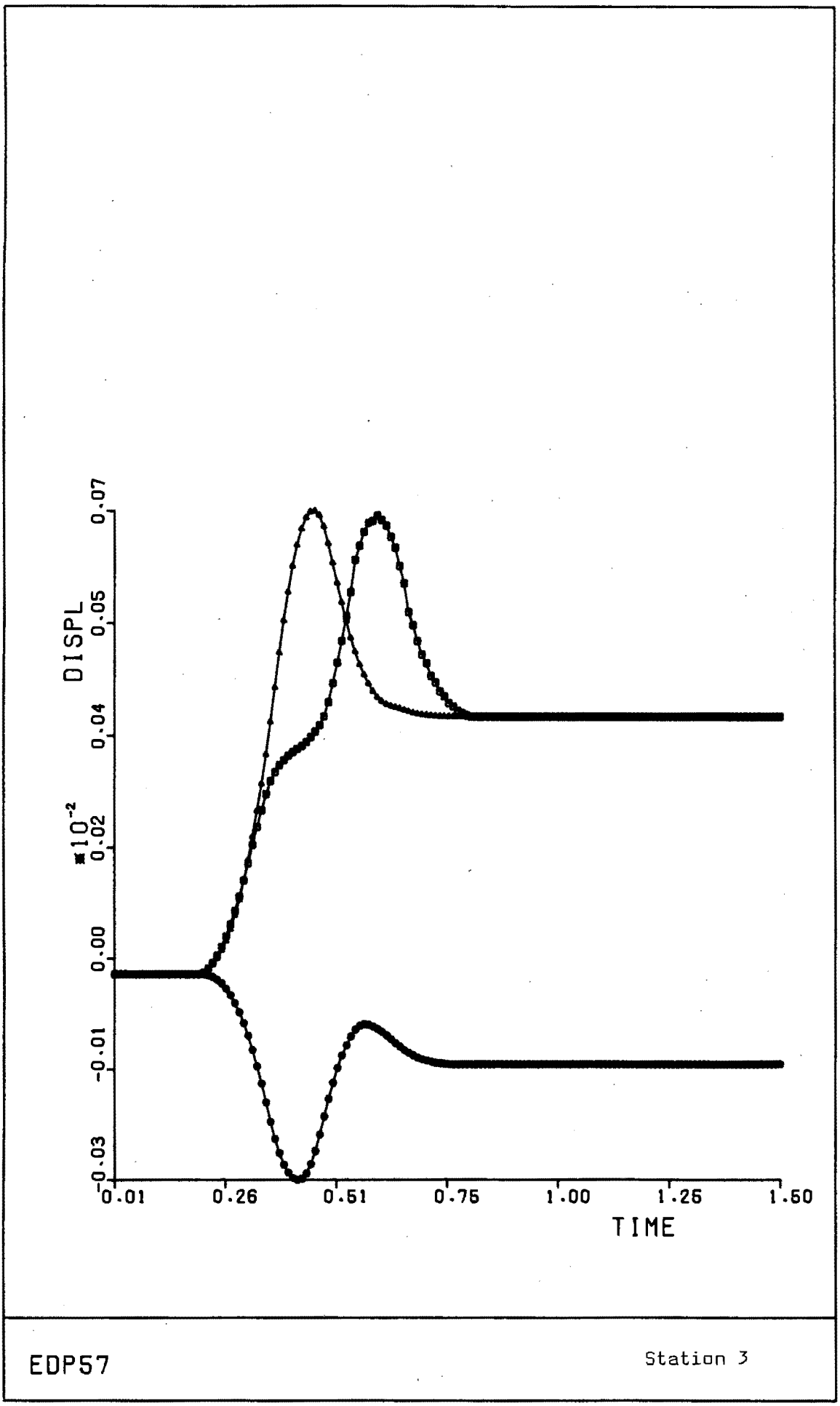

EDP57

Station 3

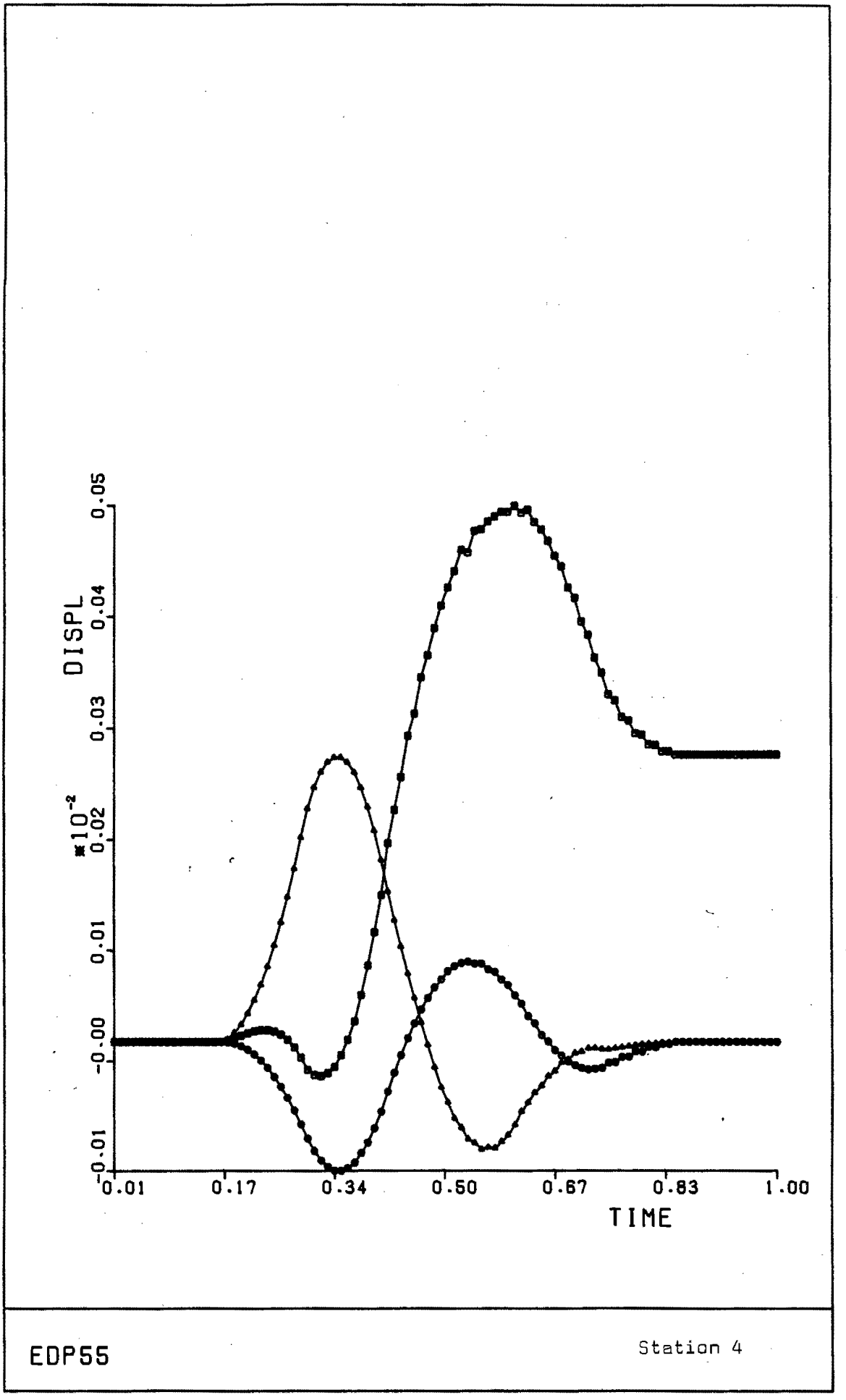
DISPL
×10⁻²
0.05
0.04
0.03
0.02
0.01
-0.00
-0.01
0.01
0.17
0.34
0.50
0.67
0.83
1.00
TIME
EDP55
Station 4

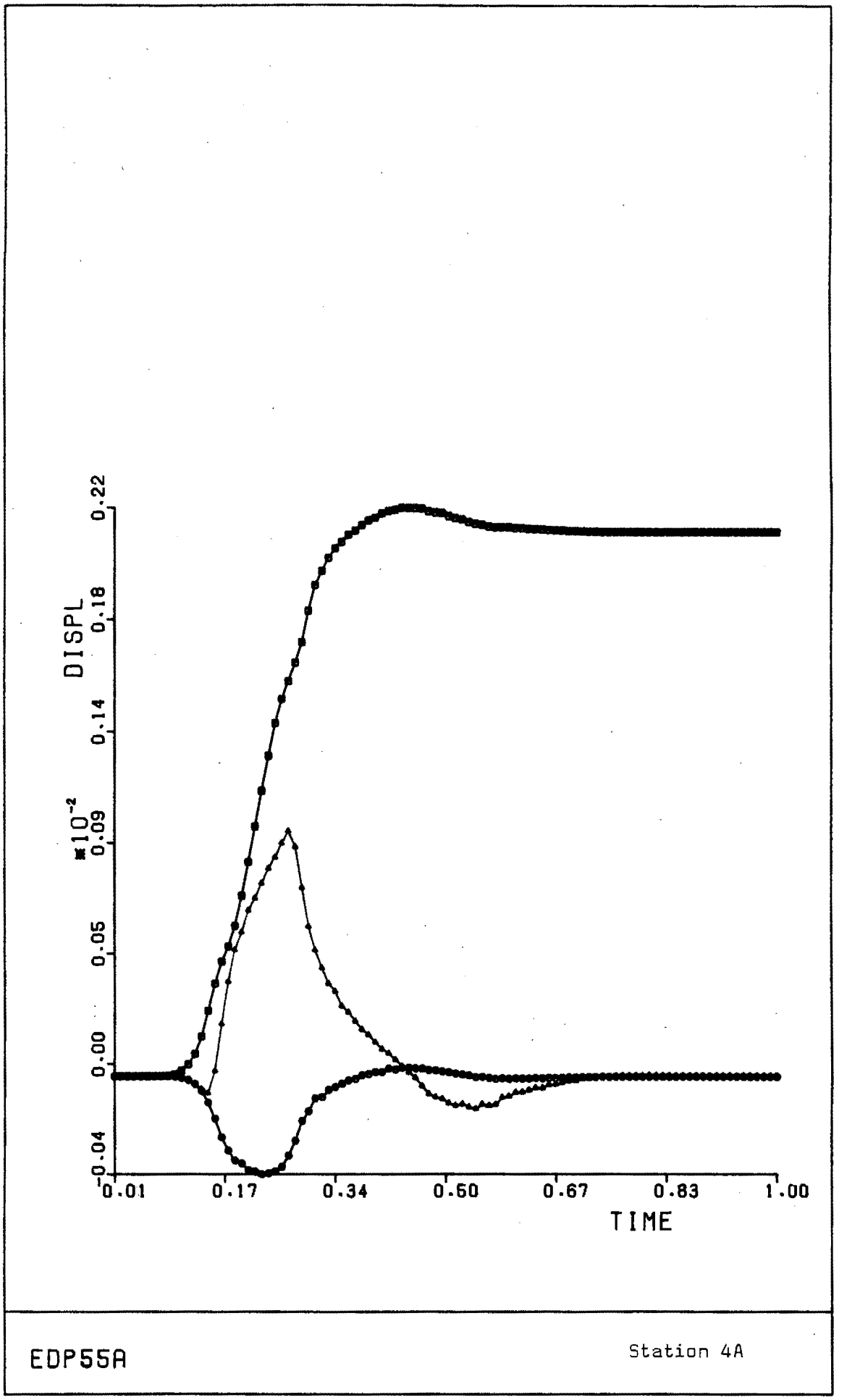

EDP55A

Station 4A

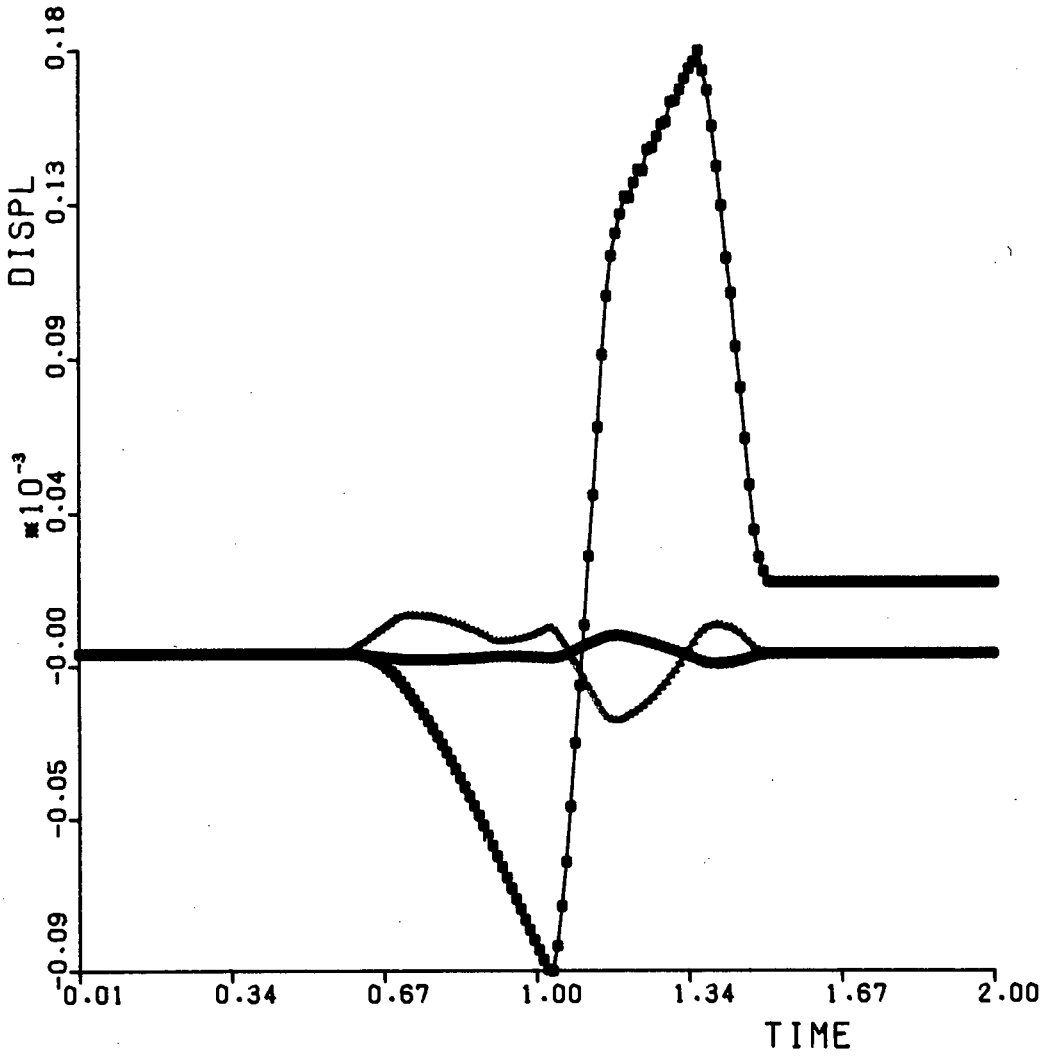

EDP55E

Station 4B

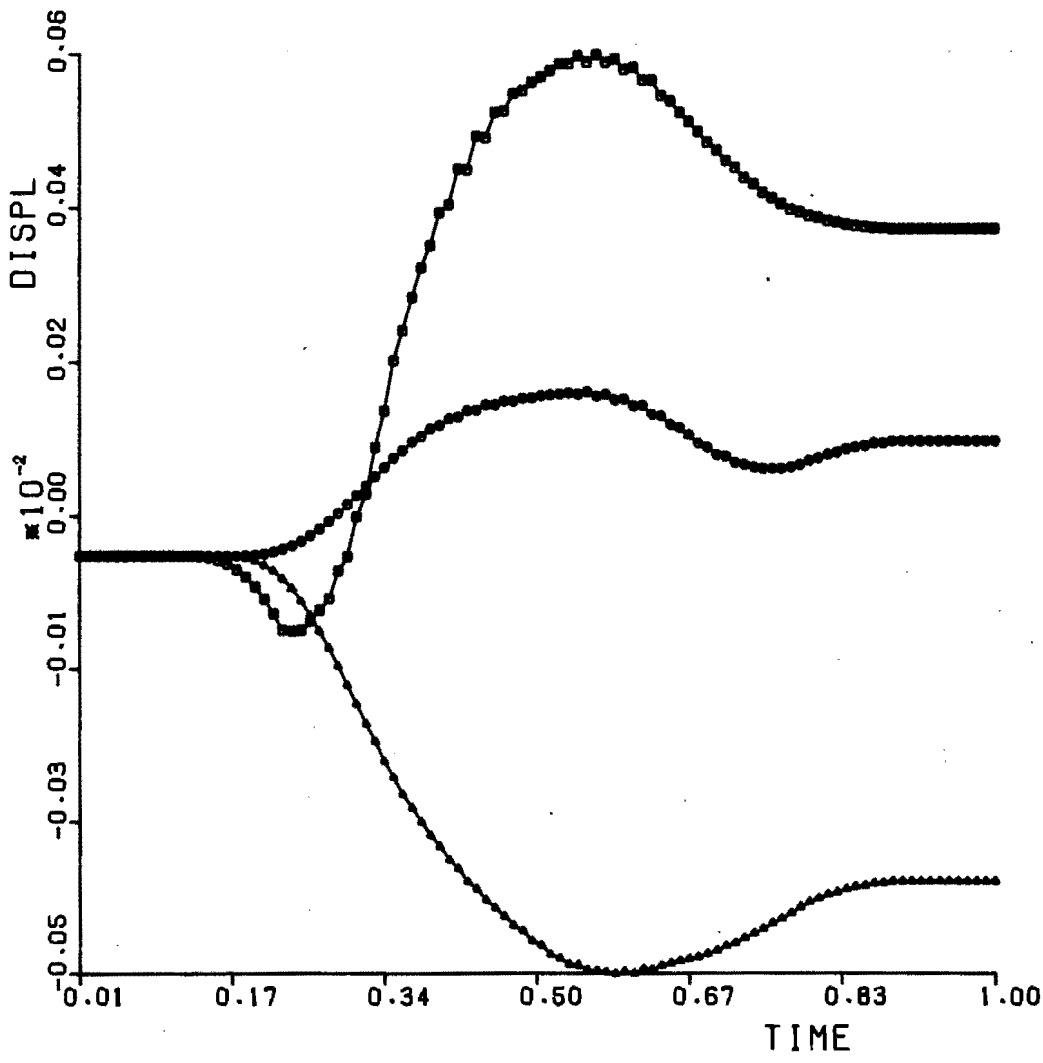

EDP58

Station 5

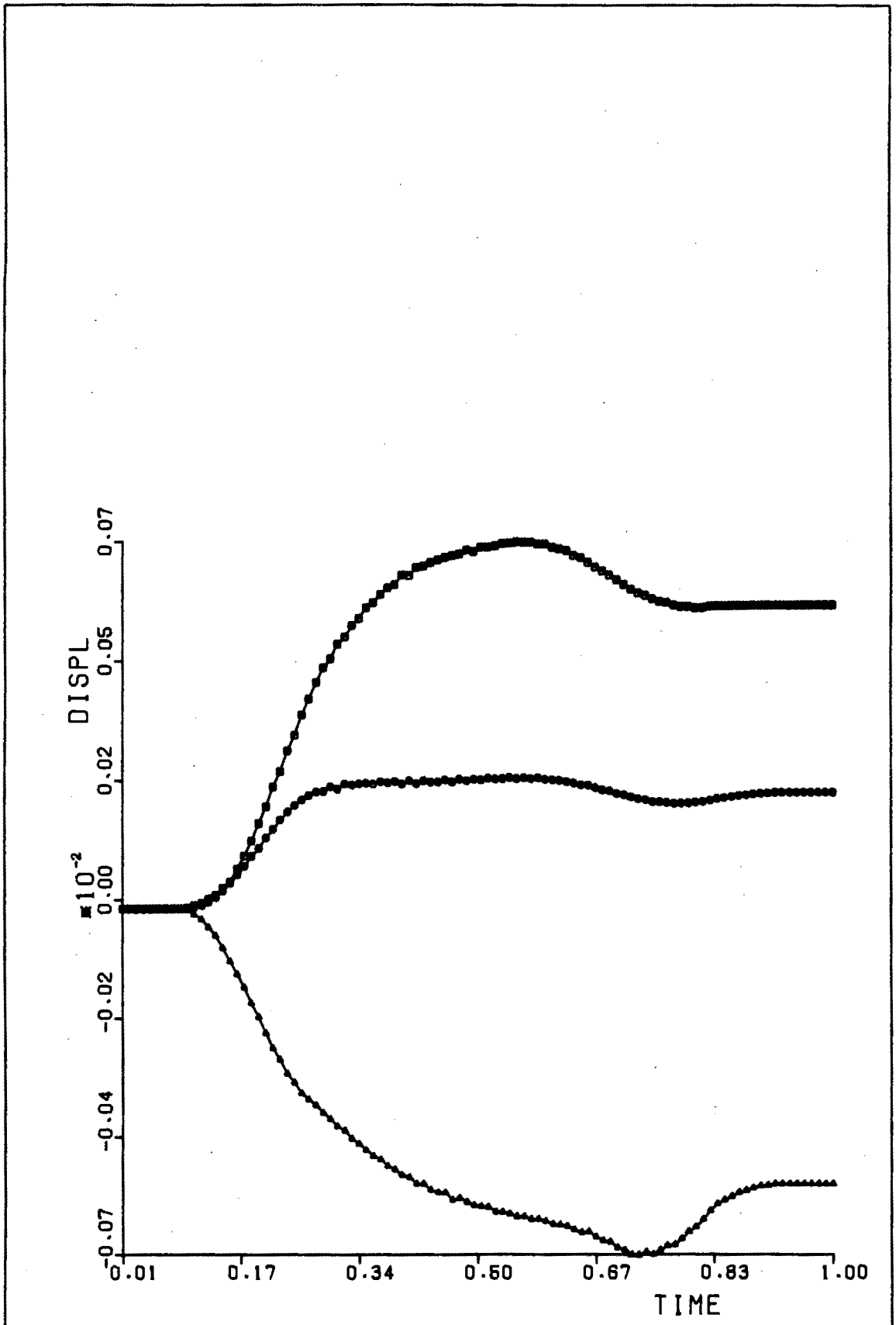

EDP52

Station 6

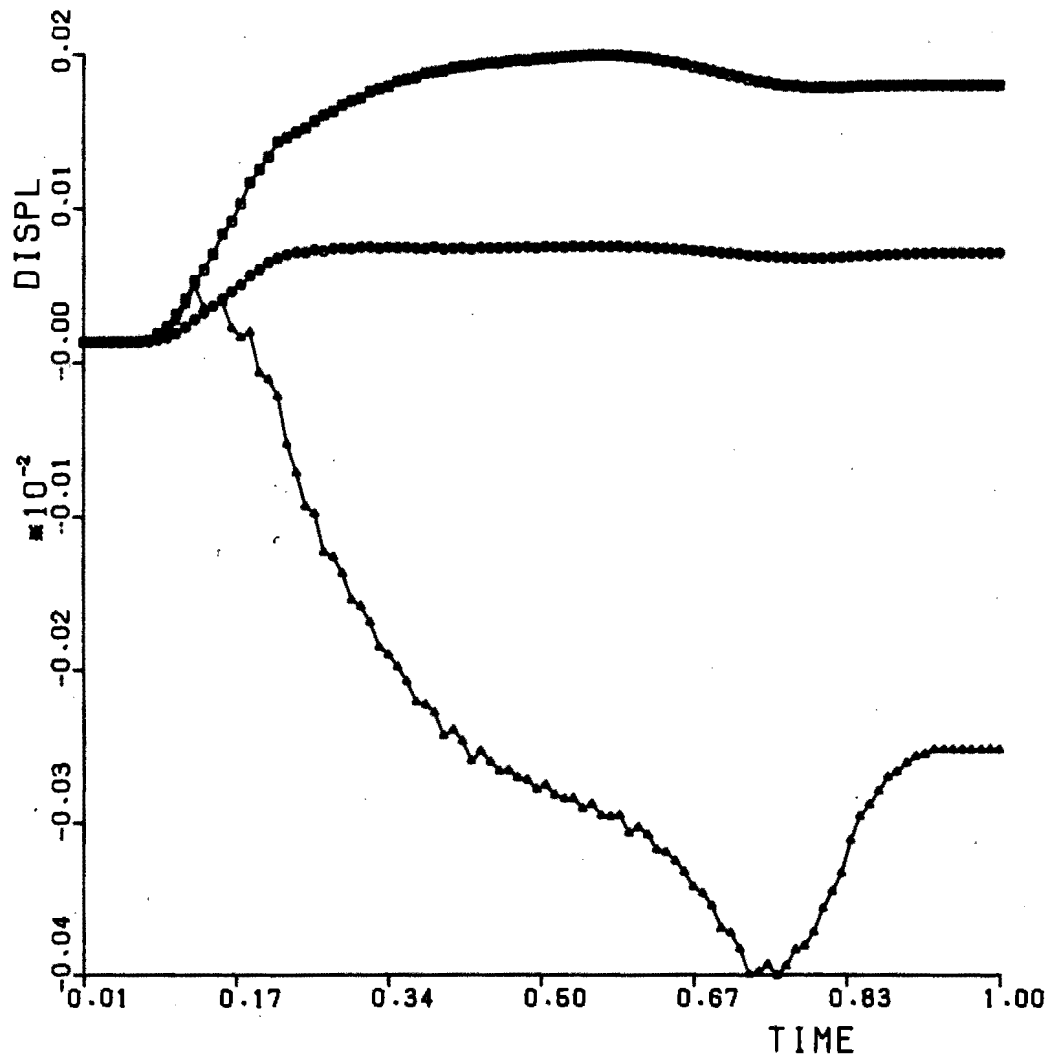

EDP64

Station 7

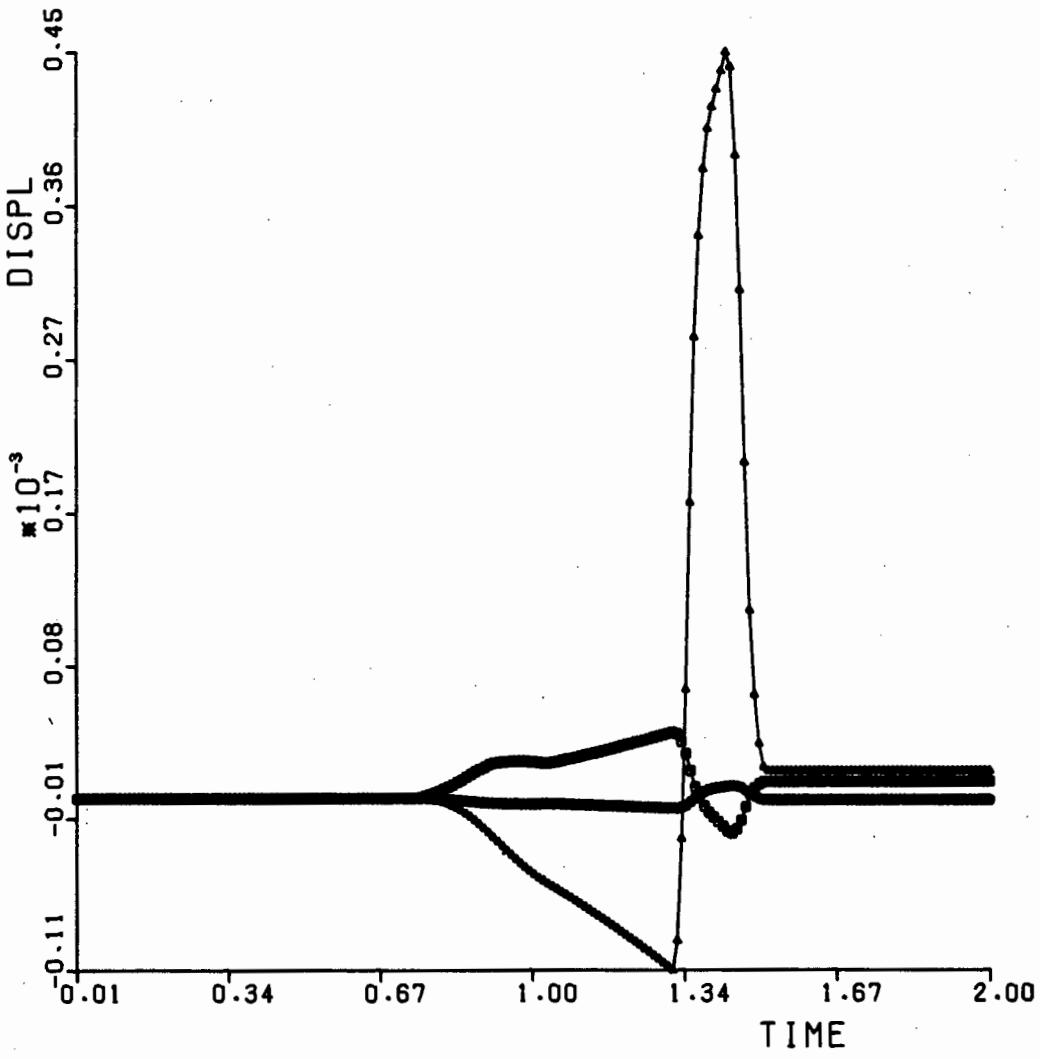

EDP54

Station 10

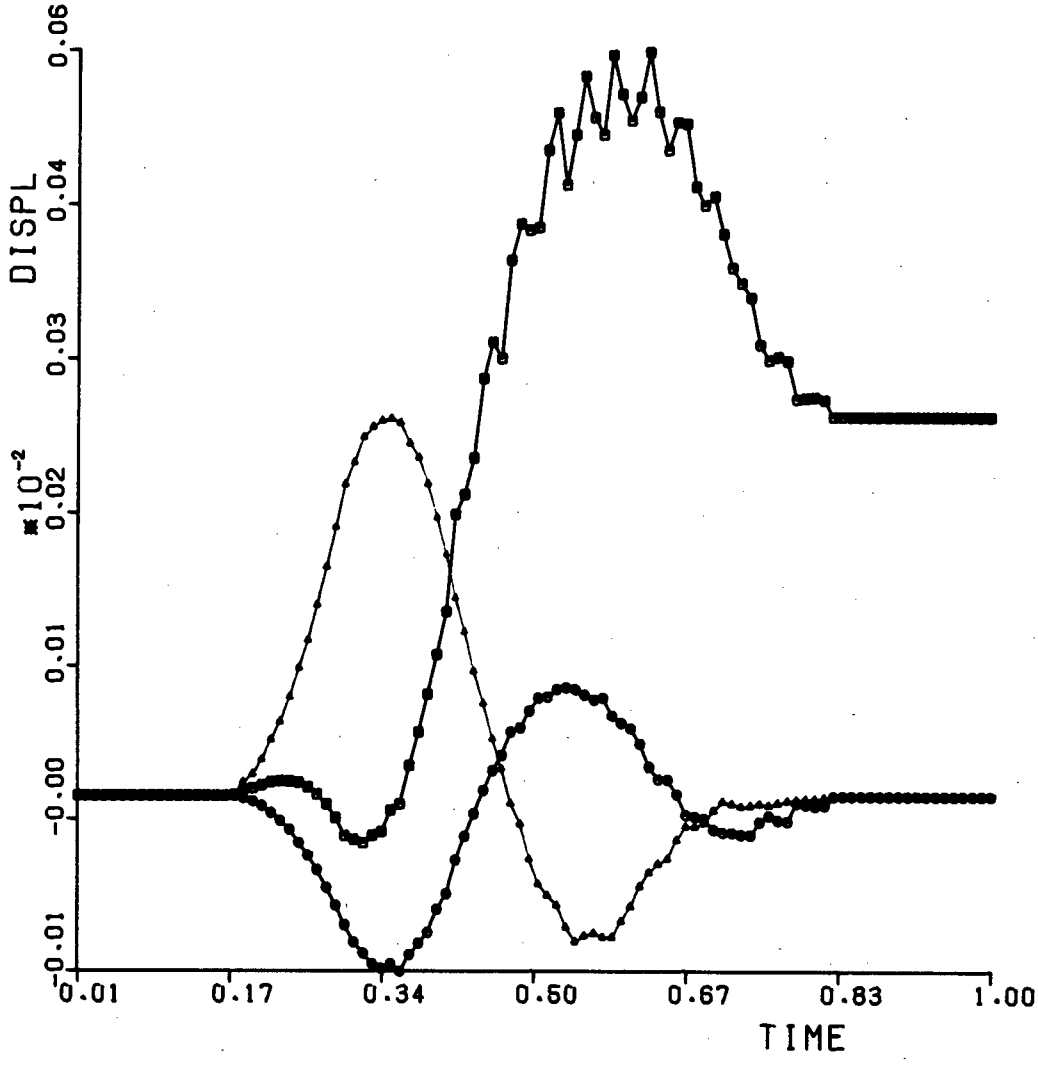

EDP55Z

STATION 4 : 10 elements in x_1-direction
5 elements in x_2-direction

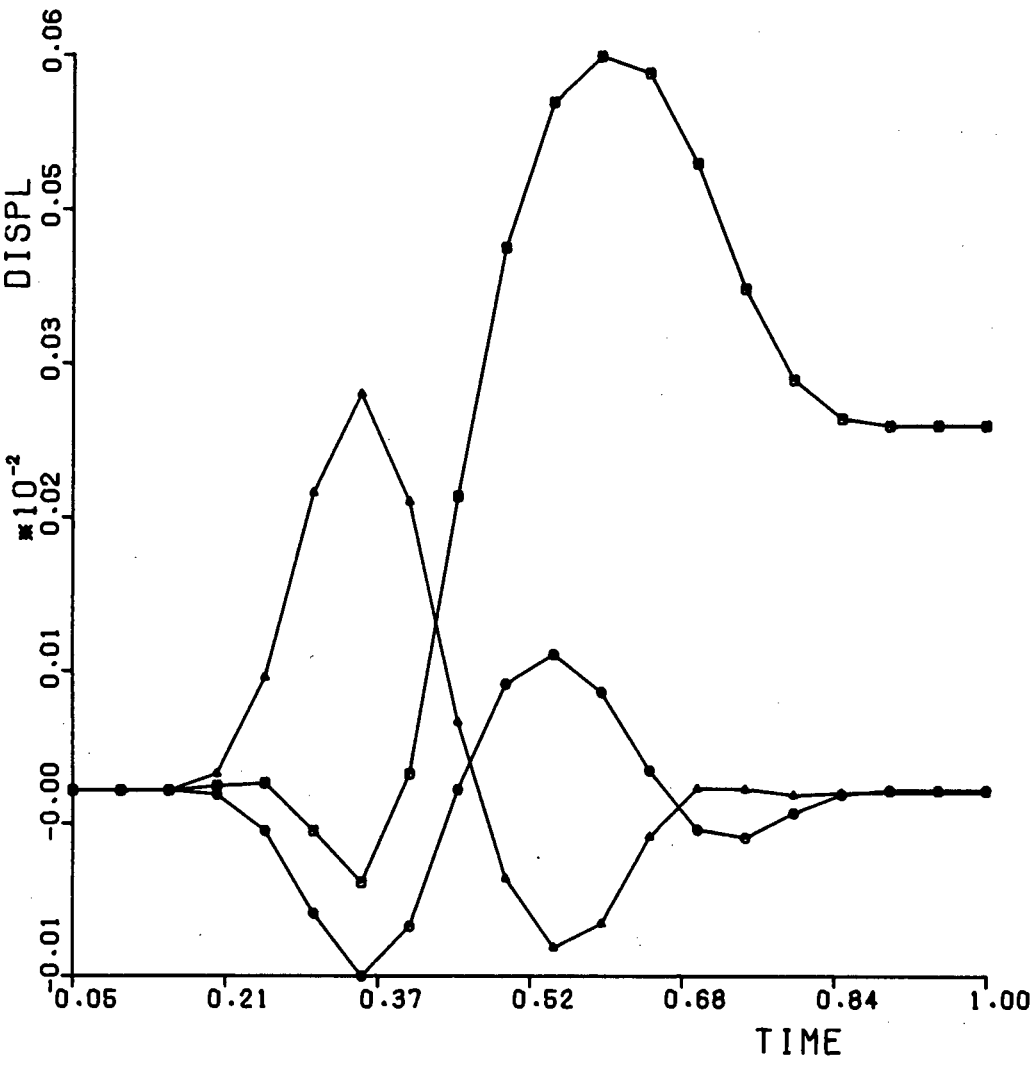

EDP55Y

STATION 4 : t = 0.05 sec.

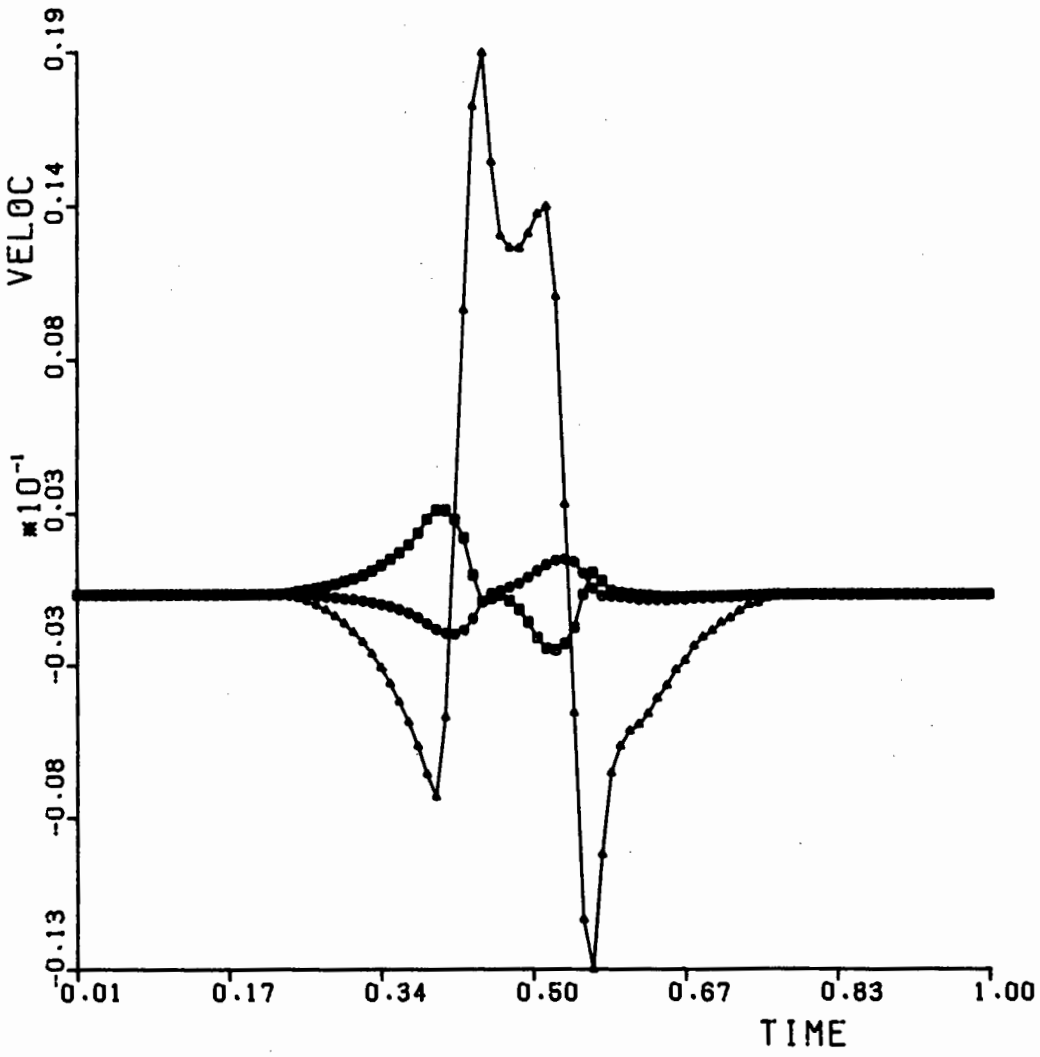

EDP63

Station 1

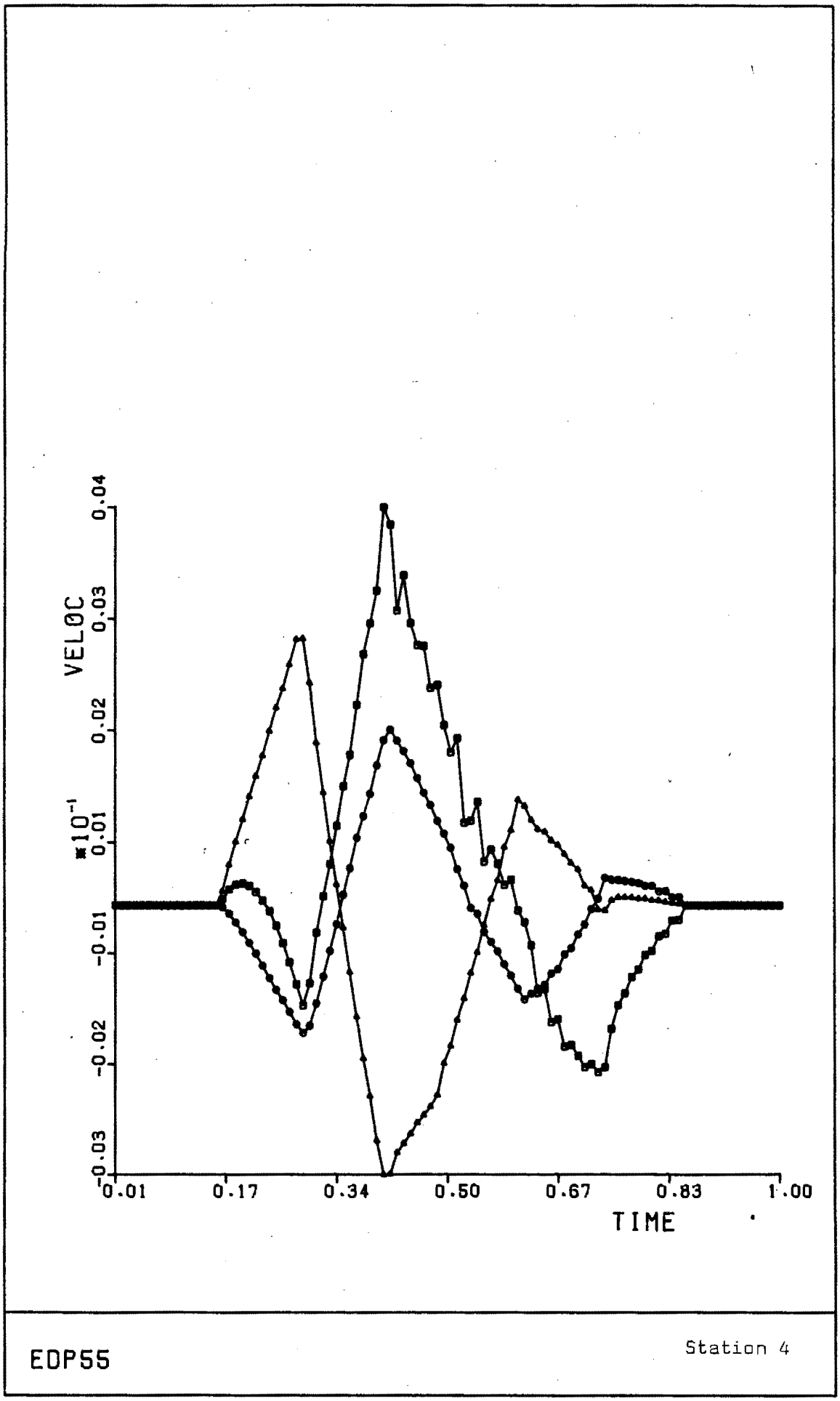

EDP55

Station 4

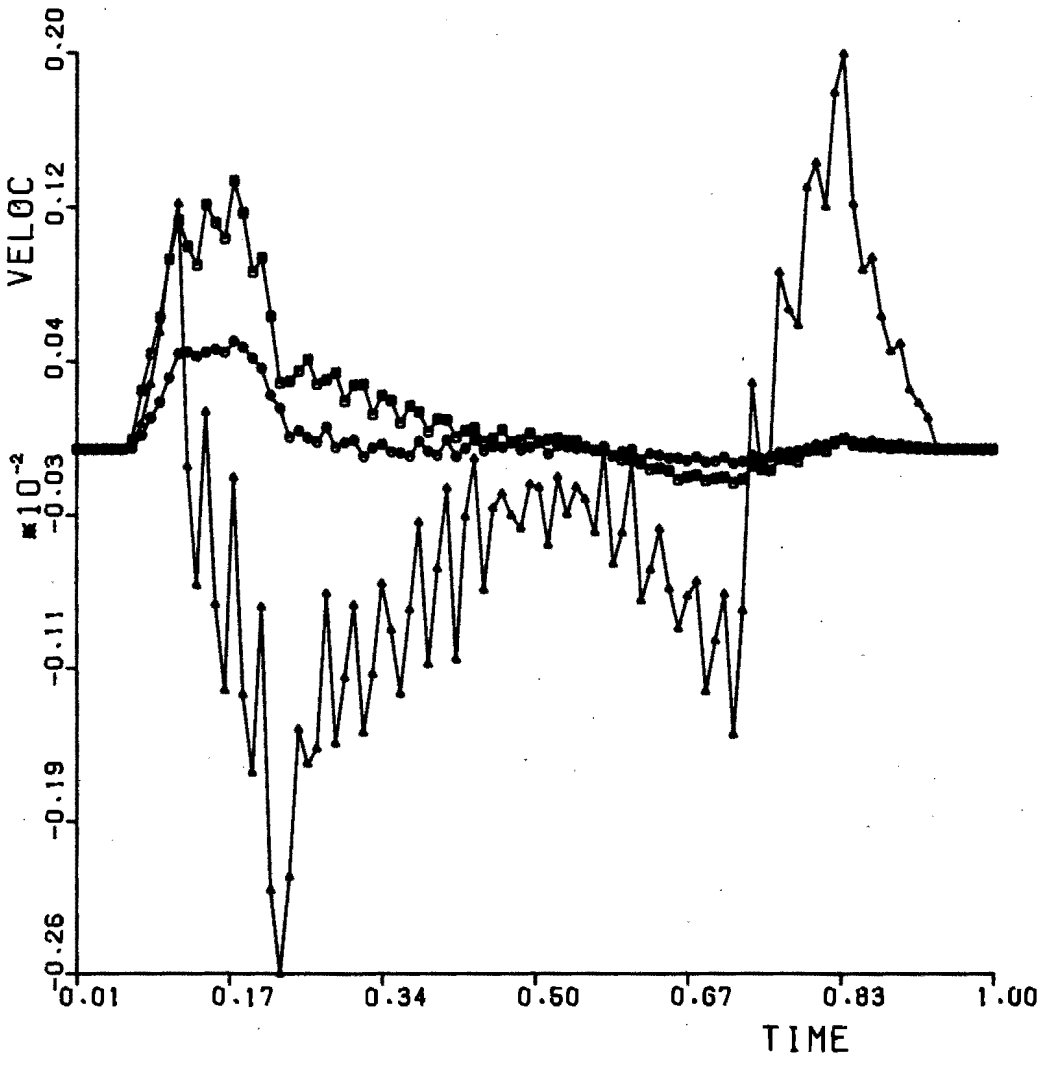

EDP64

Station 7

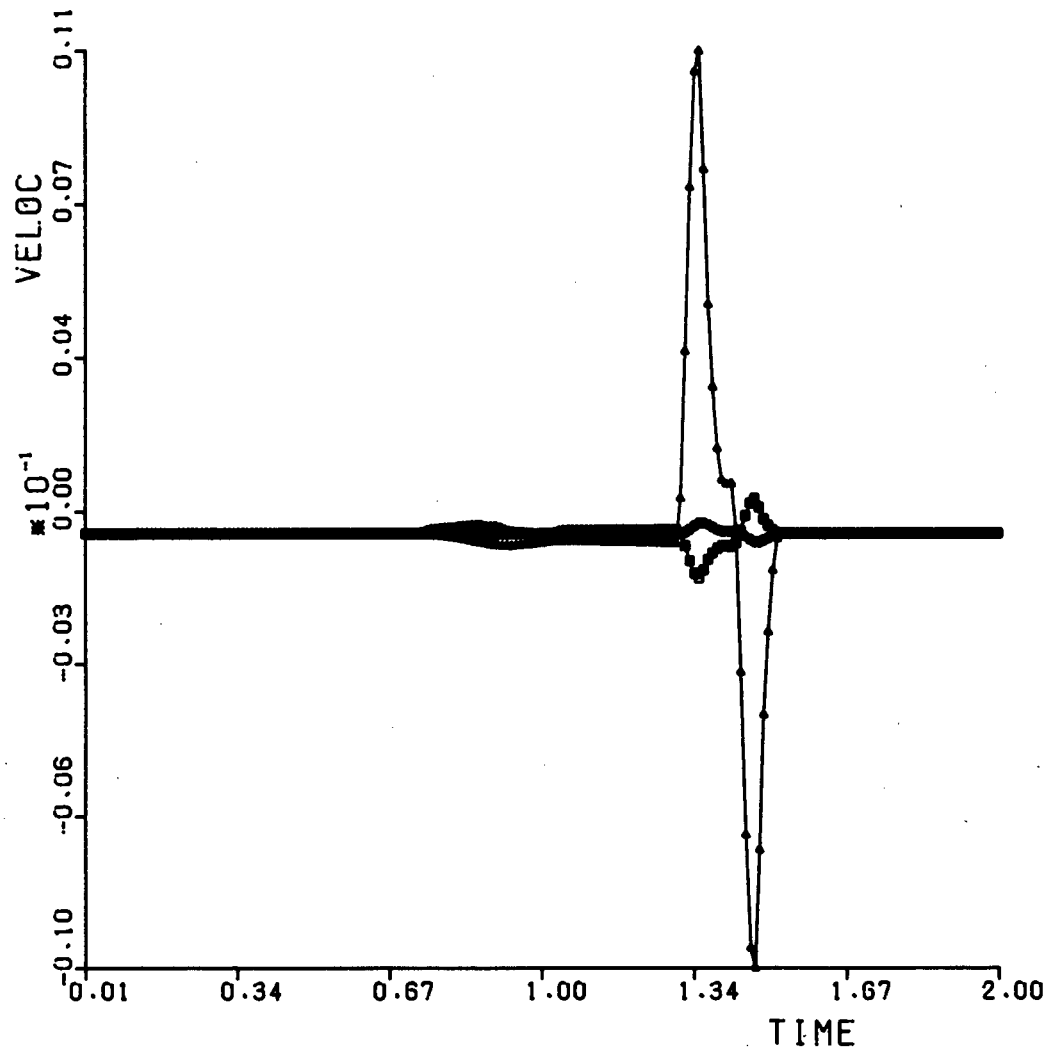

EDP54

Station 10

REFERENCES

ACHENBACH, J.D. (1973). Wave Propagation in Elastic Solids, North-Holland Series in Applied Mathematics and Mechanics, eds. H.A. Lauwerier and W.T. Koiter, 16, NH Publ. Co., Amsterdam.

AKI, K. (1967). "Scaling law of seismic spectrum", J. Geophys. Res., 72, 1217-1231.

ANDERSON, JOHN G., and RICHARDS, PAUL G. (1975). "Comparison of strong ground motion from several dislocation models",. Geophys. J. R. astro. Soc., 42, 347-373.

ANDREWS, D.J. (1976). "Rupture velocity of plane-strain shear cracks", J. Geophys. Res., 81, 5679-5687.

ANDREWS, D.J. (1985). "Dynamic plane-strain shear rupture with a slip-weakening friction law calculated by a boundary integral method", Bull. seism. Soc. Am., 75, 1-21.

ANTES, HEINZ (1985). "A boundary element procedure for transient wave propagations in two-dimensional isotropic elastic media", Finite Elements in Analysis and Design, I, 313-322.

ARCHULETA, R.J. and FRAZIER, G.A. (1978). "Three-dimensional numerical simulations of dynamic faulting in a half-space", Bull. seism. Soc. Am., 68, 573-598.

BETTI, E. (1872-73). "Teoria dell'Elasticita", Il Nuovo Ciemento t., 7-10.

BOUCHON, M. (1979a). "Discrete wave number representation of elastic wave fields in three-space dimensions", J. Geophys. Res., 84, 3609-3614.

BOUCHON, MICHEL (1979b). "Predictability of ground displacement and velocity near an earthquake fault: an example: the Parkfield earthquake of 1966", J. Geophys. Res., 84, no.B11, 6149-6156.

BOUCHON, M. and AKI, K. (1977). "Discrete wave-number representation of seismic-source wave fields", Bull. seism. Soc. Am., 67, 259-277.

BRUNE, JAMES N. (1970). "Tectonic stress and the spectra of seismic shear waves from earthquakes", J. Geophys. Res., 75, no.26, 4997-5009.

BURRIDGE, R. (1969). "The numerical solution of certain integral equations with non-integrable kernels arising in the theory of crack propagation and elastic wave diffraction", Phil. Trans. R. Soc. A, 265, 353-381.

BURRIDGE, R. and WILLIS, J.R. (1969). "The self-similar problem of the expanding elliptical crack in an anisotropic solid", Proc. Camb. phil. Soc., 66, 443-468.

COLE, D.M., KOSLOFF, D.D. and MINSTER, J.B. (1978). "A numerical boundary integral equation method for elastodynamics, I", Bull. seism. Soc. Am., 68, no.5, 1331-1357.

CRUSE, T.A. (1968). "A direct formulation and numerical solution of the general transient elastodynamic problem, II," J. Math. Anal. Appl., 22, 341-355.

CRUSE, T.A. and RIZZO, F.J. (1968a). "A direct formulation and numerical solution of the general transient elastodynamic problem, I", J. Math. Anal. Appl., 22, 244-259.

CRUSE, T.A. and RIZZO, F.J. (1968b). "A direct formultion and numerical solution of the general transient elastodynamic problem, II", J. Math. Anal. Appl., 22, 341-355.

DAHLEN, F.A. (1974). "On the ratio of P-wave to S-wave corner frequencies for shallow earthquake sources", Bull. seism. Soc. Am, 64, 1159-1180.

DAS, SHAMITA (1980). "A numerical method for determination of source time functions for general three-dimensional rupture propagation", Geophys. J. R. astro. Soc., 62, 591-604.

DAS, SHAMITA (1981). "Three-dimensional spontaneous rupture propagation and implications for the earthquake source mechanism", Geophys. J.R. astro. Soc., 67, 375-393.

DAS, SHAMITA (1985). "Application of dynamic shear crack models to the study of the earthquake faulting process", Int. J. of Fracture, 27, 263-276.

DAS, SHAMITA and AKI, KEITTI (1977). "A numerical study of two-dimensional spontaneous rupture propagation", Geophys. J.R. astro. Soc., 50, 643-668.

DAVIS, PHILLIP J. and RABINOWITZ, PHILIP (1975). Methods of Numerical Integration, in: Computer Science and Applied Mathematics series, ed. Werner Rheinboldt, Academic Press, NY.

DAY, STEPHEN M (1982). "Three-dimensional simulation of spontaneous rupture: the effect of nonuniform prestress", Bull. seism. Soc. Am., 72, 1881-1902.

DOYLE, J.M. (1966). "Integration of the Laplace transformed equations of classical elastokinetics", J. Math. Anal. Appl., 13.

DURBIN, F. (1974). "Numerical inversion of Laplace transforms: an efficient improvement to Dubner and Abate's method", Computer J., 17, 371-376.

ERINGEN, A. CEMAL and SUHUBI, ERDOGAN (1975). Elastodynamics volume III Linear theory, Academic Press, NY.

FREDHOLM, I. (1905). "Solution d'un probleme fondamental de la theorie de l'elasticite", Arkiv Mat. Astro. Fysik., 11, 28.

GELLER, R.J. (1976). "Scaling relations for earthquake source parameters and magnitudes", Bull. seism. Soc. Am., 66, 1501-1523.

GOTO, K., MATSUMOTO, M. and URAYAMA, M. (1985). "Earthquake-resistance analysis by finite element-boundary element hybrid method", Fifth International Conference on Numerical Methods in Geomechanics, Nagoya, 1-5 April 1985, T. Kawamoto and Y. Ichikawa, 1519-1524.

GRADSHTEYN, I.S. and RYZHIK, I.M. (1965). Table of Integrals, Series and Products, 4th edition prepared by Yu. V. Geronimus and M. Yu. Tseytlin, translation edited by Alan Jeffrey, Academic Press, NY.

GRIFFITH, A.A. (1921). "The phenomenon of rupture and flow in solids", Phil. Trans. R. Soc. London, Ser. A, 221, 163-198.

HAMANO, Y. (1974). "Dependence of rupture time history on the heterogeneous distribution of stress and strength on the fault plane" abstract, EOS Trans. Am. Geophys. Un., 55, 352.

HASKELL, N.A. (1964). "Total energy and energy spectral density of elastic wave radiation from propagating faults", Bull. seism. Soc. Am., 54, no.6, 1811-1841.

HASKELL, N.A. (1969). "Elastic displacements in the near-field of a propagating fault", Bull. seism. Soc. Am., 59, 865-908.

IRIKURA, KOJIRO. (1983). "Semi-empirical estimation of strong ground motions", Bull. of the Disaster Prevention Res. Inst., Kyoto Univ., Kyoto, 33, no.298, part 2, 63-104.

IRWIN, G.R. (1958). "Fracture Mechanics", Handbuch der physik, 79, 551-590, Springer-Verlag, Berlin.

KANAMORI, H. and ANDERSON, D.L. (1975). "Theoretical basis of some empirical relations in seismology", Bull. seism. Soc. Am., 65, 1073-1095.

KNOPOFF, L. and GILBERT, F. (1959). " Radiation from a strike slip fault", Bull. seism. Soc. Am., 49, 163-178.

KNOPOFF, L. and GILBERT, F. (1960). "First motions from seismic sources", Bull. seism. Soc. Am., 50, 117-134.

KOBAYASHI, S. (1985). "Applications of boundary integral equation method to geomechanics", Fifth International Conference on Numerical Methods in Geomechanics, Nagoya, 1-5 April 1985, ed. T. Kawamoto and Y. Ichikawa, 83-92.

KOBAYASHI, S. and KISHIMA, T. (1985). "Dynamic analysis of non-homogeneous ground movements by the boundary integral equation-finite element hybrid method", Fifth International Conference on Numerical Methods in Geomechanics, Nagoya, 1-5 April 1985, ed. T. Kawamoto and Y. Ichikawa, 135-142.

KOSTROV, B.V. (1964). "Selfsimilar problems of propagation of shear cracks", J. appl. Math. Mech., 28, 1077-1087.

KOSTROV, B.V. (1966). "Unsteady propagation of longitudinal shear cracks", J. appl. Math. Mech., (PMM), 30, 1241-1248.

LAMB, H. (1904). "On the propagation of tremors over the surface of an elastic solid", Phil. Trans. R. Soc. London, Ser. A, 203, 1-42.

KUPRADZE, V.D. (1963). "Dynamical problems in elasticity", Progress in Solid Mechanics, III, eds. I.N. Sneddon and R. Hill, Wiley (Interscience), NY.

LIGGET, J.A. (1982). "Singular cubature over triangles", IJNME, 18, 1375-1384.

LOVE, A.E.H. (1927). A treatise on the mathematical theory of elasticity, 4th ed., Dover Publications, NY., p.305.

MADARIAGA, R. (1976). "Dynamics of an expanding circular fault", Bull. seism. Soc. Am., 66, 639-666.

MADARIAGA, R. (1979). "On the relation between seismic moment and stress drop in the presence of stress and strength heterogeneity", J. Geophys. Res., 84, 2243-2250.

MANOLIS, G.D. (1980). "Dynamic responses of underground structures", Ph.D thesis, Univ. of Minnesota, Minneapolis, Minnesota.

MANOLIS, GEORGE D. (1983). "A comparative study on three boundary element method approaches to problems in elastodynamics", Int. J. Num. Meth. Eng., 19, 73-91.

MANOLIS, G.D. and BESKOS, D.E. (1981). "Dynamic stress concentration studies by boundary integrals and Laplace transform", Int. J. Num. Meth. Eng., 17, 573-599.

MANSUR, W.J. (1983). "A time-stepping technique to solve wave propagation problems using the boundary element method", Ph.D thesis, Univ. of Southampton.

MANSUR, W.J. and BREBBIA, C.A. (1982a). "Numerical implementation of the boundary element method for two dimensional transient scalar wave propagation problems", Appl. Math. Modelling, 6, 299-306.

MANSUR, W.J. and BREBBIA, C.A. (1982b). "Formulation of the boundary element method for transient problems governed by the scalar wave equation", Appl. Math. Modelling, 6, 307-311.

MANSUR, W.J. and BREBBIA, C.A. (1983). "Transient elastodynamics using a time-stepping technique", Boundary Elements: Proceedings of the Fifth International Conference, Hiroshima, Japan, November 1983, eds. C.A. Brebbia, T. Futagami and M. Tanaka, Springer-Verlag, 677-698.

MARUYAMA, TAKUO (1963). "On the force equivalents of dynamical elastic dislocations with reference to the earthquake mechanism", Bull. Earthquake Res. Inst., 41, 467-486.

MORSE, PHILIP M. and FESHBACH, HERMAN (1953). Methods of theoretical physics, McGraw-Hill, NY.

NARDINI, D. and BREBBIA, C.A. (1983). "Transient dynamic analysis by the boundary element method", Boundary Elements: Proceedings of the Fifth International Conference, Hiroshima, Japan, November 1983, eds. C.A. Brebbia, T. Futagami and M. Tanaka, Springer-Verlag, 719-698

NIWA, Y., KOBAYASHI. S. and AZUMA, N. (1975). "An analysis of transient stresses produced around cavities of arbitrary shape during the passage of travelling waves", Memoirs Fac. Eng. Kyoto Univ., 37, pt.2, 28-46.

NIWA, Y., KOBAYASHI, S. and FUKUI, T. (1976). "Applications of integral equation methods to some geomechanical problems", Numerical Methods in Geomechanics, ed. C.S. Desai, ASCE, NY, 120-131.

PAPOULIS, A. (1957). "A new method of inversion of the Laplace transform", Quart. Appl. Math., 14, 405-414.

POISSON, S.D. (1820). Paris Mem. Inst. t., 3.

RAJAPAKSE, R.K.N.D. and KARASUDHI, P. (1986). "An efficient elastodynamic infinite element", Int. J. Solids and Structures, 22, 643-658.

RICE, J.M. and SADD, M.H. (1984). "Propagation and scattering of SH-waves in semi-infinite domains using a time-dependent boundary element method", J. Appl. Mech., 51, 641-645.

RICHARDS, P. (1976). "Dynamic motions near an earthquake fault: a three-dimensional solution", Bull. seism. Soc. Am., 66, 1-32.

RICHARDS, PAUL G. (1979). "Elementary solutions to Lamb's problem for a point source and their relevance to three-dimensional studies of spontaneous crack propagation", Bull. seism. Soc. Am., 69, 947-956.

STEKETEE, J.A. (1958a). "On Volterra's dislocations in a semi-infinite elastic medium" Can. J. Phys., 36, 192-205.

STEKETEE, J.A. (1958b). "Some geophysical applications of the elastic theory of dislocations", Can. J. Phys., 36, 1168-1198.

STERNBERG, E. and EUBANKS, R.A. (1955). "On the concept of concentrated loads and an extension of uniqueness theorem in the linear theory and elasticity", J. Rational Mech. Anal. 4.

STERNBERG, E. and EUBANKS, R.A. (1957). "On stress functions for elastokinetics and the integration of the repeated wave equation", Quart. Appl. Math., 15.

VOLTERRA, V. (1907). "Sur l'equilibre des corps elastiques multiplement connexes", Ann. Sci. ecole norm. superieure, Paris, 24, 401-517.

ZIENKIEWICZ, O.C., BETTESS, P., CHIAM, T.C. and EMSON, C. (1981). "Numerical methods for unbounded field problems and a new infinite element formulation" in: Computational methods for infinite domain media-structure interaction, eds. Antony J. Kalinowski, ASME, AMD-46, 115-148.

BIBLIOGRAPHY

AKI, K. (1967). "Scaling law of seismic spectrum", J. Geophys. Res., 72, 1217-1231.

AKI, KEITTI and RICHARDS, PAUL G. (1980). Quantitative Seismology, I, WH Freeman, San Francisco.

BREBBIA, C.A., TELLES, J.C.F. and WROBEL, L.C. (1984). Boundary Element Techniques: Theory and Applications in Engineering, Springer-Verlag, N.Y.

COOK, ROBERT D. (1981). Concepts and Applications of Finite Element Analysis, 2nd ed., J. Wiley and Sons, NY.

CROUCH, S.L. and STARFIELD, A.M. (1983). Boundary element methods in solid mechanics, Allen and Unwin, Boston.

JAEGAR, J.C. and COOKE, N.G.W. (1979). Fundamentals of Rock Mechanics, 3rd edition, Chapman and Hall, London.

KASAHARA, K. (1981). Earthquake Mechanics, Cambridge Univ. Press, NY.

MALVERN, LAWRENCE E. (1969). Introduction to the Mechanics of a Continuous Medium, Prentice-Hall Inc., New Jersey.

STROUD, A.H. and SECREST, DON. (1966). Gaussian quadrature formulas, Prentice-Hall, Englewood Cliffs, N.J.